

SYNTHESIS AND USE OF CARBON NANOTUBES AS A SUPPORT FOR THE
FISCHER-TROPSCH SYNTHESIS

Munga Christian Bahome

A thesis submitted to the Faculty of Engineering and the Built Environment, University of the Witwatersrand, Johannesburg, in fulfillment of the requirements for the Degree of Doctor of Philosophy.

Johannesburg, 2007

Declaration

I declare that this thesis is my own, unaided work. It is being submitted for the Degree of Doctor of Philosophy in the University of the Witwatersrand, Johannesburg. It has not been submitted before for any degree or examination in any other University.

Signature of candidate

.....day of2007

Abstract

Carbon nanotubes (CNTs) were grown catalytically by a chemical vapor deposition method and characterized by a range of techniques. Fe, Ru and Co catalysts supported on the carbon nanotubes were prepared and investigated for their performances in the Fischer-Tropsch synthesis.

CNTs were synthesized in a quartz tubular reactor at atmospheric pressure and at temperatures of 700°C over iron supported on CaCO₃ using C₂H₂ as carbon source. Prior to CNT synthesis, the iron catalyst was first reduced under the same conditions (700°C and atmospheric pressure) in a flow of 5% H₂ balanced in Argon. The catalyst, for the preparation of the CNTs, was prepared by the incipient wetness impregnation. The purification of the CNTs was performed with 30 wt % HNO₃. Characterization of the CNTs using TEM, SEM, HRTEM, BET and TPR revealed that the crude product contained solely CNTs, catalysts particles and support, while no amorphous carbon was observed. The purified product is comprised of an interwoven matrix of tubes that were shown to be multi-walled (MWCNTs).

CNT supported FT based catalysts were also prepared by an incipient wetness impregnation method and tested in a plug flow reactor in Fischer-Tropsch synthesis. The TEM images of the different FT catalysts supported on CNTs revealed that the catalyst particles are well dispersed on the surface of the CNTs. The catalyst particles were very

small, and some residual Fe catalyst material, not removed by the acid treatment, could clearly be seen on the surface of the CNTs.

The reduction and metal dispersion properties of the catalysts were investigated through TPR and chemisorption techniques. A TPR study showed three reduction steps for Co catalysts, and addition of Ru to the catalyst decreased the reduction temperature of the catalysts. Gasification of the CNTs was noted to occur at temperatures higher than 600°C.

The effect of metal catalyst loading and promoters on the activity and selectivity of CNT supported FT synthesis catalysts was studied under condition of 275°C, 8 bar, CO/H₂ = 1/2 and different flow rates. The FT catalysts supported on carbon nanotubes displayed a high CO conversion and excellent stability with time on stream in the Fischer-Tropsch synthesis. Fe catalysts displayed the lowest methane selectivity compared to all other FT synthesis catalysts used in this study.

*To my wife Odette
and my sons Issa and Musa,
for your unconditional love and support*

Acknowledgements

The work presented in this thesis was made possible due to the assistance of a number of people and institutions. I would like to express my sincere gratitude to the following:

Prof. N.J. Coville, my supervisor for his enthusiasm and invaluable support throughout my research.

Prof. D. Hildebrandt, Prof. D. Glasser and Dr L.L. Jewell, my co-supervisors for their guidance and great enthusiasm as well as perseverance; to allow me to undertake this work into the new world of carbon nanotubes

B. Chassoulas for his technical support, which I really appreciated

My colleagues and members of the CatOmCer group and COMPS for their help and friendship

My parents for their unconditional love and support

The University of the Witwatersrand, Sasol, THRIP, NRF, COMPS, CatOmCer and DST Centre of Excellence for their financial support during my postgraduate studies

The Almighty God for his daily blessings

Publications and presentations arising from this thesis

Presentations

- CATSA 2004: Poster presentation
- “Fischer-Tropsch synthesis over iron catalysts supported on carbon nanotubes”
- CATSA 2005: Oral presentation
- “Fe:Ru/CNT bimetallic catalysts for Fischer-Tropsch synthesis”

Publications

- 2007: Fe:Ru small particle bimetallic catalysts supported on carbon nanotubes for use in Fischer-Tropsch synthesis. (Submitted)
- 2005: Fischer-Tropsch synthesis over iron catalysts supported on carbon nanotubes. [Applied Catalysis A: General **287** (2005) 60 – 67]

Contents

Declaration.....	i
Abstract.....	ii
Acknowledgements.....	v
Publications and presentations arising from this thesis	vi
Table of Contents	Error! Bookmark not defined.

Table of Contents

CHAPTER 1: INTRODUCTION	1
1.1. Fischer-Tropsch Synthesis	1
1.1.1. History.....	1
1.1.2. Definition	3
1.1.3. Fischer-Tropsch chemistry.....	4
1.1.4. Types of Fischer-Tropsch Reactors	7
1.1.5. Fischer-Tropsch catalysts.....	14
1.2. Catalyst supports	18
1.2.1. Carbon support.....	19
1.2.2. Carbon supports in Fischer-Tropsch synthesis	21
1.3. Carbon nanotubes	24
1.3.1. Carbon nanotube properties	24

1.3.2. Synthesis of carbon nanotubes.....	27
1.3.3. Carbon nanotube as support for Fischer-Tropsch synthesis catalysts	29
1.4. Aims of this study.....	31
References.....	32
CHAPTER 2: EXPERIMENTAL.....	38
2.1. Introduction.....	38
2.1. Synthesis of the carbon nanotubes	39
2.1.1. Gases.....	40
2.1.2. Metal and catalyst support	40
2.1.3. Catalyst preparation	40
2.1.4. Preparation of the carbon nanotubes.....	41
2.1.5. Purification of the carbon nanotubes	43
2.2. Synthesis of catalysts supported on carbon nanotubes	43
2.2.1. Gas	43
2.2.2. Metal, additives and catalyst support.....	44
2.2.3. Catalysts preparation.....	45
2.3. Reactor studies and Characterizations	48
2.3.1. Characterization	48
2.3.2. FT reactor system.....	56
References.....	68
CHAPTER 3: FISCHER-TROPSCH SYNTHESIS OVER IRON CATALYSTS	
SUPPORTED ON CARBON NANOTUBES	71
3.1. Introduction.....	71

3.2. Experimental	74
3.3. Catalyst characterization	77
3.4. Data analysis and calculations	78
3.5. Results and discussion	80
3.5.1. Catalyst synthesis.....	80
3.5.2. Catalyst characterization.....	83
3.5.3. Catalytic activity	87
3.5.4. Deactivation	91
3.5.5. Mechanistic issues	92
3.6. Conclusion	94
References	95
CHAPTER 4: Fe:Ru SMALL PARTICLE BIMETALLIC CATALYSTS SUPPORTED	
ON CARBON NANOTUBES FOR USE IN FISCHER-TROPSCH SYNTHESIS	
4.1. Introduction	98
4.2. Experimental	101
4.2.1. Catalyst Preparation	101
4.2.2. Catalyst Characterization	103
4.2.3. Catalytic measurements	104
4.3. Results and Discussion	105
4.3.1. Catalyst characterization.....	105
4.3.2. Catalytic activity	112
4.4. Conclusion	125
References	127

CHAPTER 5: COBALT CATALYSTS SUPPORTED ON CARBON NANOTUBES	
FOR THE FISCHER-TROPSCH SYNTHESIS.....	130
5.1. Introduction	130
5.2. Experimental	133
5.2.1. Catalyst preparation	133
5.2.2. Catalyst Characterization	134
5.2.3. Catalytic measurements	135
5.3. Results and discussion	136
5.3.1. Catalyst characterization.....	136
5.3.2. Catalytic activity	141
5.4. Conclusion	151
References	153
CONCLUSIONS.....	155

List of Tables

1.1: World fossil fuel reserves and consumption (EJ, 10^{18} J) [6]

1.2: Typical product selectivity from two Sasol processes

3.1: Metal content and BET surface areas of various catalysts

3.2: Activity and selectivity of iron catalyst in FTS

3.3: Results of Fe catalysts supported on various carbon materials

4.1: Actual metal content of various catalysts as determined by ICPOES

4.2: BET surface areas and pore volume of the different catalysts

4.3: Activity and selectivity of Iron- Ruthenium catalysts (Same flow rate, Large range of conversion: 60 – 36%)

4.4: Activity and selectivity of Iron- Ruthenium catalysts (Variable flow rates, conversions 20-30%)

4.5: Activity and selectivity of catalysts with same Fe/Ru ratio

4.6: Activity and selectivity of 5%Fe/ 0.25%Ru catalyst at high and low conversion

4.7: Results of Fe-Ru catalysts supported on various materials

5.1: Metal content of various catalysts

5.2: Calcination temperature, BET surface area and pore volume of various catalysts

5.3: Activity and selectivity of catalysts at the same gas hourly space velocity (GHSV = 2140. h⁻¹)

5.4: Activity and selectivity of catalysts at the different gas hourly space velocity

5.5: Activity and selectivity of catalysts at the different gas hourly space velocity

5.6: Activity and selectivity of catalysts at the different gas hourly space velocity

List of Figures

- 1.1.a: Slurry bubble column reactor
- 1.1.b: Multitubular trickle bed reactor
- 1.1.c: Circulating fluidized bed (CFB) reactor
- 1.1.d: Fluidized fixed bed (FFB) reactor
- 1.2: Structure of MWNT (a) and SWNT (b) [67]
- 1.3: SWNT zigzag (a) and SWNT armchair (b)
- 1.4: Presents a schematic of the two growth modes commonly considered for CNTs: base growth and tip growth depending on where the catalyst is located [73]

- 2.1: The furnace used for the synthesis of CNTs by the CVD method
- 2.2: Perkin Elmer Pyris 1, thermo gravimetric analyzer
- 2.3: Experimental set-up for TPR measurements
- 2.4: The TriStar analyzer and the Flowprep 060 degasser
- 2.5: Schematic representation of the plug flow reactor
- 2.6: Three plug flow reactor running in parallel
- 2.7: Schematic representation of the reactor system
- 2.8: Reactor system (Reactor, two GC and temperature controllers)
- 2.9: A trace for the calibration gas using the FID GC and hydrogen carrier gas

2.10: A trace for the FT gas product using a FID GC and a Porapak Q column

3.1: TEM image of unpurified carbon nanotubes. Dark spots represent residual Fe particles

3.2: SEM image of purified carbon nanotubes

3.3: SEM image of Fe catalyst supported on carbon nanotubes. White spots represent Fe particles

3.4: TPR profiles of the catalysts

3.5: CO conversion with time on stream

4.1a and 4.1b: TEM images of the purified carbon nanotubes

4.2a and 4.2b: TEM images of iron-ruthenium based catalysts supported on carbon nanotubes

4.3: TPR profiles of various calcined catalysts

4.4: TPR profiles of various calcined catalysts with same Fe/Ru ratio

4.5: CO conversion with time on stream (same flow rate) for promoted Fe:Ru catalysts. The drop in conversion at (a) is attributed to a change in the flowrate

4.6: CO conversion with time on stream (similar CO conversion) for promoted Fe:Ru catalysts

4.7: CO conversion with time on stream (same flow rate) for a series of Fe:Ru catalysts. The drop in conversion at (a) is due to a change in the flowrate

5.1: TEM images of Fe supported on CNT

5.2: TEM images of the Fe supported on the CNT showing small Fe particles between the graphite of the CNT support

5.3: TPR profiles of different cobalt catalysts

5.4: CO conversion with time on stream

CHAPTER 1: INTRODUCTION

1.1. Fischer-Tropsch Synthesis

1.1.1. History

Fischer-Tropsch (FT) synthesis can be said to have started in Germany in 1913 when Badische Anilin und Soda Fabrik (BASF) received patents on the preparation of hydrocarbons and oxygenates by the hydrogenation of carbon monoxide over cobalt catalysts at high pressure [1-4]. The process was further developed by Franz Fischer and Hans Tropsch [3, 4] who, in 1923, obtained what they called synthol, an oxygenate rich mixture, from a hydrogen and carbon monoxide mixture over alkalis iron and other catalysts at high pressure. In 1936 the first four FT production plants were commissioned in Germany and had a total capacity of 200 000 tons of hydrocarbon per year [3]. The catalyst used was mainly the cobalt catalyst [3].

After the Second World War, the production of fuels and chemicals from coal became uneconomic mainly due to the discovery of the huge oil fields in the Middle

East. But in 1950, the fears of an impending shortage of petroleum in the USA caused wide interest in coal-to-oil processes. A fluidised–fixed bed process was developed by Hydrocarbon Research, Trenton, New Jersey and was installed in Brownsville, Texas in 1953. This new FT reactor was used to convert syngas produced from methane over a Fe catalyst. The plant was operating correctly but it was promptly shut down due to an increase in the price of methane. At the same time, in South Africa, international isolation led to the implementation of the Sasol FT synthesis plant. This FT plant, opened in 1955, was used to convert syngas produced from coal to hydrocarbons. The Oil embargo by the Organisation of Petroleum Exporting Countries (OPEC) in 1973 and the increase in the price of petroleum led to a revival in research activities on the FT process in many countries. In South Africa, two new FT plants were designed and built in record time. These are situated in Secunda and became operational in 1980 and 1982 respectively [1, 4, 5].

FT synthesis is currently one of the most promising topics in the energy industry due to economic utilisation of natural gas and coal to environmentally clean liquid fuels, waxes, straight-chain higher alcohols and olefins for the chemical industry. The resources of coal and natural gas are very large, see Table 1.1:

Table 1.1: World fossil fuel reserves and consumption (EJ, 10^{18} J) [6]

	Reserves	Consumption (1991)
Coal (1991)	27,185	69.91
Crude oil (1992)	6,054	143.67
Natural gas (1992)	4,512	79.44

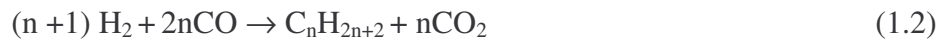
1.1.2. Definition

Fischer-Tropsch synthesis is a heterogeneous surface catalysed polymerisation process that uses CH_2 monomers, formed via the hydrogenation of adsorbed CO over transition metals, to produce hydrocarbons and oxygenates with a broad range of chain length and functionality. The major products are linear paraffins and α -olefins [7]. The FT process is the most promising source of chemicals and fuels from non-petroleum based feedstock such as coal and natural gas [8]. The FT product distribution is mainly a function of catalyst properties, kind of reactor and operating conditions (temperature, pressure) rather than thermodynamic constraints [9]. Typical operating conditions for FT synthesis are a temperature range of 200-350°C and pressures of 15-40 bar. The product selectivity is influenced by the catalyst ability to enhance chain propagation over chain termination.

1.1.3. Fischer-Tropsch chemistry

The chemistry of Fischer-Tropsch Synthesis is described by equations listed below:

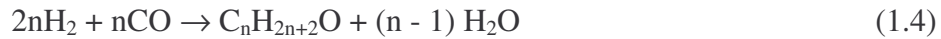
Reactions producing paraffinic hydrocarbons



Reactions producing olefinic hydrocarbons



Reaction producing alcohols



Depending on the type of catalyst used, in addition to the above equations, side reactions also occur:

Water Gas Shift (WGS) reaction



Boudouard reaction (Carbon deposition)



Bulk carbide formation



Catalyst Oxidation-Reduction



Since the cost of production of purified syngas is high it is important that the maximum amount is converted in the downstream FT reactor. For Co based FT catalysts, the typical H₂/CO usage ratio is about 2.15. When Fe based catalysts are used the overall H₂/CO ratio is changes due to the presence of the water gas shift (WGS) reaction. At higher operating temperatures, the WGS reaction is rapid and goes to equilibrium and this allows in principle all the H₂, CO and CO₂ to be converted to FT products [5].

FT synthesis is considered to be a catalysed polymerisation thus the product spectrum can be described by a chain polymerisation kinetic model. Anderson, Schultz and Flory (ASF) proposed a kinetic model that is most frequently used to describe the product distribution obtained from the FT synthesis [10, 11]. The ASF kinetic model is shown in equation (1.8):

$$\frac{W_n}{N} = (1 - \alpha^2) * \alpha^{(n-1)} \quad (1.8)$$

where n is the carbon number, W_n is the weight fraction of product containing n carbon atoms and α is the chain growth probability. The α value for product distribution ranges between 0 and 1 with the higher value indicating a greater selectivity towards waxy products and a lower value corresponding to gaseous products. However, most of the FT product distributions reported in the literature [12, 14] do not obey the simple ASF kinetic model, i.e. a high methane selectivity and a low yield of ethene relative to the predicted ASF distribution. Further the α -olefin to paraffin ratio decreases exponentially and the chain growth parameter, α , is not constant with increasing chain length.

Alpha can also be defined in terms of the rate of chain propagation (r_p) and chain termination (r_t) as:

$$\alpha = \frac{r_p}{r_t + r_p} \quad (1.9)$$

Currently there are two FT operating regimes [5, 15]. In the low-temperature FT (LTFT) process, either iron or cobalt catalyses the production of high molecular mass linear waxes in a temperature range of 200 to 240°C and at a pressure of 27 bar. In the high-temperature FT (HTFT) process iron-based catalysts are used for the production of gasoline and linear low molecular mass olefins in a temperature range of 300 to 350°C and a pressure of 20 bar. The typical product distribution for the LTFT and HTFT processes are shown in table 1.2 [16]

Table 1.2: Typical product selectivity from two Sasol processes

Product (wt%)	LTFT	HTFT
CH ₄	4	7
C2 to C4 Olefins	4	24
C2 to C4 paraffins	4	6
Gasoline	18	36
Middle distillate	19	12
Heavy Oils/Waxes	48	9
Oxygenates	3	6

1.1.4. Types of Fischer-Tropsch Reactors

Since the FT reactions are highly exothermic, the major consideration for the development of commercial FT reactors is the removal of heat. High temperatures favour the formation of undesired methane and the overheating of the catalyst which results in an increased rate of deactivation due to sintering and fouling [5]. The main types of reactor which have been developed since 1950 are [17-19]:

1. Slurry bubble column reactors with internal cooling tubes or three-phase fluidised (ebulating) bed reactors (Sasol - SSPD; Energy International - GasCat, Exxon - AGC-21, see Fig. 1.1.a)

2. Multitubular fixed bed reactor with internal cooling (Sasol - Arge; Shell - SMDS, see Fig. 1.1.b)
3. Circulating fluidised bed (CFB) reactor with circulating solids, gas recycle and cooling in the gas/solid recirculating loop (Sasol - Synthol) (Fig. 1.1.c)
4. Fluidised fixed bed (FFB) reactors with internal cooling (SAS: Sasol) (Fig. 1.1.d)

In general, the fixed bed reactors (Fig. 1.1.b) are suitable for the low temperature FT operation and for the production of wax. The gas flows through the bed in the downward direction and the wax produced trickles down and out of the catalyst bed.

There are two types of fluidised bed reactors; the circulating fluidised bed (CFB) reactor (Fig. 1.1.c) and the fluidised fixed bed (FFB) reactor (Fig. 1.1.d). In the CFB reactors, there are two phases of fluidised catalyst. In the FFB reactor, the catalyst flows down the standpipe in dense phase while it is transported up the reaction zone in lean phase. The heat of reaction is removed from the reactor by cooling coils generating steam. To avoid the inlet gas going up the standpipe the pressure over the standpipe must be higher than in the reaction zone [5].

In the slurry bed reactor, the gas flow itself provides the agitation power required to keep the catalyst bed in suspension.

The slurry bed reactor presents many advantages over the multitubular fixed bed reactor: it is cheaper to construct (only 25% of the cost of the Multitubular fixed bed reactor), it uses less catalyst and the catalyst can be removed or added on-line. It is more isothermal and so can operate at higher average temperature resulting in higher conversions. On the other hand the fixed bed is simple to operate and allows for easy separation of the catalyst from wax. Among the disadvantages of the fixed bed reactors are: high pressure drop over the reactor, a high temperature gradient (compared to other reactors) and tedious replacement of the used catalyst [5, 15, 20].

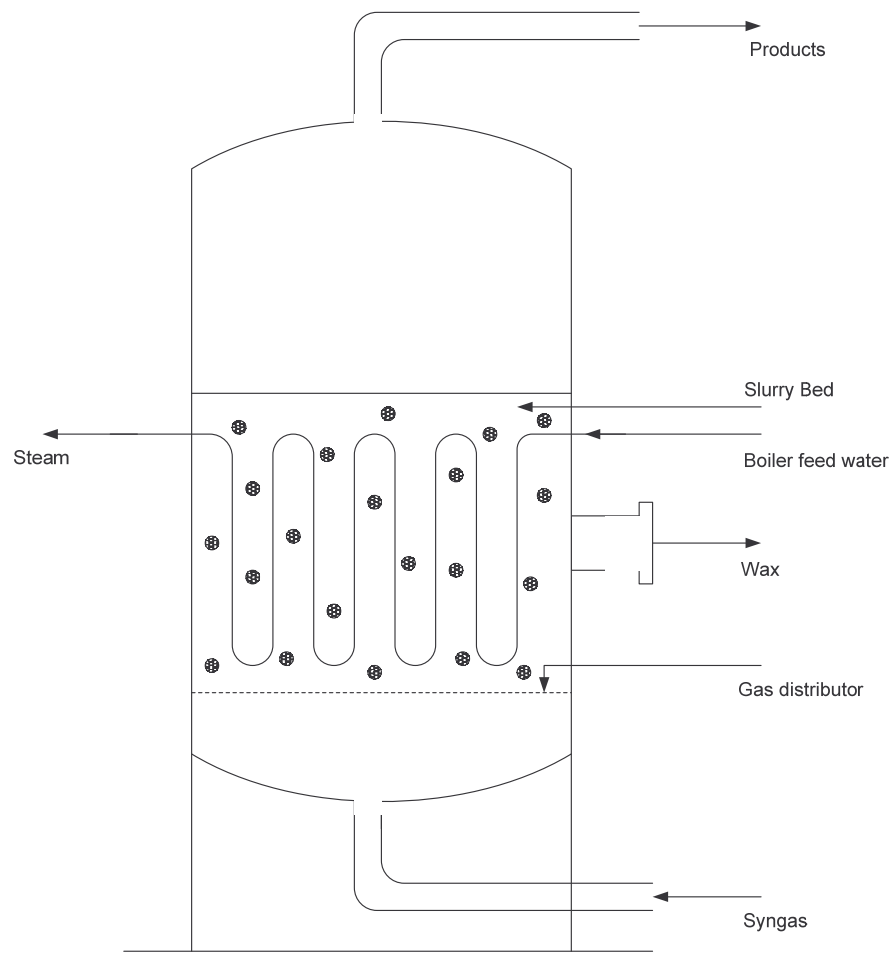


Figure 1.1.a: Slurry bubble column reactor

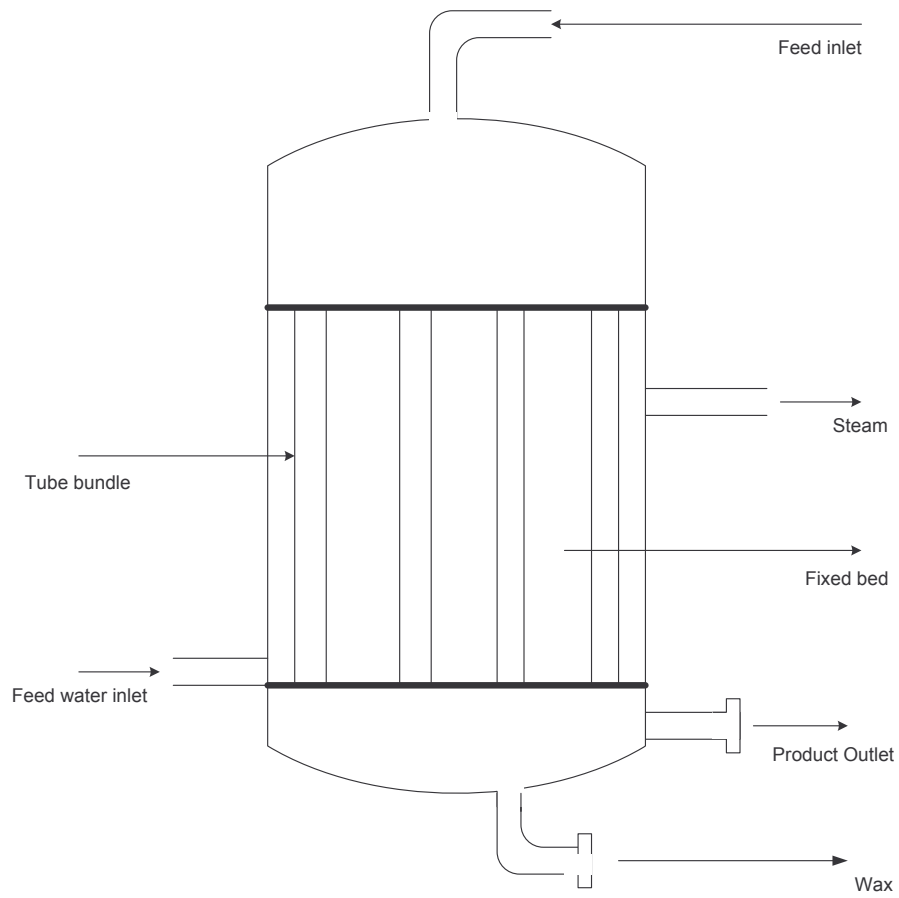


Figure 1.1.b: Multitubular trickle bed reactor

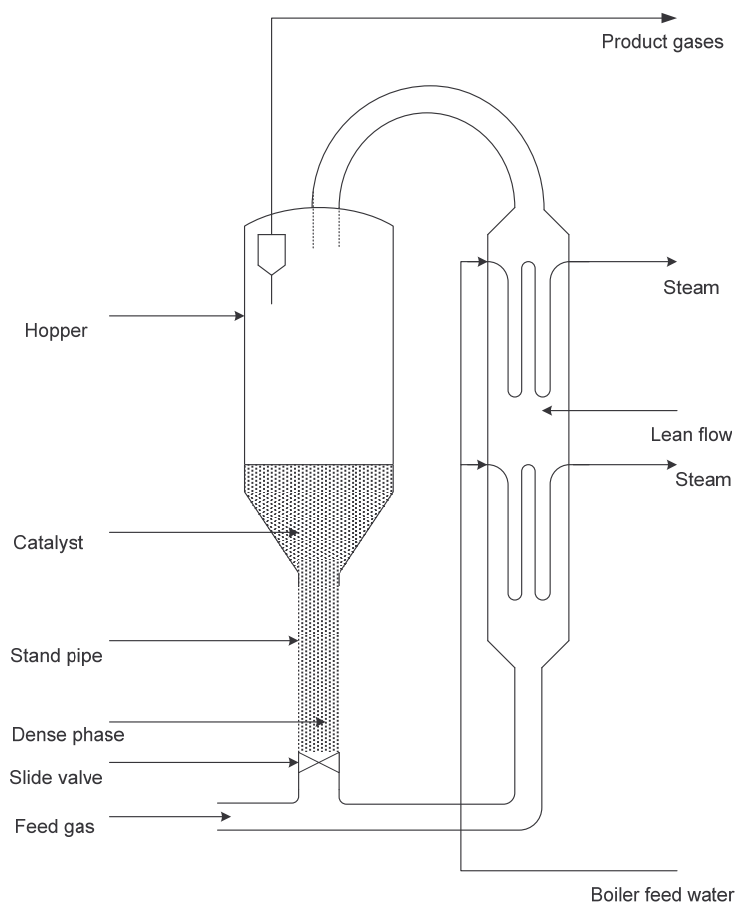


Figure 1.1.c: Circulating fluidized bed (CFB) reactor

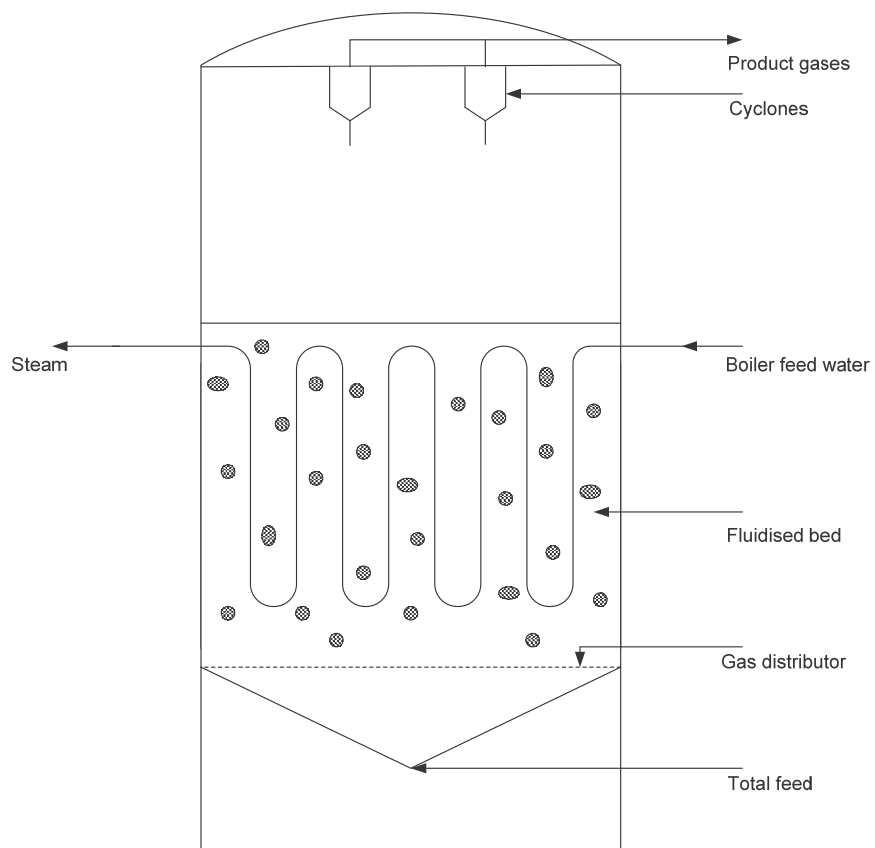


Figure 1.1.d: Fluidized fixed bed (FFB) reactor

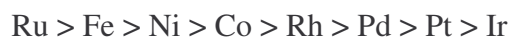
Figure 1.1: Possible reactors for Fischer-Tropsch synthesis [17, 19]. a. Slurry bubble column reactor; b. Multitubular trickle bed reactor; c. Circulating fluidized bed (CFB) reactor; d. Fluidized fixed bed (FFB) reactor.

Dry [5] compared the FFB reactor to the CFB reactor. For the same production capacity, the FFB is smaller than the CFB, it is less costly to construct (cost is 40% lower), simpler to operate (more gas can be fed by either increasing the volumetric flow rate or by increasing operating pressure) and easier to build. In the FFB the whole catalyst charge participates in the reaction at any moment, whereas in the CFB

only a portion of it does since a portion of the catalyst is in the recirculation loop and so not in contact with the reactant gas. The main disadvantage of the two fluidised bed reactors is that should any poison enter the reactor the entire catalyst bed is poisoned whereas in the fixed bed, the poison is adsorbed on the top layer of the catalyst leaving the rest of the bed intact.

1.1.5. Fischer-Tropsch catalysts

The most common catalysts for the CO hydrogenation (F-T synthesis) are group 8 to group 10 elements. Fe, Co, Ni and Ru are known as FT catalysts; however Rh has been shown to have interesting properties in FT synthesis [1] and should probably be included in this list. Since Ru is neither oxidised nor carburised during the FT synthesis many workers have chosen supported Ru as an ideal catalyst for investigation. Under typical FT operating conditions, Ni produces a large amount of methane and during the reaction Ni carbonyls are formed, which result in loss of activity [22]. Mo and W have also been tested as FT catalysts but they have displayed low activity, possibly because these metals oxidize easily [1, 20]. The specific activity for the different metals was reported to decrease in the following order [21, 22]:



Of this group, only Fe, Ni, Co and Ru have the required FT activity for commercial application. Historically, Fe has been the catalyst of choice in industrial applications

due to its low cost compared to other FT catalysts. Cobalt has also been used in industry as a catalyst for FT synthesis, as it shows greater stability than iron and can be used at lower temperatures and pressures [20, 22]. Ni has been studied widely but often under conditions for which methane is the principal product [1]. The high price of Ru and insufficient availability makes the commercial application of Ru catalysts unfeasible. Thus, Fe and Co are the only viable catalysts for use in commercial FT processes. The major difference between the two catalysts is that iron has a significant water gas shift activity. With cobalt the oxygen contained in the CO in the syngas is rejected as water and with iron the oxygen is rejected as carbon dioxide [23]

1.1.5.1. Iron catalysts

Iron catalysts are extensively used in the major FT synthesis commercial operations at Sasol and PetroSA (formerly Mossgas) in South Africa and can thus be considered as the most important FT catalyst. Fe catalysts are not only used due to their low price compared to Co and Ru but they also have the advantage of producing olefins when operated at higher temperatures or either in the low or the high alpha mode [22, 24, 25]. Iron-based catalysts are used in the LTFT for the production of wax. The product selectivity of Fe catalysts is controlled by the addition of alkali metals. In particular, promotion with potassium has been found to increase the wax and olefin selectivity and to decrease the methane production. Cu has been traditionally added to precipitated Fe catalysts in order to enhance the rate of reduction and to lower the reduction temperature of Fe oxide to metal [26]. For the iron catalysts used in HTFT

the addition of SiO_2 , Al_2O_3 and even Mn can be applied for structural promotion to enhance the olefin selectivity and to maintain high surface area and stability of the catalyst. Prior to the FT reaction the catalysts are usually reduced with hydrogen, carbon monoxide or a mixture of the two (Syngas). Iron FT catalysts can lose activity due to sintering, fouling and chemical poisoning of the surface by, for example, sulphur [27].

1.1.5.2. Cobalt catalysts

The first industrial catalyst used in FT synthesis was a precipitated cobalt catalyst. The interest in Co as the basis for a FT catalyst declined in the 1950's due to its high price and the development of successful iron based catalysts. However, cobalt catalysts are now being used in the LTFT process as at high temperatures excess methane is produced [5]. The Co catalyst is not susceptible to deactivation by carbide or oxide formation as is Fe. In addition, Co may be used at lower temperatures and pressures and Co supported on SiO_2 has the highest turnover number (TRN) of the group 8-10 metals, (synthesis conditions: 275°C , 1 atm). Iglesia [7] has reported that there is a clear correlation between activity and Co metal area irrespective of the nature of the support, i.e. the support has no chemical effect on the turnover frequency (TOF) of Co sites [5, 7].

Cobalt catalysts yield mainly linear hydrocarbons. Water is the principal oxygenate formed with alcohol production being rare [28]. Water-gas-shift activity over cobalt

catalysts is very low especially compared to iron catalysts. Both Co and Fe are poisoned by sulphur compounds and thus the sulphur content of the syngas should be kept below 0.02 mg/m^3 (STP) [5].

1.1.5.3. Ruthenium catalysts

In 1975, Vannice [30] reported the specific activities of group 8-10 metals supported on alumina. Ru catalysts displayed low selectivity towards methane and higher selectivity towards C_{5+} hydrocarbon products than any of the other common FT catalysts at temperatures from 240°C to 280°C and atmospheric pressure. In a series of studies on a $0.5\%\text{Ru}/\text{Al}_2\text{O}_3$ catalyst, Everson and co-workers [31-33] established that increasing pressure increases the activity of CO hydrogenation and selectivity towards heavier hydrocarbons while an increase in the temperature enhances activity but also increases methane selectivity. Supports and/or promoters appear to have no beneficial effect on Ru catalysts; it is most active in the pure metallic form. Studies at Sasol showed that at low conversion the Ru catalyst like Fe can produce light hydrocarbons with high olefin and alcohol content [29]. Ruthenium has a high potential as a catalyst for FT synthesis as evidenced by the fact that it is active over a wide range of temperatures ($100\text{-}300^\circ\text{C}$) and pressures (1-200 atm). The high price of ruthenium and the limited world resources exclude industrial application. However, it can be used as an additive to other FT catalyst such as Fe and Co.

1.1.5.4. Nickel catalysts

Nickel is generally regarded as a methanation catalyst and has limited use in Fischer-Tropsch synthesis. Nickel has been shown to be active for methanation in the FT synthesis when used either as alloy [34] or supported on silica [35]. Supported on Al_2O_3 , Ni catalysts have been found to result in very low conversions at temperatures below 240°C . Under typical FT synthesis conditions, poisonous volatile carbonyls are formed on Ni catalysts and carbon deposition occurs if syngas with $\text{H}_2:\text{CO}$ ratios of less than 2.5 are used. It is worthwhile to mention that the very earliest FT synthesis reaction was done in 1902 when Sabatier and Sanderens became the first to report the hydrogenation of CO over a Ni catalyst to produce methane [36, 37].

1.2. Catalyst supports

Many industrial catalysts consist of metals or metal compounds supported on an appropriate support; the purpose of the support is basically to facilitate preparation of a well dispersed, high surface area catalytic phase [38]. Spreading the active metal phase on a support allows one to obtain a metal phase with a small crystallite size on the support, which is desirable for catalysis itself. The support provides a means of obtaining small metal particles without many accompanying disadvantages. For example, the pressure drop is not excessive in a reactor (fixed bed reactor), small

catalyst particles are not entrained (fluidised reactor) and particles are easily suspended or removed by filtration (slurry reactor) [39]. The economically optimal catalyst particle size is determined by the process in which the catalyst has to be used.

The advantage of spreading the active phase on a support is to obtain a large active surface per unit weight used. A catalyst support also facilitates the flow of gases through the reactor and the diffusion of reactants through the pores to the active phase, retarding the sintering of the active phase and increasing the resistance of the catalyst to poisoning. The selection of the support is based on a series of desired characteristics: inertness; stability under reaction conditions; adequate mechanical strength, appropriate physical form for the given reactor; high surface area; porosity and chemical nature. In practice only four supports combine these characteristics optimally: alumina, silica, titania and carbon materials [40].

1.2.1. Carbon support

Carbon is the lightest atom in column 14 of the periodic table. It is a very special element because it occurs in all organic life and is the basis of organic chemistry. Carbon was discovered in prehistory and was known to the ancients, who manufactured it by burning organic material making charcoal. The five well-known allotropes of carbon are amorphous carbon, graphite, diamond, fullerenes and nanotubes. In homogeneous catalysis, carbon features as a prominent ligand in metal systems. Carbon is also used as a catalyst support material as it allows the anchoring

of catalyst particles on a substrate which does not exhibit solid acid-base properties [41-44].

1.2.1.1. Carbon chemistry

Carbon-based materials are unique in many ways. One distinction relates to the many possible configurations of the electronic states of a carbon atom, which is known as hybridisation of atomic orbitals, and the wide differences in the properties of the various forms of carbon. According to the phase diagram of carbon suggested by Bundy [45], under ambient conditions the graphite phase with strong in-plan trigonal sp^2 is the stable phase. Under application of high pressure and high temperature, a transformation to the diamond structure, with tetrahedral sp^3 bonding, takes place and once the pressure is released diamond will very slowly revert to the thermodynamically stable form of graphite [46, 47].

1.2.1.2. Carbon supports in heterogeneous catalysis

Carbon materials are established catalyst supports in heterogeneous catalysis because they can satisfy some of the desired properties required for a suitable support [40, 48]. Carbon materials are chemically inert, resistant to acidic and basic media, stable at high temperature and cheaper than conventional supports such as alumina and silica. They exhibit mechanical resistance and have a high surface area. It is easy to tailor the pore structure of carbon materials. Moreover, the active phase can be

recovered from the spent catalyst by burning off the carbon support. These properties determine the metal dispersion and the particle size, and consequently, the activity and selectivity. Carbon has thus some very valuable characteristics which are not attainable with any other support. However, a carbon support cannot be used in hydrogenation reactions above 430°C or in the presence of oxygen above 230°C, because it may gasify to produce methane and carbon dioxide, respectively [40]. In addition, the reactivity of carbon without functional groups is low with respect to most elements. In general, oxygen functional groups can be introduced on the surface of a carbonic material by treating it with an oxidising agent such as: ozone, carbon dioxide, hydrogen peroxide and nitric acid. The functional groups determine the ion exchange properties that are important for loading catalytically active components onto the support. Many oxygen groups can be found on the surface of the carbon material; carboxyl groups are of importance in heterogeneous catalysis because they give the carbon surface an acid character and they can be used as catalyst anchoring sites [49].

1.2.2. Carbon supports in Fischer-Tropsch synthesis

Numerous studies reported in the literature [50, 51] provide evidence that supports can change the activity and selectivity properties of Fe, Ni, Co, Ru and Mo for CO hydrogenation. Reuel and Bartholomew [50] observed variations in the activity of a Co supported catalyst; the decreasing order of activity in their data was Co/titania > Co/alumina = Co/silica > Co/carbon > Co/magnesia (3 and 10% Co loadings). For a

given Co supported catalyst activity was found to increase with increasing loading and decreasing dispersion (dispersion generally decreases with increasing metal loading). The FT product distribution obtained from these catalysts was also support dependent. Furthermore Fu and Bartholomew [51] have shown that for a Co/alumina as the Co loading is increased from 3 to 15% the product selectivity shifts to the heavier product with the alpha value increasing from 0.70 to 0.90.

Studies on Fe supported catalysts [51, 52] revealed the influence of the support on the activity and selectivity. The data obtained from these studies showed that for highly loaded and poorly dispersed catalysts the specific activity decreases in the order Fe > Fe/carbon > Fe/silica > Fe/alumina and the olefin to paraffin molar ratio varies from 0.72 for Fe/alumina to 4.1 for Fe/carbon. The above observations suggest that these changes in the activity and selectivity with the support used and/or the metal loading might be due to the change in metal crystallite size or dispersion due to the metal-support interaction. Catalyst preparation and pre-treatment conditions also have been found to have a great influence on the performance of the carbon supported catalysts because of their impact on the structure and stability of the supported metal [53, 54].

Vannice and co-workers [55, 56] have demonstrated that using carbon as a support could alter catalytic behaviour of metals such as iron and ruthenium. Carbon supported Fe catalysts were found to be very active and highly selective for the production of olefins compared to unsupported, unpromoted Fe/alumina and

Fe/silica. From an economic point of view, the production of short chain olefins is very attractive, as they are the most valuable bulk hydrocarbons [57].

Jung et al. [56] reported that poorly dispersed Fe/C catalysts are more active for CO hydrogenation than Fe/alumina, while well-dispersed iron on carbon black has a high and stable activity when using a H₂/CO ratio of 3 at 1 atm [55, 56, 58]. Jung et al. [59] have also reported a decrease in the specific activity with decreasing crystallite size for the Fe/carbon system.

In the past three decades, the use of different forms of carbons as heterogeneous catalyst supports has grown drastically. Graphite and diamond have received some attention, with activated carbon being the most studied catalyst support of the other carbon materials [52]. With the discovery of carbon nanotubes and their large scale synthesis, attention is now being focused on potential applications in various fields of materials research such as catalysis, superconductivity, etc. [60]. In heterogeneous catalysis especially, activated carbon has many advantages if used as a catalyst support. On the other hand, carbon nanotubes possess similar properties and in most cases surpass activated carbon [61]. Carbon nanotubes have revealed great potential as a new type of support material in ammonia synthesis, Fischer-Tropsch synthesis, crotonaldehyde hydrogenation and other reactions [61-65].

1.3. Carbon nanotubes

Carbon nanotubes - long, tiny tubes of carbon about 10,000 times thinner than a human hair - were discovered accidentally in 1991 by Iijima [66, 67]. These are large carbon macromolecules that are unique for their size, shape, and remarkable physical properties. They can be thought of as a sheet of graphite (a hexagonal lattice of carbon) rolled into a seamless cylinder. A simple nanotube has a structure similar to a fullerene where each carbon is bonded to three neighboring carbon atoms through sp^2 hybridization, but a nanotube is cylindrical, with ends often being capped with half a fullerene molecule. Their name derives from their size since nanotubes are only a few nanometers in width, with lengths in the range of several micrometers to millimeters [66, 67].

1.3.1. Carbon nanotube properties

Currently, the physical properties are still being explored and disputed because nanotubes have a very broad range of electronic, thermal, and structural properties that are function of the kinds of nanotube (defined by diameter, length, and structure) [66].

Carbon nanotubes can be classified essentially into two categories as shown in Fig 1.2, single-walled nanotubes (SWNT) and multi-walled nanotubes (MWNT) [68, 70].

SWNT's are made of a perfect graphene sheet rolled up into a cylinder and closed by two caps (semi-fullerenes). Their internal diameter can vary between 4.0 and 2.5 nm.

MWNT's contain several concentric coaxial cylinders of graphitic shells with diameters ranging between 2 and 100 nm. Recent studies have shown that the intershell spacing can range from 0.34 to 0.39 nm. In addition, the intershell spacing decreases with increasing carbon nanotube diameter, and this effect is more pronounced in small diameter nanotubes (< 15 nm) [70, 71].

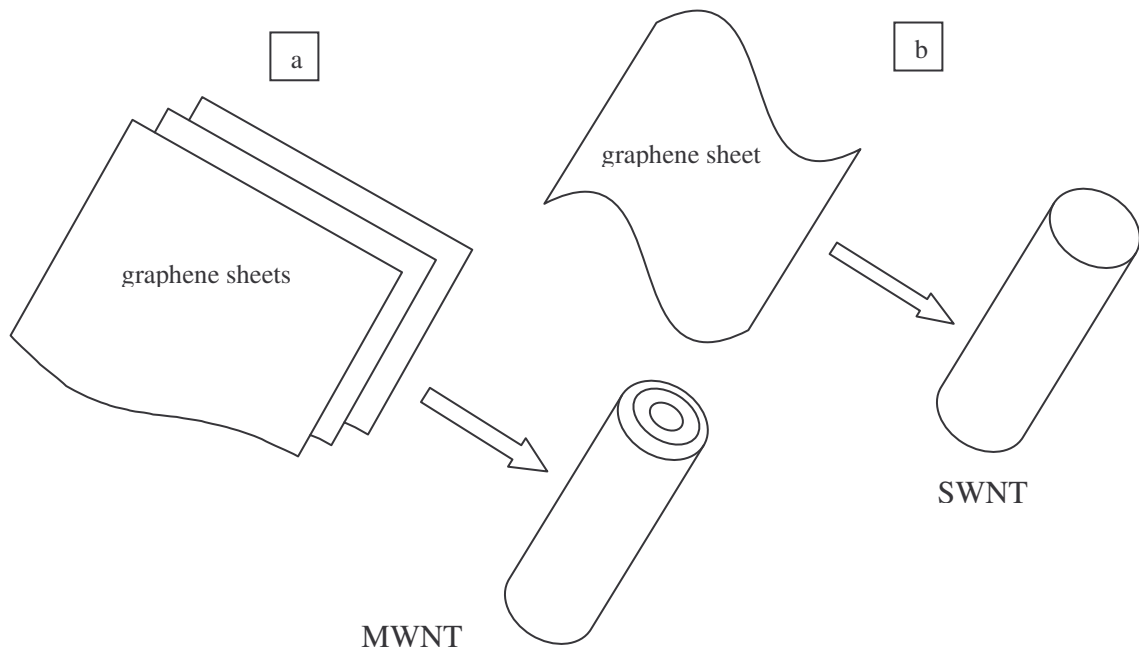


Figure 1.2: Structure of MWNT (a) and SWNT (b) [67]

Electronic properties of the carbon nanotubes are mainly governed by the diameter and the helicity which is defined by the orientation of the hexagons with respect to

the axis. In addition, the electronic properties are also influenced by the presence of defects such as pentagons, heptagons, vacancies or impurities.

SWNTs can be classified in two groups when its graphene sheet is folded along its axis: zigzag SWNTs (Fig.1.3.a) and armchair SWNTS (Fig.1.3.b). In particular, armchair SWNTs are metallic and zigzag ones are semi-conductors. The SWNTs behave like pure quantum wires (1D-system). At low temperature, the MWNTs reveal 2D-quantum transport features [60].



a. Zigzag



Armchair

Figure 1.3: SWNT zigzag (a) and SWNT armchair (b)

In theory, carbon nanotubes could be the most resistant filament obtainable because they are made exclusively of carbon atoms covalently bonded. They are also very inert, as there are very few open edges and hanging bonds in their structures which

implies that there is mainly the possibility of physical adsorption onto the graphene layers instead of chemical reaction.

It comes as no surprise that the combination of these properties makes CNT attractive and competitive catalyst supports by comparison with activated carbon [60].

1.3.2. Synthesis of carbon nanotubes

Carbon nanotubes were first identified accidentally by a Japanese scientist, Sumio Iijima in 1991 [67]. Since then it has been realized that these materials can be prepared by various techniques.

At present, there are several approaches used to producing nanotubes, such as arc discharge, laser ablation, and chemical vapor deposition (CVD). Each method has its advantages and disadvantages. The CVD method involves the catalytic decomposition of certain hydrocarbons or organics (such as acetylene, ethylene, ethanol, carbon monoxide, etc.) in the presence of various unsupported or supported metal catalysts (usually cobalt, nickel or iron) at temperatures above 600 °C [69].

The carbon arc method and the laser ablation can be classified as high temperature methods (operating temperature 2700°C) with short reaction times (μ s-ms), whereas the CVD method is a medium temperature (500 – 1100°C) method with a relatively long reaction time (minutes to hours).

In general, the CVD method produces large amounts of carbon nanotubes at low cost. Good purification facilities are required. The size of the carbon nanotubes varies with the particle size of the catalysts; however the carbon nanotubes produced are relatively poor in crystallinity in comparison with those prepared by the carbon-arc method. The carbon-arc method, on the other hand, produces thin and straight carbon nanotubes. This method appears very simple but it requires careful control of the operating conditions and its carbon nanotube productivity is low [72].

Carbon nanotubes production involves several steps: hydrocarbon decomposition, diffusion, dissolution and precipitation of the catalysts [73-75]. The hydrocarbon molecule dissociates into molecular hydrogen and carbon on the exposed surface of the metal catalyst. The carbon dissolves into the metal and diffuses through the bulk of the metal. Diffusion through the support cannot be excluded. Precipitation of the graphite on the other side of the metal particle occurs [76]. Two modes, namely base growth and tip growth have been proposed depending on the interaction between the catalyst and its support (Fig. 1.4). Strong interactions can anchor the catalyst and induce the base growth mode while weak interactions cause the tip growth mode. The tip growth mode is confirmed by the presence of the metal particles at the tips of carbon nanotubes, while the metal particles remain attached to the substrate for the base growth mode [73, 77].

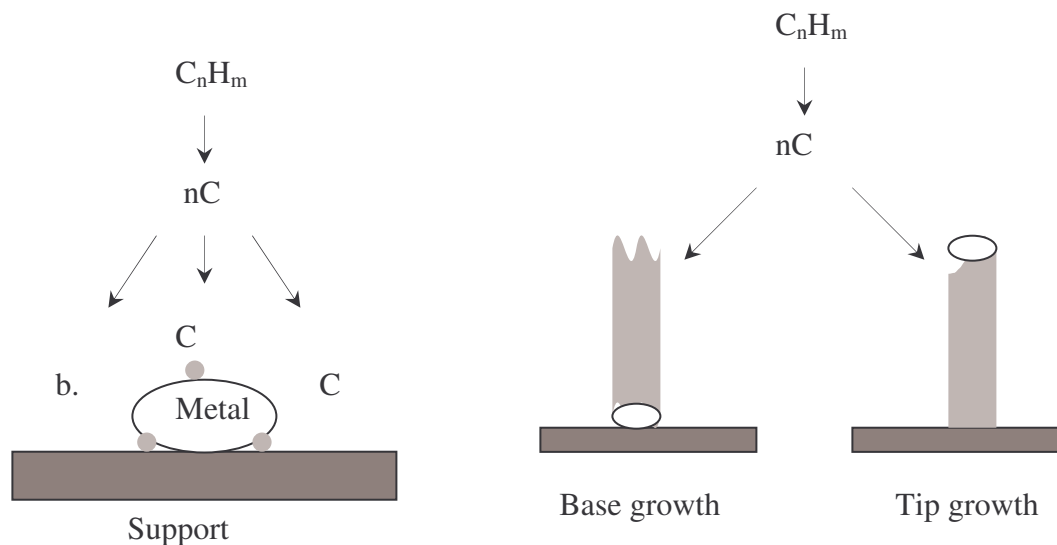


Figure 1.4: Presents a schematic of the two growth modes commonly considered for CNTs: base growth and tip growth depending on where the catalyst is located [73]

1.3.3. Carbon nanotube as support for Fischer-Tropsch synthesis catalysts

The use of carbon nanotubes as a support for the FT reaction was first reported by van Steen and Prinsloo [61] who studied the effect of the method of preparation and promoters of CNT supported iron catalysts on the FT synthesis. In this study [61], it was claimed that the activity of the Fe/CNT catalysts in the FT synthesis varied significantly with the methods of preparation of the catalyst. The catalyst prepared by incipient wetness was the more active, although its activity declined with time. They have speculated that the differences in the performance of the catalysts could be attributed to the difference in the crystallite particle size distribution, which would

result in the variation in the amount of the active phase present in the catalyst under reaction conditions. In addition, the FT product selectivity over Fe/CNT catalysts used in this study seemed to be independent of the method of preparation.

Bezemer et al. [78] also studied the potential of CNT supported catalysts in FT synthesis, but used cobalt rather than iron; different cobalt loadings on CNT were prepared by the incipient wetness impregnation method. They found that carbon nanotubes were a promising support for FT synthesis. They observed the cobalt particle size effect which is well known for FT synthesis using cobalt supported on metal oxides; at 1 bar the activity decreased with the decrease in the particle size of the metal catalysts particles. These catalysts displayed stable activity and a remarkable high selectivity for C₅₊ hydrocarbons. The C₅₊ selectivity was 86 wt%, which is high for an unpromoted catalyst.

The actual relationship between support and metal catalyst and how they interact to affect the activity or selectivity of a catalyst system is a subject of debates and speculations. It is difficult to predict the catalyst behaviour of an untreated catalyst system subjected to any particular pre-treatment [36]. Comparison between the different supported catalysts reported in the literature is difficult, since different authors have used different supports, methods of preparation, and metal loadings. However, in this thesis, an attempt will be made to relate the data from this study to other relative studies on related catalysts.

1.4. Aims of this study

In this study, we have investigated the effect of the carbon nanotubes as a support for metal catalysts such as: Fe, Co and Ru. Various characterization techniques (CO chemisorption, TPR, BET and Scanning Electron Microscopy) have been utilized to relate the performance of the catalysts to the physical and chemical properties of the catalyst and their performance in the FT synthesis been compared with that of other carbon material supports as reported in the literature.

References

- [1]. Anderson, R.B., The Fischer-Tropsch Synthesis, Academic Press, New York, 1984
- [2]. BASF: German Pat. 293, 787 (1913)
- [3]. Frohning, C.D., Fischer-Tropsh-Synthese, Chemierohstoffe aus Khole (Falbe J., ed.) Stuggart: Thieme 1977
- [4]. Fischer, F., Tropsch, H., Brennst.-Chem., 4 (1923) 276
- [5]. Dry, M.E., Catal. Today, 71 (2002) 227
- [6]. Choi, G.N., Kramer, S.J., Tam, S.T., Fox, J.M., Design/economics of natural gas based Fischer-Tropsch plant, in Spring National Meeting, American Institute of Chemical Engineers, Houston, 1996
- [7]. Iglesia, E., Appl. Catal. A: Gen. 161 (1997) 59
- [8]. Gradassi, M.J., Stud. Surf. Sci. Catal., 119 (1998) 35
- [9]. Storch, H.H., Golumbic, N., Anderson, R.B., 1951. The Fischer-Tropsch and related synthesis. John Wiley & Sons; New York p. 610
- [10]. Stenger, H.G., Askonas, C.F., Ind. Eng. Chem. Fundam. 25 (1986) 410
- [11]. Bartholomew, C. H., Stud. Surf. Sci. Catal. 64 (1991) 158
- [12]. Dictor, R.A., Bell, A.T. J., Catal., 97 (1986) 121
- [13]. Komaya, T., Bell, A.T. J., Catal., 146 (1994) 237
- [14]. Madon, R.J., Reyes, S.C., Iglesia, E. J., Phys. Chem. 95 (1991) 7795
- [15]. Esponzoza, R.L., Steynberg, A.P., Jager, B., Vosloo, A.C., Appl. Catal. A: Gen. 186 (1999) 13

- [16]. Jager, B., Stud. Surf. Sci. Catal., 119 (1998) 26
- [17]. Sie, S.T., Rev. Chem. Eng. 14 (1998) 109
- [18]. Saxena, S.C., Rosen, M., Smith, D.N., Ruether, J.A., Chem. Eng. Comm., 40 (1986) 97
- [19]. www.dissertations.ub.rug.nl/FILES/faculties/science/1999/g.p.van.der.laan/c1.pdf
- [20]. Dry, M.E., Appl. Catal., A: Gen. 138 (1996) 319
- [21]. Mokoena, E.M., Synthesis and Use of Silica Materials as Supports for the Fischer-Tropsch Reaction, PhD Thesis, University of the Witwatersrand, Johannesburg, 2005
- [22]. Marura, A.E., Influence of the Preparation Techniques on the Fischer-Tropsch Performance of Supported Cobalt Catalysts, PhD Thesis, University of Cape Town, 2002
- [23]. Davis, B., Catal. Today, 84 (2003) 83
- [24]. Dry, M.E., Mol. J.Catal., 17 (1982), 133
- [25]. Rao, V.U.S., Stiegel, G.J., Bose, A.C., Cinquegrane, G.J., Am. Chem. Soc. Div. Fuel Chem. 37 (1982) 184
- [26]. Storch, H.H., Golumbic, N., Anderson, R.B., 233 (1951) 283
- [27]. Dry, M.E., The Sasol Fischer-Tropsch Process, Vol 2, Chap. 5 (1983) Academic Press Inc
- [28]. Adesina, A.A., Appl. Catal. A: Gen. 138 (1995) 17
- [29]. Dry, M.E., Catalysis: Science and Technology, Anderson, J.R., Boudart, M. eds., Vol. 1, Springer-Verlag Berlin Heidelberg, New York, 1981, p. 195
- [30]. Vannice, M.A., J. Catal. 37 (1975) 449

- [31]. Everson, R.C., Mulder, H., Keyser, M., ChemSA, oct, (1986) 243
- [32]. Everson, R.C., Woodburn, E.T., Kirk, A.R.M., J. Catal. 53 (1978) 186
- [33]. Everson, R.C., Mulder, H., J. Catal. 143 (1993) 166
- [34]. Habazaki, H., Yamasaki, M., Zhang, B., Kawashima, A., Khono, S., Takia, T., Hashimoto, K., Appl. Catal. 172 (1998) 131
- [35]. Louis, C., Cheng, Z., Che, M., J. Phys. Chem. 97 (1993) 5703
- [36]. Price, J., G. An Investigation into Novel Bimetallic Catalysts for Use in the Fischer-Tropsch Reaction, PhD Thesis, University of the Witwatersrand, 1994
- [37]. Crowell, J.H., Benson, H.E., Field, J.H., Storch, H.H., Ind. Eng. Chem. 42 (1950) 2376
- [38]. Reuel, R.C., Bartholomew, C.H., J. Catal., 85 (1999) 189
- [39]. Satterfield, C.N., Mass Transfer in Heterogeneous Catalysis, M.I.T Press, Cambridge, Massachusetts, and London, England, 1970
- [40]. Rodriguez-Reinoso, F., Carbon, 36(3) (1998) 159
- [41]. Radovic L.R. and Rodriguez-Reinoso, F., Chem. Phys. Carbon, 25 (1997) 243
- [42]. Rodriguez-Reinoso, F., Carbon, 36 (1998) 159
- [43]. Moreno-Castilla, C., Mahajan, O. P., Walker Jr., P. L., Jung, H-J., and Vannice, M. A., Carbon, 18 (1980) 271
- [44]. http://www.mpg.de/pdf/europeanWhiteBook/wb_materials_055_057.pdf
- [45]. Bundy, F.P., Solid State Physics under Pressure: Recent Advance with Anvil Devices, S. Minomura, ed. Reidel, Dordrecht, 1985
- [46]. Ebbesen, T.W., Carbon nanotubes, Preparation and Properties, Boca Raton, New York, London, Tokyo, CRC Press, 1997

- [47]. Saito, R., Dresselhaus, G., Dresselhaus, M.S., Physical Properties of Carbon Nanotubes, Imperial College Press, 1998
- [48]. Radivic, C L., Sudhakar, R., Carbon as a Support, H. Marsh, Heintz, E.A., Rodriguez-Reinoso, F. eds., Introduction to Carbon Technologies, University of Alicante, Alicante, Spain, 1997
- [49]. Stiles, A. B., Catalyst Supports and Supported Catalysts, Butterworths, Boston, 1987
- [50]. Reuel, R.C., Bartholomew, C.H., J. Catal., 85 (1984) 78
- [51]. Fu, L., Bartholomew, C.H., J. Catal, 92 (1985) 367
- [52]. Jones, V.K., Neubauer, L.R., Bartholomew, C.H., J. Phys. Chem., 90 (1986) 4832
- [53]. Chen, A.A., Vannice, M.A., Phillips, J., J. Phys. Chem. 91 (1987) 6257
- [54]. Peters, U., Greb, H., Jockers, R., Klein, J., Preparation of Catalysts IV: Scientific Bases for Preparation of Heterogeneous Catalysts; Delmon et al., Eds.; Elsevier: Amsterdam, 1987; p 493
- [55]. Vannice, M.A., Walker, P.L., Jung, H.-J., Moreno-Castilla, C., Mahajan, O.P., Proc. Int. Cong. Catal. 7th 1980, paper A31
- [56]. Jung, H.-J., Walker, P.L. Jr., Vannice, M.A., J. Catal. 75 (1982) 416
- [57]. Sommon, A.P.B., Stoop, F., van der Wiele, K., Appl. Catal. 14 (1985) 277
- [58]. Dandekar, A., Baker, R.T.K., Vannice, M.A., J. Catal., 183, 131 (1999)
- [59]. Jung, H.-J., Mulay, M.L., Vannice, M.A., Stanfield, R.M., Delgass, W.N., J. Catal. 76 (1982) 208

- [60]. Planeix, J.M., Coustel, N., Coq, B., Brotons, V., Kumbhar, P.S., Dutartre, R., Geneste, P., Bernier, P., Ajayan, P.M. *J. Am. Chem. Soc.* 116 (1996) 7935
- [61]. van Steen, E., Prinsloo, F.F. *Catal. Today*, 71 (2002) 327
- [62]. Li, K. Yao, C., Liang, J. *Appl. Catal. A: Gen.* 261 (2004) 221
- [63]. Luo, J.Z., Gao, L.Z., Leung, Y.L., Au, C.T. *Catal. Lett.* 66 (2000) 91
- [64]. Cai, Y., Lin, J.D., *Chin. Chem. Lett.* 11 (2000) 373
- [65]. Salman, F., Park, C., Baker, R.T.K. *Catal. Today* 53 (1999) 385
- [66]. <http://www.pa.msu.edu/cmp/csc/ntproperties/>
- [67]. Iijima, S. *Nature* 354 (1991) 56
- [68]. <http://www.nanotech-now.com/nanotube-buckyball-sites.htm>
- [69]. Merkoci, A., Pumera, M., Llopis, X., Pérez, B., Del Valle, M., Alegret, S. *Trends in Anal. Chem.*, 24 (2005) 826
- [70]. Serp, P., Corrias, M., Kalck, P. *Appl. Catal. A: Gen.* 253 (2003) 337
- [71]. Fischer, J.E., Johnson, A.T. *Curr. Opin. Solid. State Matter. Sci.* 4 (1999) 28
- [72]. Chen, P., Zhang, H.-B., Lin, G.-D., Hong, Q., Tsai, K.R. *Carbon*, 35 (1997) 1495
- [73]. Wung, Y.Y. *Synthesis and Field Emission Properties of Carbon Nanotubes*, PhD Thesis, North Carolina State University, 2004
- [74]. Bower, C., Zhou, O., Zhu, W., Werder, D. J. S. Jin, *Appl. Phys. Lett.* 77 (2000) 2767
- [75]. Li, D., Dai, L., Huang, S., Mau, A.W.H., Wang, Z.L. *Chem. Phys. Lett.* 316 (2000) 349

[76]. Baker, R.T.K., Barber, M.A., Harris, P.S., Feates, F.S., Waite, R.J. *J. Catal.* 26

(1972) 51

[77]. Baker, R.T.K. *Carbon* 27 (1989) 315

[78]. Bezemer, G.L., van Laak, A., van Dillen, A.J., Jong, K.P. *Stud. Surf. Sci. Catal.*,

147 (2004) 259

CHAPTER 2: EXPERIMENTAL

2.1. Introduction

Several methods have been used to synthesize the carbon nanotubes (CNTs). The chemical vapour deposition (CVD) procedure was the method used in this study. CNTs synthesized by CVD method usually are mixed with the support and even the CNTs contain other types of carbon containing species. The type and amount of impurities depend on the method of preparation. A range of techniques has been used for the purification of the CNTs i.e. removal of the support and other carbon types. The simplest procedure is by use of acids. However, surface oxidation of the carbon nanotubes occurs during nitric acid treatment and this introduces surface oxygen functionalities (e.g. carboxylic and acid groups) on the outer and possibly inner walls of the CNTs [1, 2, 3]. This method can also destroy the CNTs.

The method of preparation, support employed, addition of additives, the sequence in which precursors are mixed, thermal pre-treatment, etc. play a decisive role in the behaviour of catalysts used in FTS [4, 5]. A number of Characterization techniques have been developed to correlate these parameters with the behaviour of the catalysts in the Fischer-Tropsch (FT) synthesis. Information about surface structure and

composition of the catalysts at the atomic scale can be obtained using these Characterization techniques [6].

The FT synthesis results in the synthesis of a wide range of products ranging from methane to waxes. The products can not be analysed in one attempt. A variety of approaches using different GC analysis configurations have been reported in the literature [7, 8, 9].

The focus in this chapter will be on the experimental methods used in this study, and includes the synthesis and characterization of the carbon nanotubes and carbon nanotube supported FT catalysts, FT catalyst testing, and reactor studies.

2.1. Synthesis of the carbon nanotubes

Carbon nanotubes can be grown by many techniques (e.g., arc discharge, laser ablation and catalytic methods) [10]. The chemical vapour decomposition (CDV) of carbon molecular precursors at high temperatures, assisted by the catalytic activity of small transition metal particles, is considered as the method of choice for the mass production of carbon nanotubes [11, 12]. This was the method used in this study.

The preparation of the catalyst for the synthesis of the carbon nanotubes was achieved by using a number of gases and chemicals as illustrated below:

2.1.1. Gases

All the gases used in this study were supplied by AFROX (African Oxygen) Ltd. All the gas cylinders were accompanied by a certificate that indicated the purity of the components available in a particular gas mixture. All the pure gases used in this study were Ultra High Purity (UHP) grade gases (.99.997% purity)

2.1.2. Metal and catalyst support

$\text{Fe}(\text{NO}_3)_3 \cdot 9\text{H}_2\text{O}$ was used as source of iron for the preparation of the CNTs. The Fe salt was loaded onto a calcium carbonate (CaCO_3) support. Both chemicals were supplied by MERCK.

2.1.3. Catalyst preparation

The catalyst for the synthesis of the carbon nanotubes was prepared by the incipient wetness impregnation method [13].

In this preparation, a calculated amount of metal salt $\text{Fe}(\text{NO}_3)_3 \cdot 9\text{H}_2\text{O}$ (7.21 g) was dissolved in 30 ml distilled water and subsequently added drop-wise to 10 g of

CaCO₃ support contained in a beaker. The total concentration of catalyst was about 10 wt%. The resulting mixture was placed under continuous stirring on a hot plate kept at room temperature. The as-prepared sample was dried at 120°C overnight and then collected as dry powder. The latter was then calcined in a furnace at 400°C for 16 hours in the presence of air.

2.1.4. Preparation of the carbon nanotubes

Once the catalyst has been calcined, it was milled to an adequate size. The size of the catalyst particles produced is important and affects on the nanotubes characteristics. Acetylene was used as the carbon source to make the CNTs.

The decomposition of acetylene was carried out in a tubular quartz reactor (51 cm x 1.9 cm i.d) [14], which was placed horizontally in a furnace (Fig. 2.1). The furnace was under electronic control and thus temperature ramping of 10°C min⁻¹, was readily achieved. The front end of the tube was connected to a glass manifold that allowed the free flow of gases (hydrogen or acetylene) at atmospheric pressure to be passed through the tube. A quartz glass wool plug was placed in the rear end of the quartz tube, which was situated outside the oven. All reactions were carried out at atmospheric pressure in the absence of oxygen.

The catalyst (100 mg) was loaded into a quartz boat (120 mm x 15 mm) at room temperature and the boat was placed in the centre of the quartz tube, which was

situated in the heating region of the furnace. Before deposition could take place, the catalytic surface was first activated. Hydrogen gas was used to reduce the catalyst for 1 hour in situ (700°C , 100 ml min^{-1}). The heating and cooling were automatically controlled and a temperature ramping rate of $10^{\circ}\text{C min}^{-1}$ was used. The H_2 gas was then replaced with acetylene and the gas was then passed through the reactor for 3 hours (700°C , 100 ml min^{-1}). At this temperature the carbon source was converted into an activated carbon species which diffused onto the surface of the reduced catalyst. Graphitisation of the walls of the nanotubes then occurred. The reactor was then cooled to room temperature in a H_2 atmosphere. The boat was removed from the reactor and weighed to establish the amount of carbon nanotube material that had been formed. This reaction was repeated and the products collected were combined and mixed.

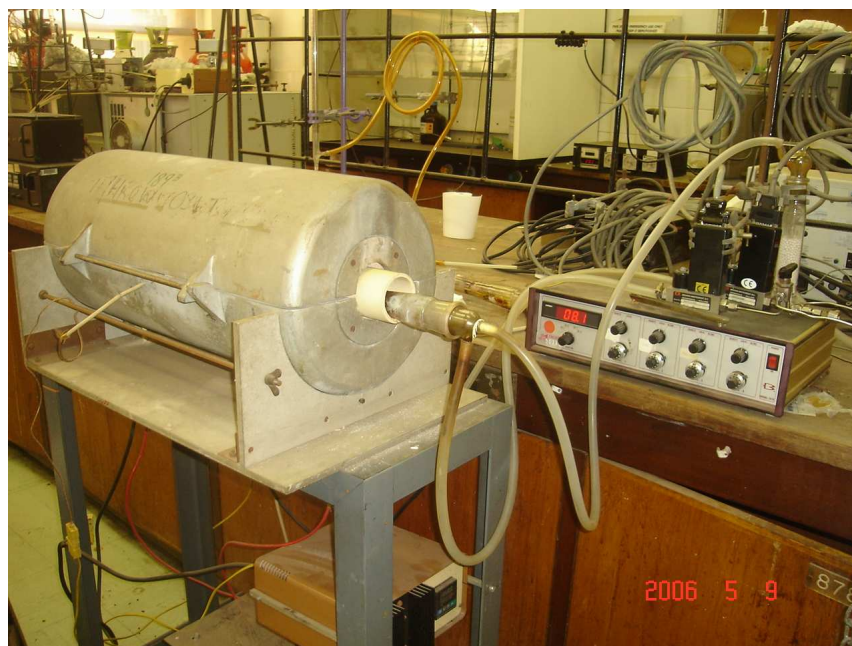


Figure 2.1: The furnace used for the synthesis of CNTs by the CVD method.

2.1.5. Purification of the carbon nanotubes

The catalyst precursor was separated from the carbon nanotubes by dissolving the crude product in nitric acid (30% HNO₃, 2 h, at room temperature) [13]. The acid dissolved away the Fe catalyst, the CaO and some of the amorphous insoluble carbon. The carbon nanotubes were then recovered by filtration; thoroughly washed with distilled water and finally dried at 120°C overnight.

2.2. Synthesis of catalysts supported on carbon nanotubes

The catalysts were prepared according to the incipient wetness impregnation and deposition precipitation methods [15].

The preparation of the catalyst for the synthesis of the carbon nanotubes was achieved by using a number of chemicals and nitrogen gas as described in detail below:

2.2.1. Gas

The nitrogen cylinder used in the preparation of these catalysts was supplied by AFROX (African Oxygen) Ltd. The cylinder was accompanied by a certificate the indicated the purity of the gas, which was ultra high purity (UHP) grade (>99.997%).

2.2.2. Metal, additives and catalyst support

Three metals, iron, cobalt and ruthenium, were loaded onto the carbon nanotube support as active metals. Copper and potassium were used as additives or promoters for iron and ruthenium based catalysts. Iron and cobalt were loaded as $\text{Fe}(\text{NO}_3)_3 \cdot 9\text{H}_2\text{O}$ and $\text{Co}(\text{NO}_3)_2 \cdot 6\text{H}_2\text{O}$ respectively. Iron nitrate was supplied by MERCK and cobalt nitrate was supplied by SAARCHEM. The ruthenium was loaded as $\text{C}_8\text{H}_{12}\text{O}_8\text{Ru}_2$, which was prepared in our laboratory according to the method described in the literature [16]. This compound contains no halide ions and is soluble in water.

Copper and potassium were also loaded as promoters to the iron and ruthenium based catalysts. $\text{Cu}(\text{NO}_3)_2 \cdot 3\text{H}_2\text{O}$ and KNO_3 were used as Cu and K sources and were added successively.

The incipient wetness technique required the determination of the pore volume of the support prior to the preparation of the catalysts.

The total pore volume of the carbon nanotube support was determined by adding distilled water drop wise from a burette to a certain known amount of the support. This is done until the addition of the last drop result in the formation of a thick slurry, indicating that the entire pore volume has been filled. The pore volume of the nanotubes is then read from the burette [15].

It is known that iron nitrate, cobalt nitrate and ruthenium acetate are soluble in water. Therefore, for the impregnation method, one salt (for the monometallic catalyst) or two salts (for the bimetallic catalyst) of the three salts mentioned earlier were dissolved in water prior to the impregnation step.

The support used, for the preparation of the FT catalysts used in this study, was the carbon nanotube material prepared and purified as described earlier on.

2.2.3. Catalysts preparation

2.2.3.1. Deposition Precipitation Method

The carbon nanotube supported catalysts were prepared by the deposition precipitation (DPU) method using urea [15].

In the DPU method, $\text{Fe}(\text{NO}_3)_3 \cdot 9\text{H}_2\text{O}$ (7.21 g, 10%) and urea (1.61 g; 1.5 moles urea per mole of iron) were dissolved in de-ionized water (18 ml) and added to 10 g of the carbon nanotube support.

After allowing sufficient time (at least two hours) for the hydrolysis of the urea (Eqn 2.1), the sample was dried by evaporating the water under vacuum at 90°C for 40

minutes. The urea was added to facilitate the uniform formation of metal hydroxides onto the surface of the carbon nanotube support [17].



Three other catalysts (DPUCu, DPUK and DPUKCu) were prepared by promoting the Fe/CNT catalyst with Cu, K or Cu/K. Thus KNO_3 (0.052 g; 0.2% K) and/or $\text{Cu}(\text{NO}_3)_2 \cdot 3\text{H}_2\text{O}$ (0.228 g ; 0.6% Cu) were added to an iron solution prepared above and the mixture added drop-wise to 10 g of the carbon nanotube support.

All the samples were further dried in an oven (120°C, overnight) and then heated in nitrogen at 220°C for 2.5 hours to decompose the iron nitrate.

2.2.3.2. Incipient Wetness Impregnation Method

Fe catalyst: $\text{Fe}(\text{NO}_3)_3 \cdot 9\text{H}_2\text{O}$ (7.21 g; 10% Fe) was dissolved in de-ionized water (18 ml) and added to 10 g of carbon nanotubes support. The resulting slurry was dried in a rotary evaporator at 90°C for 2 hours. The sample was further dried in an oven (120°C, overnight) and then heated in nitrogen at 220°C for 2.5 hours.

Co catalyst: $\text{Co}(\text{NO}_3)_2 \cdot 6\text{H}_2\text{O}$ (4.938 g) were successively dissolved in de-ionized water (18ml) and added to 10 g of the carbon nanotube support. The total

concentration of the catalyst was 10%Co on the carbon nanotube support. The resulting mixture was dried at 120°C overnight and then collected as dry powder.

Four other cobalt based catalysts were similarly prepared by incipient wetness impregnation and calcined at different temperatures 220, 250, 300 and 350°C (Co220, Co250, Co300 and Co350).

Prior calcination, all the samples thus prepared were dried overnight at 120°C in an oven.

Fe/Co and Fe/Ru bimetallic catalysts: Three catalysts with a Fe/Ru molar ratio of 7.23 were also prepared. A 10%, 5% and 2.5% iron catalyst supported on CNT and promoted by 0.25%, 0.125% and 0.0625%Ru successively were prepared by the incipient wetness (IW) impregnation method. For the preparation of these catalysts, the metal loading was successively divided by 2 and then by 4. $\text{Fe}(\text{NO}_3)_3 \cdot 9\text{H}_2\text{O}$ (7.21g, 3.605g and 1.8025g) and $\text{C}_8\text{H}_{12}\text{O}_8\text{Ru}_2$ (0.07g, 0.35g and 0.175g) were successively dissolved in de-ionized water (18 ml) and added to 10 g of the carbon nanotube support. All the samples prepared were further dried in an oven (120°C, overnight) and then heated in nitrogen at 220°C for 2.5 hours.

Fe/Ru/K and Fe/Ru/Cu: Three iron-ruthenium based catalysts (FeRuCu, FeRuK and FeRuCuK) were similarly prepared by promoting the 10% Fe/ 0.25%Ru/ CNT catalyst with Cu, K or Cu/K. Thus KNO_3 (0.052g; 0.2% K) and/or $\text{Cu}(\text{NO}_3)_2 \cdot 3\text{H}_2\text{O}$

(0.228g; 0.6% Cu) were added to an iron-ruthenium solution prepared above and the mixture added drop-wise to 10 g of the carbon nanotube support. The resulting mixture was dried at 120°C overnight and then collected as dry powder. All the samples prepared were further dried in an oven (120°C, overnight) and then heated in nitrogen at 220°C for 2.5 hours.

2.3. Reactor studies and Characterizations

2.3.1. Characterization

2.3.1.1. ICP-OES Analysis

Inductively Coupled Plasma Optical Emission Spectroscopy (ICP-OES) is a major technique used for obtaining elemental analysis of a material. In this method, the determination of trace concentrations of elements in a sample is achieved using atomic emission spectroscopy. The atomic spectroscopy method is based on the measurement of the amount of electromagnetic radiation absorbed or emitted by an analyte atom to determine the concentration of the sample [18].

The solid sample to be analyzed is first dissolved and then diluted with water before it is fed into the plasma. Atoms in the plasma emit light (photons) with characteristic

wavelength. The light is recorded as a signal by one or many optical spectrometers. The signal recorded provides a quantitative analysis of the original sample. The type of element determined is based on the position of the photon rays, and the content of each element is determined based on the X-ray's intensity [19].

2.3.1.2. Thermogravimetric analysis

Thermogravimetric analysis was performed with a Perkin Elmer Pyris 1 TGA thermogravimetric analyzer (Fig. 2.2) using nitrogen or air as purge gas and a heating rate of 5°C per minute. Prior to the analysis the sample is weighed on a balance and then placed in a crucible. The crucible is suspended on the balance of the TGA apparatus before the furnace is lifted up to cover the balance. Then a temperature programme allowed the temperature to be ramped linearly from room temperature to 1000°C under a flow of nitrogen or air. The temperature of the sample was monitored by a PC and the loss of the weight of the sample was expressed on a percentage basis.



Figure 2.2: Perkin Elmer Pyris 1, thermo gravimetric analyzer

2.3.1.3. Temperature programmed reduction

Temperature programmed reduction (TPR) is a commonly used method in catalysis and is used to assess the reducibility of a catalyst, as well as to analyse catalyst support interactions [20]. The home-build apparatus used (Fig. 2.3) was the same as that used by Mokoena [21] and Duvenhage [22].

The catalyst sample to be analysed is first weighed before being loaded into a U-shaped quartz tube. Typical mass values required for this procedure range between 10 mg and 50 mg. A glass wool is inserted into the U-tube before the sample is inserted. This is to prevent any of the catalyst material being carried into the outlet which leads

to the thermally coupled detector (TCD). The ends of the U-tube are attached to the gas-inlet and outlet points of the apparatus.

Initially, the catalyst was heated in a nitrogen atmosphere at 150°C for half an hour. This was done to remove moisture from the catalyst sample. Then a temperature programme allowed the temperature ramping linearly from room temperature to 800°C under a flow of 5% H₂ balanced in argon. The temperature of the sample was monitored by a thermocouple situated in the catalyst bed. Hydrogen consumption was monitored by a PC using thermal conductivity detectors.



Figure 2.3: Experimental set-up for TPR measurements

2.3.1.4. Physisorption (BET surface area)

A gas sorption measurement (Physisorption) is a non-destructive method used to analyze porous materials. The method is used to determine the specific surface area, pore volume and pore size distribution of a sample.

The determination of surface area is considered to be an important requirement in catalyst characterization, although the catalytic activity may only be indirectly related to the total surface area [20]. In addition, it is usually necessary to access the pore volume structure since it may control the transport of the reactants and products of a catalytic reaction, in this case the Fischer-Tropsch reaction [21].

This measurement is done via the isothermal adsorption of N₂ at the temperature of liquid N₂. The surface area is calculated using the equation developed by Brunauer, Emmett and Teller, the BET equation. The BET equation reduces to the Langmuir equation in the area of low relative pressures and describes adsorption relatively in the area of relative pressures of 0.05 – 0.35. The specific surface area is obtained from the equation:

$$p/V(p_0 - p) = 1/V_m c + [(c - 1)/V_m c][p/p_0] \quad (2.2)$$

where, V is the volume of gas adsorbed at relative pressure p/p₀, V_m is the volume of gas required for monolayer coverage of the catalytic surface and c is a constant.

Thus, a plot of $p/V(p_0 - p)$ versus p/p_0 allows for the determination of c and V_m . The total surface area can be determined if the cross-sectional area of the adsorbed species is known.

The specific adsorption pore volumes were calculated by the Barrett-Joyner-Halenda (BJH) method [23] that is assumed to cover the cumulative adsorption pore volume of pores in the range 1.7 to 300 nm in diameter.

The analysis of the samples was performed on a Tristar 3000, Micromeritics instrument [24]. The TriStar 3000 is an automated gas adsorption analyzer which contains three ports, allowing the analysis of up to three samples simultaneously. It consists of the TriStar analyzer and a Flowprep 060 degasser [25] (fig. 2.4) for preparing samples a vacuum pump, and a control module for entering analysis and report options.

The FlowPrep 060 Degasser prepares samples for the adsorption analysis. It uses flowing gas passed over a heated sample to remove moisture and other contaminants. The degasser has six heating stations for degassing samples and six cooling stations. The desired temperature is set on the temperature controller pad located at the front of the instrument. Gas flow control valves are accessible and provide a constant indication of the valve state (fig. 2.4) [25].



Figure 2.4: The TriStar analyzer and the Flowprep 060 degasser

2.3.1.5. Chemisorption Analysis

Chemisorption measurements were performed on an ASAP 2010C, Micromeritics instrument. The sample was first heated under a flow of nitrogen at a heating rate of 1°C per minute until 70°C and then at a heating rate of $0.5^{\circ}\text{C min}^{-1}$ to the final reduction temperature (350°C).

2.3.1.6. Transmission Electron Microscopy

Transmission Electron Microscopy (TEM) was developed in the 1930's by Knoll and Ruska. It works on the same principle as a light microscope except electrons are used

instead of light to observe the finer details of a specimen. This results in much higher resolving power (up to 10 000 times greater than a light microscope).

The transmission electron microscope (Joel JEM 100S) and a High Resolution Transmission Electron Microscope (Phillips CM200) were used to characterize the catalyst samples. This apparatus consists of a 2 metre metal column, with a tungsten filament (the cathode) at the top. This filament is then heated and a high voltage is applied between the cathode and the anode. This creates the electron beam. The beam is focussed by electro-magnets, located along the column onto the sample. As the beam passes through the specimen, some electrons are scattered whilst the remainder are focused by the objective lens onto photographic film to form an image.

Preparation of the specimen is important: the sample must be very thin (due to the penetrating power of the electron beam) and must be exposed to a high vacuum (10^{-8} Torr). The contrast (the sharpness of the image) is dependant on the atomic number since the higher the atomic number, the more electrons are scattered and the finer the contrast [26, 27]

2.3.1.7. Scanning Electron Microscopy

A Scanning Electron Microscope (Joel JSM 840) was used to study the morphology and particle size of the catalysts.

Scanning Electron Microscopy (SEM) differs from Transmission Electron Microscopy in the manner in which the electron beam strikes the surface. The electron beam strikes the surface at an angle, causing the emission of secondary electrons from the surface atoms. These electrons strike a detector which is also placed at an angle to the surface. The signal is enhanced by a photomultiplier and this is followed by the generation of an image. This form of microscopy yields information about the surface structure of a sample [26, 27].

2.3.2. FT reactor system

2.3.2.1. Gases

All the gases that were used were supplied by AFROX (African Oxygen) Ltd. All the gas cylinders were accompanied by a certificate that indicated the purity of the components available in a particular gas mixture. The gases used for the catalyst characterization and catalyst reduction prior to the FT synthesis were Ultra High Purity (UHP) grade gases (99.997% purity). Gas cylinders containing H₂/CO/Ar mixtures (0.60/0.30/0.1 vol. Purity: 99.99) were used to supply the reactant gas stream to the catalyst. Ar was used as an internal standard in order to ensure accurate mass balances. UHP hydrogen gas was used as carrier gas for the gas chromatograph (G.C).

2.3.2.2. Catalyst evaluation

The plug flow reactor (PFR) system is shown in Figure 2.5, and is similar to that used by Mokoena [21] and described by Snel [28]. In the reactor, there are three zones, the pre-heater zone where the gas is heated through a bed of 2mm stainless steel balls, the catalyst chamber where the reaction is taking place in the catalyst bed and the reactor bottom, the region below the catalyst bed (fig. 4).

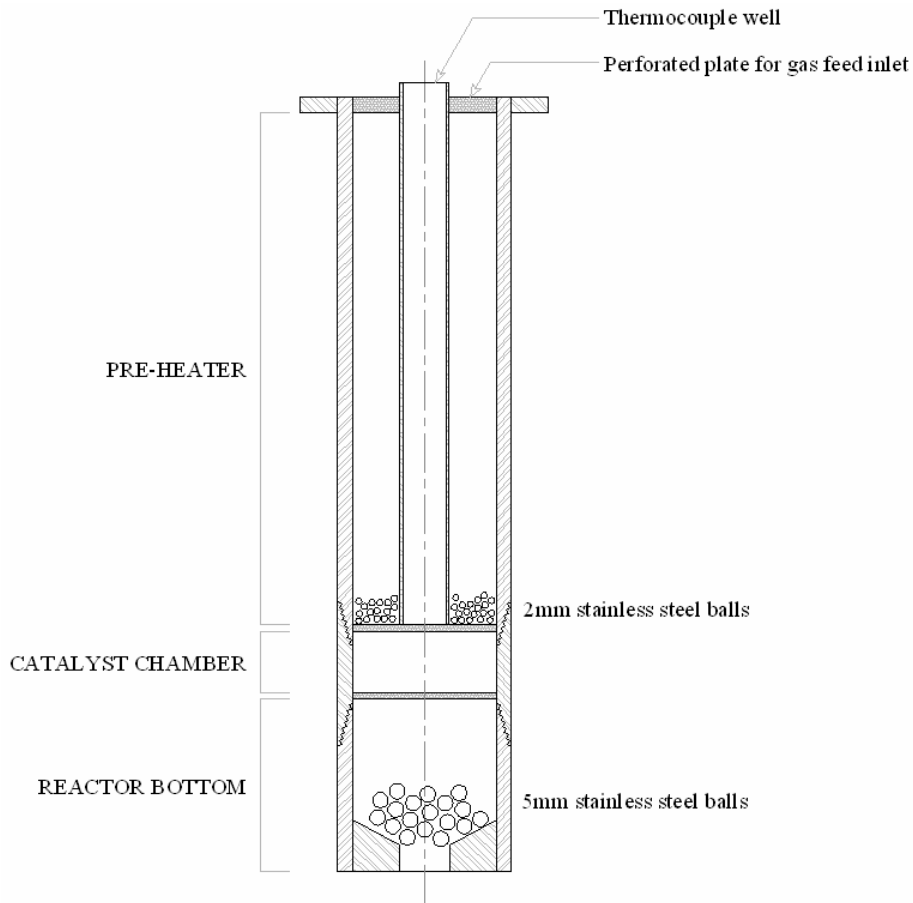


Figure 2.5: Schematic representation of the plug flow reactor

Catalyst (0.5 g) was added to the reactor and reduced in situ at 350°C for 24 hours under a stream of H₂ (2 bar pressure, 20 ml min⁻¹). After reduction, the temperature was decreased to 275°C, synthesis gas was introduced and the pressure was increased gradually to 8 bar.

Up to three plug flow reactors were run in parallel (fig. 2.6) with supply gases being split in a manifold that directed the gases to each reactor. In addition, a bypass line was used in the system to allow the analysis of the feed or the calibration gas before the beginning of the reaction.



Figure 2.6: Three plug flow reactor running in parallel

All gas lines after the reactor were kept at 150°C as shown in Figure 5 and a hot trap placed immediately after the reactor was held at this temperature in order to collect

wax. A second trap kept at ambient temperature was used to collect the oil and water mixture. The flow was controlled using a metering valve and measured by a bubble meter. A three way valve was placed in the line after the metering valve to direct the gaseous product from the reactor either to the G.C. for analysis or vented to atmosphere. These valves were connected to the timers that automated the sampling of the gaseous sample. Each sample was analyzed individually and the system automatically cycled between the reactors.

A series of valves were used to feed hydrogen gas or syngas to the reactor system (fig. 2.7). The pressure of the system was controlled using the feed regulators placed on the gas cylinders and the temperature of the system was also electronically controlled as shown in Figure 6.

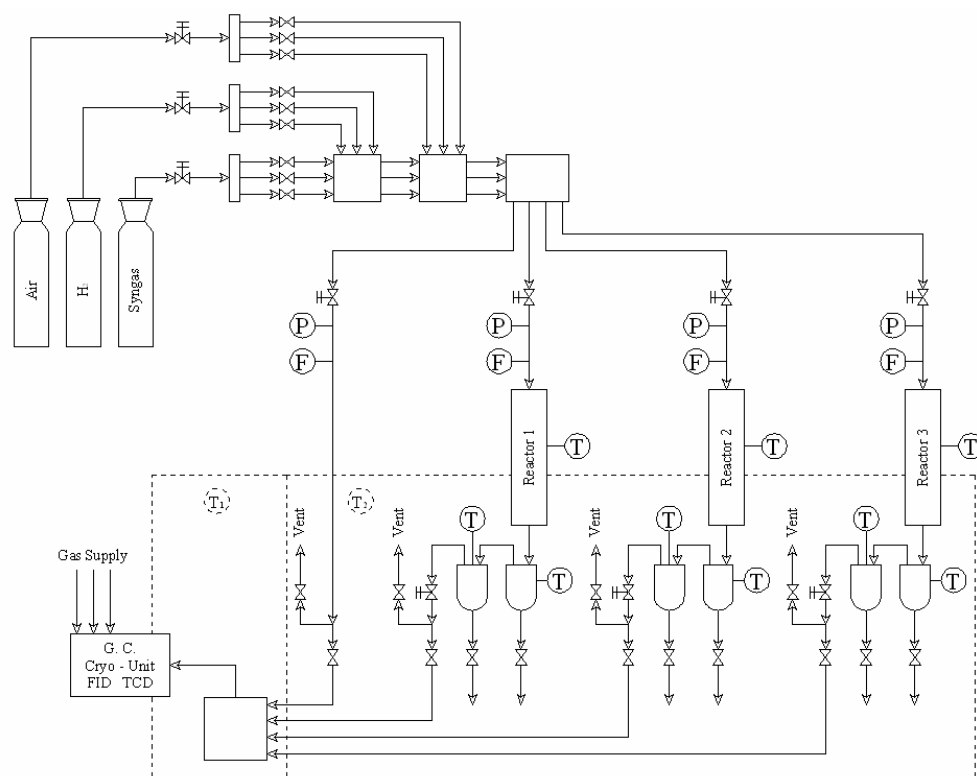


Figure 2.7: Schematic representation of the reactor system

All the lines used in the system were 1/4" or 1/8" stainless steel tubing and the fittings used were Swagekock stainless steel fittings. The on/off valves were SS Valco valves with viton seals and the needle valves were Whitey valves. The reactor system is shown in Figure 2.8.



Figure 2.8: Reactor system (Reactor, two GC and temperature controllers)

2.3.2.4. Product analysis

The analysis of the product spectrum was divided into two parts. The gas product stream was analyzed online using two gas chromatographs. A thermal conductivity detector (TCD), equipped with a Carbosieve S-II (1.50 m x 1/8 inch, stainless) packed column, was used to analyze Ar, CO and CO₂. And a flame ionization detector (FID), equipped with a Porapak Q packed column, was used for the analysis of hydrocarbons. Prior the gas product analyses, the two online gas chromatographs (GC) are calibrated using a gas mixture with a known concentration. Typical traces of a calibration analysis and hydrocarbon gas analysis are shown in Figure 2.9 and Figure 2.10.

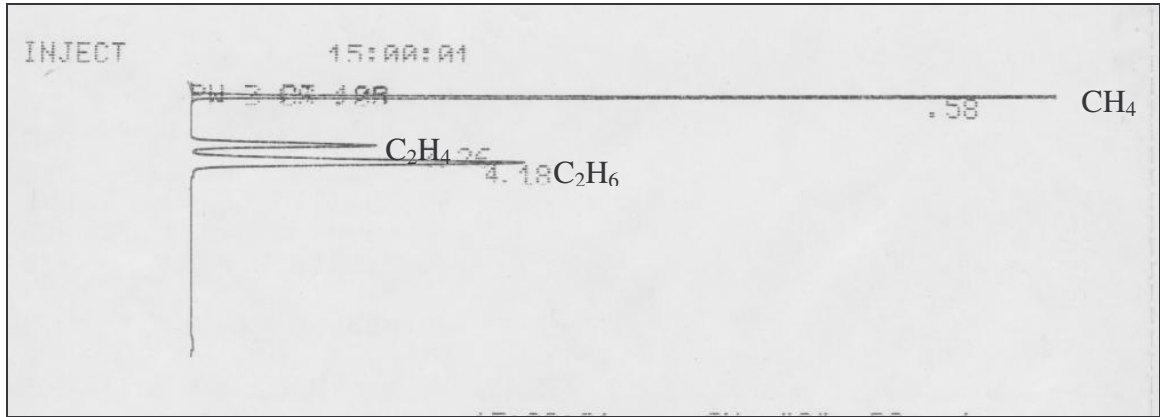


Figure 2.9: A trace for the calibration gas using the FID GC and hydrogen carrier gas.

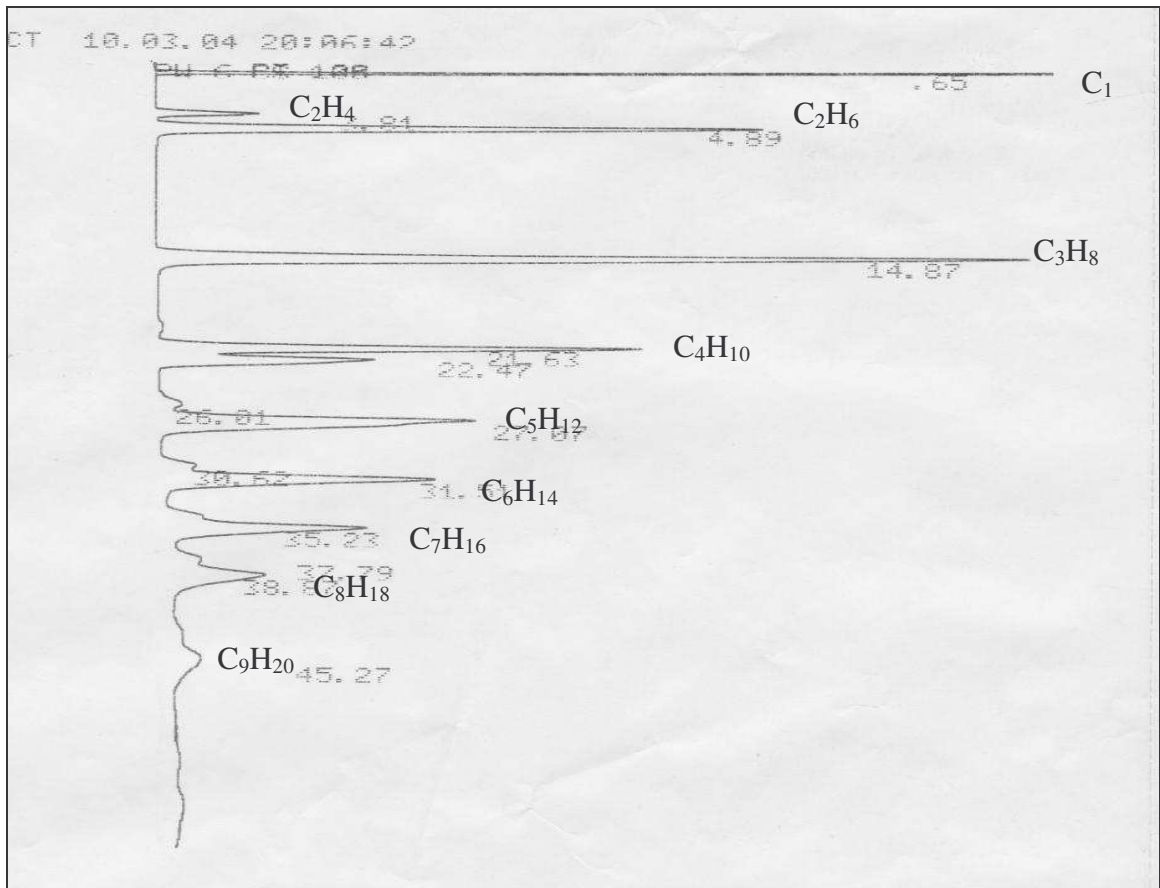


Figure 2.10: A trace for the FT gas product using a FID GC and a Porapak Q column

A ZB-1 capillary column (30 m x 0.5 mm) was also used to separate the higher boiling point hydrocarbons (up to C₁₂).

An offline GC, equipped with a ZB-5 capillary column, was used to analyze the oil and the wax, collected from the hot trap, by using two different temperature programs.

2.3.2.5. Mass balance calculations

The calculations used to determine the mass balance are similar to those used by, Nijs et al [7], Mokoena [21], Duvenhage [22] and Price [28]. The mass balance was performed on carbon and oxygen. Mass balance data of $100 \pm 5\%$ was accepted as adequate.

The analysis of feed and products in the two gas chromatographs was recorded and printed out as areas with an integrator. The areas of the components were converted to molar composition by calculation.

The steady state is typically reached 24 hours after the beginning of the reaction. From this time the mass balance period was recorded and the liquid and wax traps were emptied. At the end of the experiment, the time was recorded as well. This time

was taken as the end of the mass balance period. The oil and water mixture, and the wax were collected separately from the cold trap and hot trap successively and weighed. The oil was separated from water before analysis on an offline GC.

The outlet flow stream was measured on a daily basis using a bubbler at ambient pressure and temperature. The feed inlet flow rate to the reactor was determined using Ar gas contained in the syngas cylinder. The equation used to determine the feed flow rate is given below:

$$F_{in} = \left[\frac{X_{Ar,in}}{X_{Ar,out}} \right] x F_{out} \quad (2.3)$$

where F_{in} is the total feed flow rate in mol/s, $X_{Ar,in}$ and $X_{Ar,out}$ are mole fractions of Argon in the feed (Syngas) and reactor exit streams respectively and F_{out} is the total reactor exit stream in mol/s

The number of moles of carbon in the feed stream in the total mass balance period was calculated by:

$$N_{C,in} = F_{in} \cdot t \cdot X_{CO,in} \quad (2.4)$$

where $N_{C,in}$ is the moles of carbon in the feed, F_{in} is the total feed flow rate in mol/s, t is the total mass balance time and $X_{CO,in}$ is the mole fraction of CO in the feed gas.

Calibration of the components was carried out with a premixed gas of known composition containing CH₄, C₂H₆, C₂H₄, CO, CO₂, and Ar. The moles product of each of the component present in the calibration gas was calculated using the following equation:

$$N_{c, \text{out}} = \frac{A_c}{A_{c, \text{cal}}} \cdot X_{c, \text{cal}} \cdot F_{\text{out}} \cdot t \quad (2.5)$$

where A_c is the GC integrated area of component c , $A_{c, \text{cal}}$ is the area of the component c in the calibration gas and $X_{c, \text{cal}}$ is the mole fraction of the component c in the calibration gas.

The hydrocarbon product areas were corrected for C₂H₄ (olefins) and C₂H₆ (paraffins) by using the response factors based on those presented by Dietz [29], and Scanlon and Willis [30]. The mole fractions of hydrocarbons $X_{\text{HC}, i}$ were calculated using the equation below:

$$X_{\text{HC}, i} = \frac{\text{RF}_i \cdot A_{\text{HC}, i}}{A_{\text{C}_2, \text{cal}}} \cdot X_{\text{C}_2, \text{cal}} \quad (2.6)$$

where RF_i is the response factor for carbon number i , $A_{\text{HC}, i}$ is the integrated GC area for a hydrocarbon with carbon number i , $A_{\text{C}_2, \text{cal}}$ and $X_{\text{C}_2, \text{cal}}$ refer to peak area and mole fraction of the C₂ hydrocarbon in the calibration gas [21, 22].

The mole fractions obtained were used to determine the number of carbon atoms in the vapour product stream. The C₇ peak which was presented on the traces from both the PPQ and Megabore columns was used as a link to adjust all the areas to one standard.

The mass of the product for oil and wax measurements were determine in the same manner and added to the gas fraction. The mass response factors for the hydrocarbon with carbon number greater than 15 were assumed to be one. The mass fractions of these hydrocarbons (i > 15) were thus determined directly from the GC integrated areas using the following equation:

$$m_i = \frac{A_{HC,i}}{\sum A_{HC,i}} \quad (2.7)$$

The % CO conversion was calculated as:

$$\left[\frac{CO_{in} - CO_{out} \times \text{Gas contraction}}{CO_{in}} \right] \times 100 \quad (2.8)$$

where the gas contraction was determined from the $\frac{Ar_{in}}{Ar_{out}}$ calibration

The product selectivity for hydrocarbons S_i was calculated for component x_i as follows:

$$S_i = \left[\frac{\text{mass component } x_i}{\sum x_i} \right] \times 100\% \quad (2.9)$$

The individual rates of reaction for FTS (r_{FTS}) and water gas shift WGS (r_{WGS}) were calculated from experimentally obtained quantities as:

$$r_{\text{WGS}} = r_{\text{CO}_2} \quad (2.10)$$

$$r_{\text{FTS}} = r_{\text{CO}} - r_{\text{CO}_2} \quad (2.11)$$

where r_{CO_2} is the rate of carbon dioxide formation and r_{CO} is rate of carbon monoxide conversion.

The olefin to paraffin ratio x_2 was given as:

$$\text{Olefin to Paraffin ratio } x_2 = \frac{\text{Mass olefin } x_2}{\text{Mass total hydrocarbon } x_2} \quad (2.12)$$

Carbon and oxygen mass balances were determined using the information obtained from the above analysis and calculations:

$$\% \text{ Mole balance} = 100 \times \frac{N_{\text{CO},\text{in}} - N_{\text{CO},\text{out}} - N_{\text{CO},\text{in solid}} - N_{\text{CO},\text{in vapour}} - N_{\text{CO}_2}}{N_{\text{CO},\text{in}}} \quad (2.13)$$

References

- [1] Serp, P., Corrias, M., Kalck, P. *Appl. Catal. A* 253 (200) 337
- [2] Kusnetzova, K., Popova, I., Yales, J.T., Bronikowski, M.J., Huffman, C.D., Liu, J., Smalley, R.E., Hwu, H.H., Chen, J.G. *J. Am. Chem. Soc.* 123 (2001) 10699
- [3] Kyotani, T., Nakazaki, S. W.H. Xu, A. Tomita, *Carbon*, 39 (2001) 771
- [4] van de Loosdrecht, J.M., van der Kraan, A.M., van Dillen, A.J., Geus, J.W. *Appl. Catal. A: General* 150 (1997) 365
- [5] Lupidus, A., Krylova, A., Kazanskii, V., Zaitsev, A., Rathousky, J., Zukal, A., Jancalkova, M. *Appl. Catal.* 73 (1991) 65
- [6] Madikizela, N.N. Cobalt Fischer-Tropsch Catalysts Promoted by Zinc, PhD Thesis, University of the Witwatersrand, Johannesburg, (2002)
- [7] Nijs, H.H., Jacobs, P.A.J. *Chrom. Sci.* 19 (1981) 40
- [8] Rofer-DePoorter, C.K. *Chem. Rev.* 81 (1981) 447
- [9] Chronis, T. A Fischer-Tropsch Study of Co/Ru Catalysts, PhD Thesis, University of the Witwatersrand, Johannesburg, (1999)
- [10]. Collins, P.G., Zettl, A., Bando, H., Smalley, A.R.E. *Science* 278 (1997) 100
- [11]. Laurent, C., Flahaut, E., Peigney, A., Rousset, A. *J. Chem.* 22 (1998) 1229
- [12]. Fan, Y.Y., Cheng, H.M., Wei, Y.L., Su, G., Shen, Z.H. *Carbon*, 38 (2000) 789
- [13]. Couteau, E., Hernadi, K., Seo, J. W., Thiên-Nga, L. Cs. Mikó, R. Gaál, L. Forró. *Chem. Phys. Lett.* 378 (2003) 9
- [14]. Mabudafhasi, M. L., Bodkin, R., Nicolaides, C. P., Liu, X-Y., Witcomb, M. J., Coville, N. J. *Carbon*, 40 (2002) 2737

- [15]. van Steen, E., Prinsloo, F. F. *Catal. Today*, 71 (2002) 327
- [16]. Legzdins, P., Mitchell, R.W., Rempel, G.L., Ruddick, J.D., Wilkinson, G., J. *Chem. Soc. A* (1970) 3322
- [17]. De Jong, K., Van Dillen, A. J., *Heterogeneous Catalysis. Preparation, Characterization and Application*, Publicard: Utrecht. (1999) 274
- [18]. Szefer, P. *Chem. Geo.*, 120 (1995), 111
- [19]. Hulanicki, A. *Problems of Analytical Specification in Biological Samples*, *Wiadomosci Chemiczne* 51 (3-4) (1997) 189
- [20]. Haber, J. *Pure Appl. Chem.* 63 (1991) 1227
- [21]. Mokoena, E. M. *Synthesis and use of silica materials as support for the Fischer-Tropsch reaction*, PhD Thesis, University of the Witwatersrand, Johannesburg, 2005
- [22]. Duvenhage, D.J. *The preparation, Characterization and Evaluation of Titania Supported Fe:Co Bimetallic Catalysts for the Hydrogenation of CO*, PhD Thesis, University of the Witwatersrand, Johannesburg, 1994
- [23]. Berrett, E.P., Joyner, L.G., Halenda, P.P. *J. Am. Chem. Soc.* 73 (1951) 373
- [24]. Micromeritics Instrument, TriStar 3000, Operator's manual, Part No. 300-42832-01, April 2005
- [25] Micromeritics Instrument, FloPrep 060, Operator's manual, Part No. 060-42803-01, March 2002
- [26]. <http://www.biologie.uni-hamburg.de/b-online/e03/03e.htm>
- [27] Lin, H., Chen, Y., Li, C. *Thermochimica Acta*, 400 (2003) 61

[28]. Price, J.G. An Investigation into novel bimetallic catalysts for use in the Fischer-Tropsch reaction, PhD Thesis, University of the Witwatersrand, Johannesburg, 1994

[29]. Dietz, A.W. J. Gas Chrom. (1967) 62

[30]. Scanlon, J.T., Willis, D.E. J. Chrom. Sci. 23 (1985) 333

CHAPTER 3: FISCHER-TROPSCH SYNTHESIS OVER IRON CATALYSTS SUPPORTED ON CARBON NANOTUBES

3.1. Introduction

The Fischer-Tropsch (FT) synthesis has long been recognized as a heterogeneous surface catalyzed polymerization process [1, 2]. During this process CH_x monomers, formed via hydrogenation of adsorbed CO on transition metals, produce hydrocarbons and oxygenates with a broad range of chain lengths and functional groups. The major products are linear paraffins and α -olefins [3].

Among the reported Fischer-Tropsch synthesis catalysts, iron and cobalt are used commercially at temperatures between 200 and 300°C, and at 10 to 60 bar pressure [3-5]. The performance of these catalysts is affected by numerous factors, one of which is the nature and structure of the support materials. Most studies on FT catalysts have been performed with the metals supported on silica, alumina or titania [6].

However, other supports have been investigated for use in the FT reaction and one of these is carbon [3]. Indeed, a series of studies by Vannice in the 1980s reported on the use of organometallic iron complexes supported on graphitic carbon supports in the FT reaction [7-11]. Since these studies were reported, very little further work has appeared in the literature on the use of carbon supported metals in this reaction [12]. This is surprising since carbon supported iron catalysts give high selectivities to olefins in the FT reaction [3]. From an economic point of view the production of short chain olefins is attractive, as these are valuable bulk hydrocarbons [7, 13-15].

The recent discovery of carbon nanotubes (CNTs), followed by extensive studies of the unique properties associated with this form of carbon, has resulted in some preliminary investigations into the use of CNTs as a carbon support in catalysis [16-18], and specifically on their use as a support in FT synthesis [19, 20].

Currently CNTs are synthesized by a wide range of routes and produce a range of structures with both tubular and herring bone arrangements [16, 21-23]. While herring bone CNTs will certainly provide a better interaction of a metal with a carbon surface than will tubular CNTs, reduction of the metal will also be inhibited. To facilitate the Fe reduction (i.e. reduce the Fe-CNT interaction) we have thus chosen to use tubular CNTs in this study.

In summary, this work has been motivated by the following issues:

- Early comparative studies have revealed selectivities for olefin formation in the Fischer-Tropsch synthesis to be Fe/C > Fe/silica > Fe/alumina [24].
- Sommen et al. [13] observed high olefin selectivities for Fe/carbon catalysts, but found a strong tendency for these catalysts to deactivate due to formation of carbon deposits at a H₂/CO ratio of 1. Thus, it is not clear from the previous work whether Fe/carbon catalysts are stable under typical synthesis conditions, i.e., at a H₂/CO ratio of 2.
- Carbon supported iron catalysts are suggested to be able to maintain high catalyst activities and high throughput per unit volume as a consequence of high dispersions and/or strong metal-support interactions [11].
- CNTs differ from graphite in that CNTs present a curved surface to metal ions. Theoretical calculations have indicated that this effect impacts on the metal interaction with the carbon support [25]
- Since CNTs produced by different procedures have different surface areas, dimensions etc, it is not clear whether these factors will influence the catalyst behaviour in a significant manner [19, 20]. Indeed, the poor reactivity and rapid deactivation of some Fe/CNT FT catalysts [19] is unexpected.

3.2. Experimental

Carbon nanotubes were synthesized by the catalytic decomposition of acetylene at 700°C over an iron catalyst supported on CaCO₃ [26]. In the preparation, Fe(NO₃)₃·9H₂O (7.21 g ; 10% Fe) was dissolved in 30 ml distilled water and added drop-wise to 10 g of CaCO₃ support. The resulting slurry was dried at 120°C overnight and then calcined at 400°C in air for 16 hours [26].

The decomposition of acetylene was carried out in a tubular quartz reactor (51 cm x 1.9 cm i.d) [27], which was placed horizontally in a furnace. The furnace was under electronic control and thus temperature ramping was readily achieved. The front end of the tube was connected to a glass manifold that allowed the free flow of gases (hydrogen and acetylene) at atmospheric pressure to be passed through the tube. A quartz glass wool plug was placed in the rear end of the quartz tube, which was situated outside the oven. All reactions were carried out at atmospheric pressure in the absence of oxygen.

The catalyst (100 mg) was loaded into a quartz boat (120 mm x 15 mm) at room temperature and the boat was placed in the centre of the quartz tube. H₂ was used to reduce the catalyst for 1 hour in situ (700°C, 100 ml min⁻¹). The heating and cooling were automatically controlled and the temperature ramping rate used was 10°C min⁻¹. The H₂ gas was then replaced with acetylene and the gas was then passed through the

reactor for 3 hours (700°C , 100 ml min^{-1}). The reactor was then cooled to room temperature in a H_2 atmosphere. The boat was removed from the reactor and weighed to establish the amount of carbon nanotube material that had been formed. This reaction was repeated and the products collected were combined and mixed.

The catalyst precursor was separated from the carbon nanotubes by dissolving the crude product in nitric acid (30% HNO_3 , 2 h, at room temperature) [26]. The acid dissolved away the Fe catalyst, the CaO and some amorphous insoluble carbon. The carbon nanotubes were then recovered by filtration thoroughly washed with distilled water and finally dried at 120°C overnight.

The F-T supported catalysts were prepared by the deposition precipitation (DPU) method using urea [19, 28]. In the DPU method, $\text{Fe}(\text{NO}_3)_3 \cdot 9\text{H}_2\text{O}$ (7.21 g) and urea (1.61 g; 1.5 moles urea per mole of iron) were dissolved in de-ionised water (18 ml) and added to 10 g of the carbon nanotube support. Three other catalysts (DPUCu, DPUK and DPUKCu) were prepared by promoting the Fe/CNT catalyst with Cu, K or Cu/K. Thus KNO_3 (0.052 g; 0.2% K) and/or $\text{Cu}(\text{NO}_3)_2 \cdot 3\text{H}_2\text{O}$ (0.228 g; 0.6% Cu) were added to an iron solution prepared above and the mixture added drop-wise to 10 g of carbon nanotube support. After allowing sufficient time (at least two hours) for the hydrolysis of the urea, the sample was dried by evaporating the water under vacuum at 90°C for 40 minutes. The urea was added to facilitate the uniform formation of metal hydroxides onto the surface of the carbon nanotube support [29].

A Fe/CNT sample was also produced by the incipient wetness (IW) impregnation process. In this instance $\text{Fe}(\text{NO}_3)_3 \cdot 9\text{H}_2\text{O}$ (7.21 g; 10% iron) was dissolved in de-ionised water (18 ml) and added to 10 g of carbon nanotubes support. The resulting slurry was dried in a rotary evaporator at 90°C for 2 hours.

All the samples were further dried in an oven (120°C , overnight) and then calcined in nitrogen at 220°C for 2.5 hours.

The Fischer-Tropsch synthesis was performed in a fixed-bed micro reactor [30]. Gas cylinders containing $\text{H}_2/\text{CO}/\text{Ar}$ mixtures (0.60/0.30/0.1 vol. Purity: 99.99) were used to supply the reactant gas stream to the catalyst with a space velocity of 2120 h^{-1} . Ar was used as an internal standard in order to ensure accurate mass balances.

Catalyst (0.5 g) was added to the reactor and reduced in situ at 350°C for 24 hours under a stream of H_2 (2 bar pressure, 20 ml min^{-1}). After reduction, the temperature was decreased to 275°C , synthesis gas was introduced and the pressure was increased gradually to 8 bar.

All gas lines after the reactor were kept at 150°C and a hot trap placed immediately after the reactor was held at this temperature in order to collect wax. A second trap kept at ambient temperature was used to collect the oil and water mixture. The flow was controlled using a metering valve and measured by a bubble meter.

The product stream was analyzed online using two gas chromatographs. A thermal conductivity detector (TCD), equipped with a Porapak Q (1.50 m x 3 mm) packed column, was used to analyze Ar, CO and CO₂ and a flame ionization detector (FID), equipped with a Porapak Q packed column, was used for the analysis of hydrocarbons. A ZB-1 capillary column (30 m x 0.5 mm) was also used to separate the higher boiling point hydrocarbons (up to C₁₂). An offline GC, equipped with a ZB-5 capillary column, was used to analyze the oil and the wax by using two different temperature programs.

3.3. Catalyst characterization

A Du Pont 951 TGA (Thermo gravimetric analyser) using a linear temperature programme (heating rate, 10°/min; nitrogen flow rate, 30 ml min⁻¹) was used to analyze the decomposition of the CNTs and to determine the catalyst decomposition temperature.

The average particle size was determined from TEM (Transmission electron microscopy) (Jeol JEM 100S) images. Samples for TEM analysis were prepared by sonicating about 1 mg of material in 1 ml methanol for 10 min. A few drops of the resultant suspension was added onto a holey Cu grid coated with a carbon film.

BET surface areas were determined by nitrogen physisorption (Micromeritics ASAP 2010) A TPR (temperature programmed reduction) apparatus constructed in our laboratory was used for reduction studies. Samples (5 mg) were placed within a quartz U tube reactor as a thin packed bed, heated in pure N₂ (30 ml min⁻¹) to 150°C at 10°C min⁻¹, and held at this temperature for 30 minutes in order to remove water. The sample was then cooled down to room temperature in N₂ and the gas was switched to 5% H₂/Ar. The sample temperature was then increased to 800°C at 7.5°C min⁻¹.

3.4. Data analysis and calculations

Mass balance calculations similar to those proposed by Duvenhage et al. were used [30]. The % CO conversion was calculated as:

$$\left[\frac{\text{CO}_{\text{in}} - \text{CO}_{\text{out}} \times \text{Gas contraction}}{\text{CO}_{\text{in}}} \right] \times 100 \quad (3.1)$$

where the gas contraction was determined from the $\frac{\text{Ar}_{\text{in}}}{\text{Ar}_{\text{out}}}$ calibration

The product selectivity for hydrocarbons S_i was calculated for component x_i as follows:

$$S_i = \left[\frac{\text{mass component } x_i}{\sum x_i} \right] \times 100\% \quad (3.2)$$

The individual rates of reaction for FTS (r_{FTS}) and water gas shift WGS (r_{WGS}) were calculated from experimentally obtained quantities as:

$$r_{\text{WGS}} = r_{\text{CO}_2} \quad (3.3)$$

$$r_{\text{FTS}} = r_{\text{CO}} - r_{\text{CO}_2} \quad (3.4)$$

where r_{CO_2} is the rate of carbon dioxide formation and r_{CO} is rate of carbon monoxide conversion.

The olefin to paraffin ratio x_2 was given as:

$$\text{Olefin to Paraffin ratio } x_2 = \frac{\text{Mass olefin } x_2}{\text{Mass total hydrocarbon } x_2} \quad (3.5)$$

The specific activity was expressed as μmol of CO converted per gram catalyst per second and was calculated as a function of the CO conversion. Mass balance data of $100 \pm 5\%$ was accepted as adequate.

3.5. Results and discussion

3.5.1. Catalyst synthesis

Carbon nanotubes (CNTs) can be made by a range of different procedures, but the most facile process relies on passing a gaseous carbon source over a metallic catalyst (preferably Ni, Fe or Co) supported on an inorganic material at high temperature [16, 31]. Many different metal/support combinations have been reported in the literature that applies this general process to the synthesis of both multi-walled (MW) and single walled (SW) carbon nanotubes. The different processes also yield two types of CNTs – herringbone and tubular CNTs. While the synthesis and characterization of CNTs is straightforward, purification and functionalization of the CNTs are still non-trivial exercises. To minimize this issue we have used a procedure in which a metal catalyst was supported on CaCO_3 [26]. This support was chosen since:

- The process gives high yields of MWCNTs.
- The formation of amorphous carbon is suppressed by non porous materials and therefore selective formation of CNTs is promoted over non porous materials like CaCO_3 .

- The support can readily be removed from the CNTs by a mild acid treatment after completion of the reaction. A mild acid treatment will also remove residual catalyst and not chemically destroy the carbon nanotubes.

The Fe/CaCO₃ catalyst was prepared by a procedure similar to that described by Couteau et al. [26] and this catalyst produced high yields of MWCNTs. After washing, some residual iron particles were observed in the CNTs by TEM (see below). A blank FT catalytic run on the purified CNTs was hence performed to establish the activity of the support. Very little production of methane was observed and no other hydrocarbons were formed.

Residual Ca²⁺ is not expected to affect the FT activity of the catalysts. Extensive studies by Luo and Davis have indicated that calcium ions hardly affect the catalyst reactivity or selectivity [32]. To further ensure that the presence of Ca²⁺ did not affect the study the same batch of CNT support was used in all the reactions described in this study, thus allowing for a meaningful comparison between the data. The use of the same CNT support material also eliminated the effect of residual Fe content on the FT results.

TEM analysis was performed on the unpurified and purified CNTs. The data confirmed:

- The samples contained solely CNTs and catalyst particles,
- That after purification only nanotubular carbon (no amorphous material) was observed,
- The CNT wall structure was well graphitized,
- The removal of most of the Fe and Ca was achieved by acid treatment,
- The CNTs tubes were open at both ends,

Thus the mild acid treatment did not generate substantial carboxylic acid groups on the tube ends or even on the tube walls [16]. Thus, only moderate interaction of metal ions with the CNT support is expected.

The Fe (and promoter ions) was then added to the CNTs by classical deposition precipitation (DPU) procedures [33] to produce four different catalysts: DPU, DPUCu, DPUK and DPUKCu (Table 3.1). For comparison, a catalyst prepared by the incipient wetness technique was also synthesized.

3.5.2. Catalyst characterization

ICPOES (ICP Optical Emission Spectroscopy) analysis of the catalysts revealed that the metal ratios obtained are very close to those predicted from the catalyst preparation (Table 3.1).

Table 3.1: Metal content and BET surface areas of various catalysts

Catalyst Name ¹	%Fe	%Cu	%K	Pore volume (mm ³)	BET surface areas (m ² /g) Fresh catalyst
IW	12.1	0.0	0.0	3.4	35.0
DPU	10.5	0.0	0.0	5.6	18.5
DPUCu	11.4	0.7	0.0	23.8	9.3
DPUK	9.3	0.0	0.7	5.4	15.5
DPUKCu	8.9	0.5	0.5	1.3	17.0

¹IW = incipient wetness; DPU = deposition precipitation

TEM analysis performed on the unpurified CNT revealed that the crude product contained solely CNTs with opened pores, catalyst particles and support, while no amorphous carbon was observed (Figure 3.1). Purification of the CNT resulted in removal of the Fe and CaO, and enhancement of the CNT density (Figure 3.2).

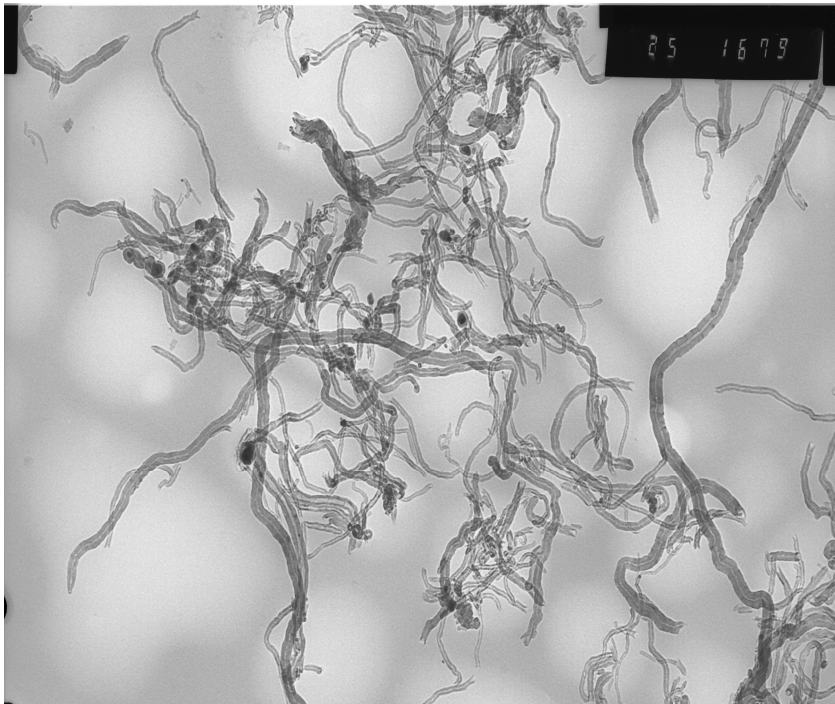


Figure 3.1: TEM image of unpurified carbon nanotubes. Dark spots represent residual Fe particles.

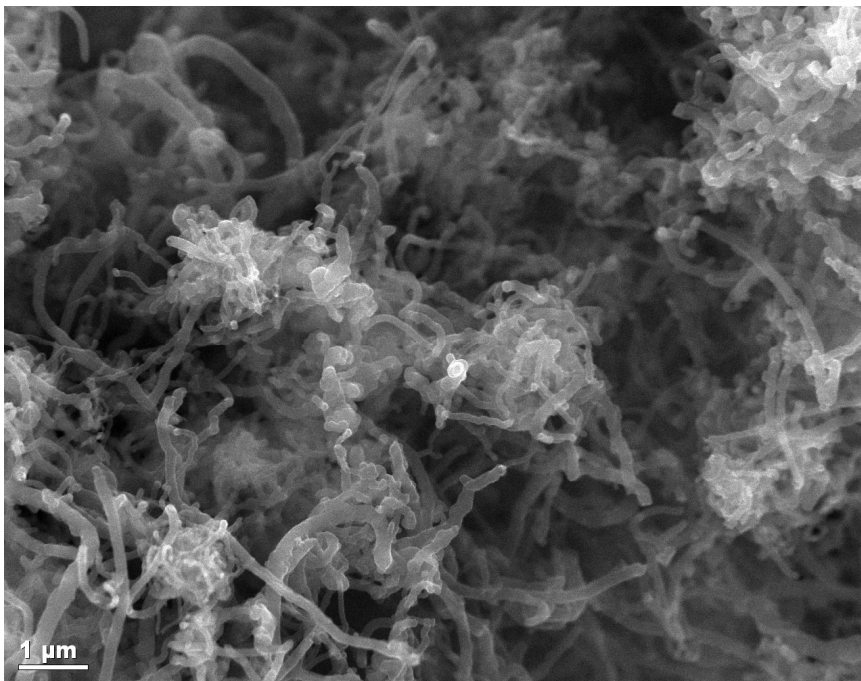


Figure 3.2: SEM image of purified carbon nanotubes

The purified CNTs have a BET surface area of $113 \text{ m}^2 \text{ g}^{-1}$. Addition of the Fe and the promoters to the CNT resulted in an expected reduction of the surface area ($< 20 \text{ m}^2 \text{ g}^{-1}$ for the DPU catalysts; Table 3.1). This arises since the metal covers the outside of the CNTs and also blocks the CNT pores.

Addition of the metal ions (Fe, Cu, K) did not affect the morphology of the CNTs. Figure 3.3 shows a SEM image of a representative reduced Fe/CNT catalyst. The iron particles appear on the surface of the CNTs. The images show a homogeneous coverage with small iron particles (average diameter approximately 15 nm).

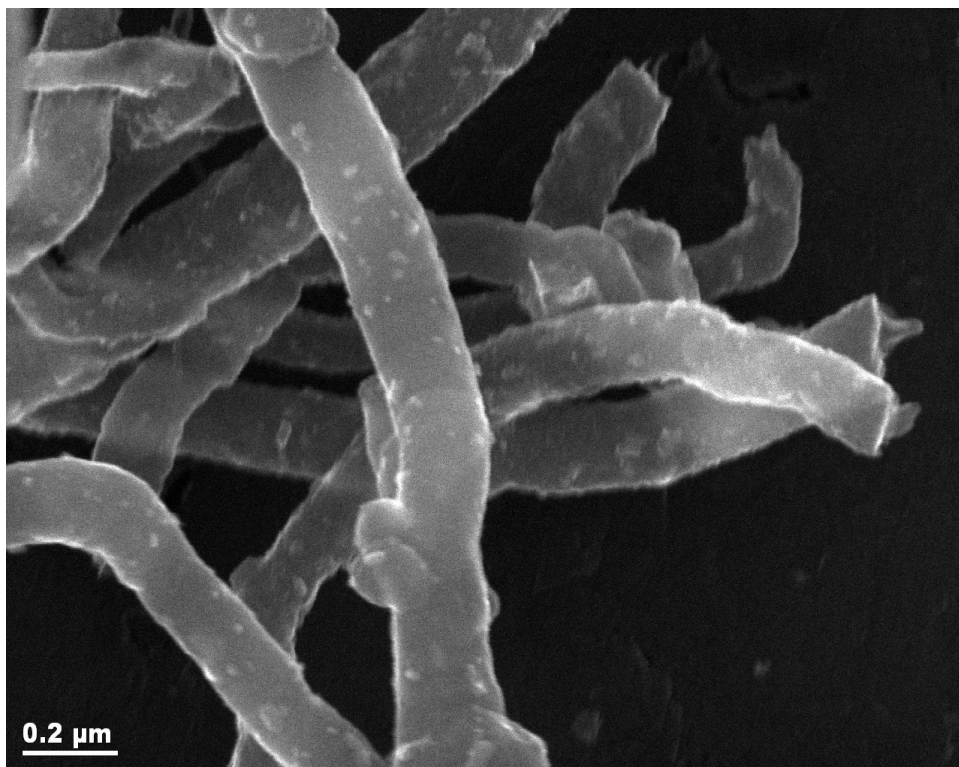


Figure 3.3: SEM image of Fe catalyst supported on carbon nanotubes. White spots represent Fe particles.

The reduction behaviour of the various catalyst precursors was studied by temperature-programmed reduction (TPR) (Figure 3.4).

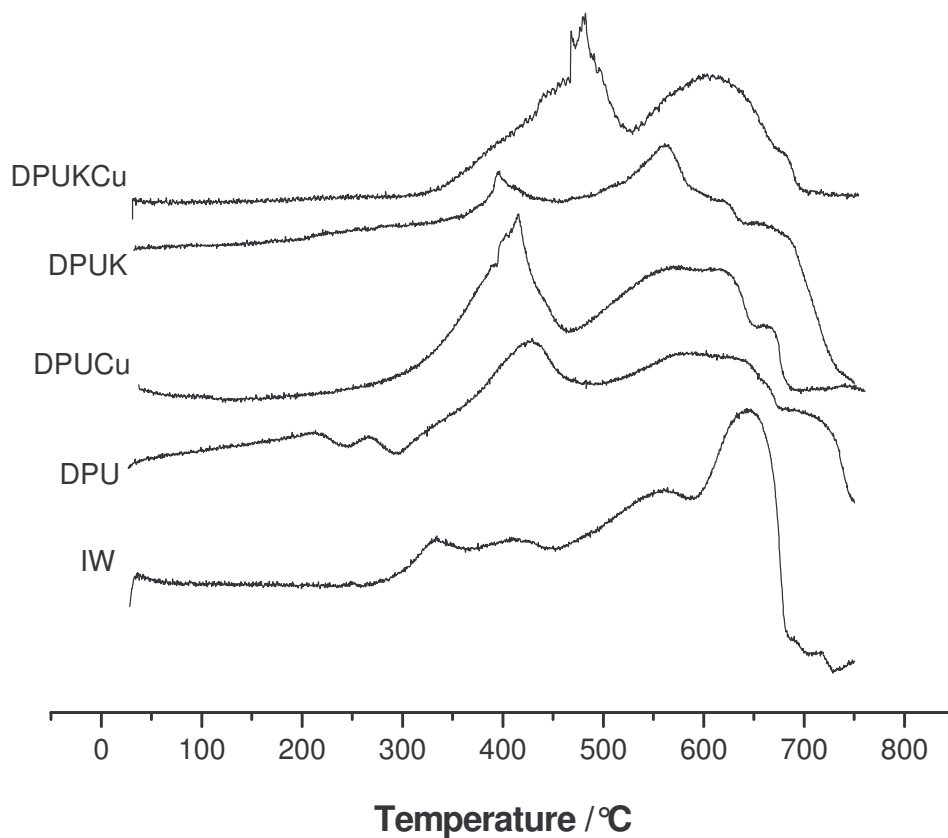


Figure 3.4: TPR profiles of the catalysts

Two peaks are present in all the TPR-profiles. Since transition metals can act as catalysts for the formation of methane through reaction of hydrogen with carbon nanotubes when $T > 600\text{ }^{\circ}\text{C}$ [19, 28], the peak observed at temperature above $550\text{ }^{\circ}\text{C}$ in all the profiles can be attributed to the gasification of the CNT support. The carbon

gasification process was substantiated by passing the outlet gas from the TPR reactor through a GC. Methane was detected in this outlet gas at temperatures above 550°C. This suggests that gasification of the CNTs occurs at high temperatures, presumably catalyzed by the Fe, even in the absence of oxygen. However, no gasification occurred at the temperatures used in the FT study.

3.5.3. Catalytic activity

Fig. 1.5 shows a plot of the catalytic activity in terms of the percentage conversion of CO, as a function of reaction time. All the reactions were performed under a set of standard conditions (275°C, 8 bar, H₂:CO = 0.5) as established from preliminary experiments in our laboratory. The activity, for all the catalysts studied, was initially low but increased significantly within 15 hours and became stable for the entire experiment (20-120 h). This contrasts with data reported on similar Fe/CNT catalysts where activities and stability were poor [19].

A comparison of the data for the 10% catalysts (no promoters) prepared by IW and DPU procedures reveals that the CO conversions are very similar and that the conversion is not dependent on the method of preparation of the catalysts. The small differences noted could relate to the differing surface areas and the different Fe content. Indeed the activity measured per g Fe reveals that the DPU prepared catalyst is more active since its metal content is low. Finally, selectivity data and alpha values

(See table 3.2) also suggest very little difference between the two catalysts. The main difference relates to CO₂ content.

Addition of Cu to Fe/CNT (DPUCu catalyst) resulted in an increase in CO reaction rate and activity as well as CO₂ production rate (Figure 3.5, Table 3.2).

Table 3.2: Activity and selectivity of iron catalyst in FTS

Catalysts	IW	DPU	DPUCu	DPUK	DPUKCu
CO rate ¹	-2.25E-06	-1.71E-06	-3.02E-06	-2.95E-06	-2.77E-06
CO ₂ rate (WGS)	6.97E-07	5.96E-07	1.07E-06	1.28E-06	1.23E-06
FTS rate	1.55E-06	1.11E-06	1.95E-06	1.67E-06	1.54E-06
Activity ($\mu\text{mol}/\text{sec}\cdot\text{gFe}$)	45.06	56.81	60.50	58.90	55.45
Alpha (α)	0.65	0.65	0.64	0.73	0.69
Selectivity (%)					
C ₁	14.59	15.43	16.10	10.97	9.90
C ₂ -C ₄	42.11	39.86	39.99	29.50	36.15
C ₅ -C ₁₁	41.62	42.16	41.79	51.66	50.75
C ₁₂₊	1.69	2.55	2.12	7.87	3.20
$C_2^= / (C_2 + C_2^=)^2$	0.11	0.09	0.10	0.72	0.67
CO ₂	6.83	9.81	10.58	12.59	12.16

¹ Rate (mol/sec)

² Olefin to total C₂ hydrocarbon weight ratio

These trends are expected and are consistent with the ability of Cu to lower the reduction temperature of Fe thus providing more active iron sites for catalysis [34, 35]. The low Cu loading did not however modify the catalyst selectivity significantly. It is noted that the Cu reduced the catalyst surface area from 18.50 m²/g before Cu addition to 9.26 m²/g after addition (Table 1).

Addition of K to Fe/CNT gave the DPUK catalyst, which showed the expected increase in olefinity and alpha value and a decrease in CH₄ content relative to the DPU catalyst [36-40]. The effect of the K on the olefinicity of the C₂ hydrocarbon (9.1% to 71.9%) is remarkable.

Finally a catalyst prepared containing Cu and K (DPUKCu) displayed a low CO conversion activity. From Table 3.2, it can be seen that the Fe content is lower in this catalyst when compared to the other catalysts. van Steen and Prinsloo have also observed a decrease in CO conversion using an iron catalyst supported on CNT and promoted with Cu and K [19].

A comparison of our data with other related Fe/C FT catalysts is given in Table 3.3. The data in Figure 3.5 and Table 2.2 show that, despite the high CO conversion (65%-89%) generated in this study, the olefin to paraffin ratio is high for the catalysts DPUK and DPUKCu. This contrasts with typical literature reports where increases in

CO conversion have been shown in general to decrease the olefin to paraffin ratio [7, 8].

Table 3.3: Results of Fe catalysts supported on various carbon materials

Catalyst	Temp (K)	H ₂ /CO Ratio	Act $\mu\text{mol.g}^{-1}.\text{s}^{-1}$	Conv (%)	Selectivity	
					C ₁ %	C ₂ ⁼ /C ₂
IW	548	2:1	45.06	80.0	13.39	0.11
DPU	548	2:1	56.81	76.7	14.17	0.09
DPUCu	548	2:1	60.50	86.1	14.80	0.10
DPUK	548	2:1	58.90	84.9	9.99	0.72
DPUKCu	548	2:1	55.45	69.1	9.03	0.67
10%Fe/ C ¹	473	2:1	-	3.7	12	-
4.8% Fe /Act. Saran ²	503	3:1	-	3.1	18	0.43
5.9% Fe /Ox. Saran ²	503	3:1	-	3.6	20	0.50
5.0% Fe /Carbolac ²	503	3:1	-	3.0	23	0.35
4.4% Fe /R0 0.8 ³	674	2:1	322.7	5.8	22	0.65
8.8% Fe /R1 ³	674	1:1	84.09	5.9	26	0.67

¹ Bartholomew et al. [6]; comparable activity and C₂⁼ selectivity data not available.

² Vannice et al. [13]; comparable activity data not available

³ Van Der Wiele et al. [13]

The wide range of conditions used in the various studies shown in Table 3.3 does not allow for a simple comparison of the data. However, the data do indicate that in the Fe/CNT catalysts that (i) the methane selectivity is decreased and (ii) the olefin

selectivity is high relative to other Fe/C catalysts. This issue will need to be explored in more detail to evaluate the generality of the finding.

3.5.4. Deactivation

Controversy still surrounds the deactivation phenomenon for Fe/C FT catalysts. Jones et al. [24] found, using temperatures in the range of 473-513 K and a H₂:CO ratio of 2, that Fe/C of either moderate or high dispersion underwent 1-2 orders of magnitude loss of activity within a period of 24 hours of CO hydrogenation. By contrast, Vannice and Jung et al [7, 8] reported well-dispersed Fe/C catalysts had a high stability at a temperature of 508 K and a H₂: CO ratio of 3.

In this study no catalyst deactivation has been observed during the first 120 hours of reaction with all the catalysts used (See figure 3.5). By contrast, van Steen and Prinsloo using a Fe/CNT catalyst noted that their catalyst did deactivate with time. This could have been due to their use of a herringbone CNT rather than the use of a tubular CNT as the catalyst support. This will be an issue that will need to be explored in future studies.

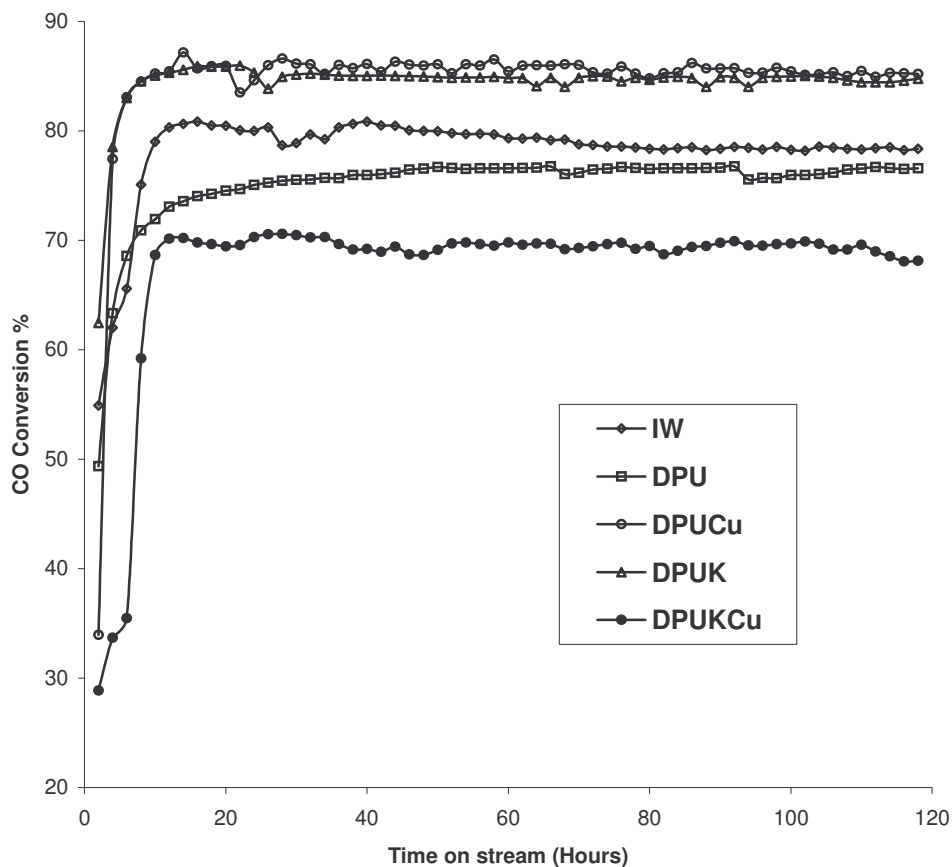


Figure 3.5: CO conversion with time on stream

3.5.5. Mechanistic issues

We also used $\text{Ni}(\text{NO}_3)_2$ supported on Al_2O_3 to produce CNTs. The reaction gave high yields of MWCNTs while TEM and EDX revealed the presence of some residual Ni. However, as the Ni was observed to be *in the tubes*, we initially assumed that the Ni would not interfere with the FT reaction.

Blank FT reactions were then performed on the purified CNTs (8 bar P, 275°C) in the catalyst F-T reactor i.e. in the absence of added Fe metal catalyst. The main product formed was methane (80% in the gas product) with almost no liquid and wax product. The data thus revealed that access to the Ni by the reactant gases was possible and that the CNTs synthesized from Ni did not produce a suitable support material for use in the FT reaction. This is an important finding and suggests that care must be taken to ensure that when CNTs are used as catalyst supports, the source of the materials be adequately described.

The CNTs produced in this study were shown by TEM analysis to be MWCNTs. Thus the interaction with the support surface is expected to be weaker than that to be found when herring bone CNTs are used. The analysis reveals that the Fe is well dispersed on the CNTs, but the influence of particle size (and the curvature of the tube) cannot be assessed from this study.

It is important to note that the catalytic activity for a catalyst supported on the CNT herring bone-type may differ from that of CNT parallel-type. For example, when Rodriguez et al [41] introduced an active phase (e.g. FeCu) onto carbon nanofibers (CNF) via an incipient wetness technique, the FeCu/CNF catalysts displayed a higher activity for ethene hydrogenation than FeCu/activated carbon. The authors ascribed this high activity to a unique (metal-support) interaction. Unfortunately, no characterization data was provided that could explain the activity differences observed. In a more intensive study, Hoogenraad [42] compared the hydrogenation

activity of Pd/CNF (herring bone), Pd/CNF (parallel) and Pd on activated carbon. The herring bone-type fibers displayed (even at low Pd content) a much higher activity than the Pd/CNF (parallel) and Pd on activated carbon. Once again, insufficient characterization data are available to explain these interesting phenomena in detail.

3.6. Conclusion

In this study, the effect of catalyst promotion on the FTS activity, stability, and product selectivity of a series of Fe/CNT catalysts were investigated. Iron supported on CNTs produces a very stable and active catalyst. The method of preparation does not have an effect on the CO conversion and product selectivity. The addition of potassium leads to decreased hydrogenation and increased chain growth during FT synthesis reaction, producing higher molecular weight products (i.e., a higher α). The production of C₂ olefins is also increased. Potassium also decreases methane production and increases WGS activity. Copper, introduced to facilitate reduction of the iron did increase FTS reaction rate but did not have a major effect on the product spectrum.

References

- [1]. Herington, E. F. G. *Chemistry and Industry*, 1946, 346
- [2]. Friedel, R. A., Anderson. R. D. *J. Am. Chem. Soc.* 72 (1950) 1212
- [3]. Dry, M.E. in: Anderson, J.R., Boudart, M. *Catalysis Science and Technology*, Vol. 1, Springer, New York, 1981, 159 pp. 319
- [4]. Fischer, F., Tropsch, H. German Patent 484337 1925
- [5]. Jager, B., Espinoza. R. *Catal. Today* 23 (1995) 17
- [6]. Bartholomew, C. H. "New Trends in CO Activation" ed. Guzzi, L. Elsevier, Amsterdam, 1991, 225
- [7]. Jung, H. J., Walter Jr., P. J., Vannice, M. A. *J. Catal.* 75 (1982) 416
- [8]. Jung, H. J., Vannice, M. A., Mulay, L. N., Stanfield, R. M., Delgass, W. N. *J. Catal.* 76 (1982) 208
- [9]. Venter, J., Kaminsky, M., Geoffroy, M., Vannice, M. A. *J. Catal.* 103 (1987) 450
- [10]. Venter, J., Kaminsky, M., Geoffroy, M., Vannice, M. A. *J. Catal.* 105 (1987) 155
- [11]. Venter, J., Chen, A. A., Phillips, J., Vannice, M. A. *J. Catal.* 119 (1989) 451
- [12]. Ma, W-P., Ding, Y-J., Lin, L-W. *Ind. Eng. Chem. Res.* 43 (2004) 2391
- [13]. Sommen, A. P. B., Stoop, F., Van der Wiele, K. *Appl. Catal.* 14 (1985) 277
- [14]. Bi, Y.H., Dalai, A.K. *Can J Chem Eng.*, 81 (2003) 230
- [15]. Davis, B.H. *Catalysis Today*, 84 (2003) 83
- [16]. Serp, P., Corrias, M., Kalck, P. *Appl. Catal. A* 253 (2003) 337
- [17]. Marsh, H., Heintz, E. A., Rodriquez-Reinoso, F., *Introduction to Carbon Technologies*, University of Alicante, Alicante, 1997

- [18]. Rodriguez-Reinoso, F. Carbon 36 (1998) 159
- [19]. van Steen, E., Prinsloo, F. F. Catal. Today 71 (2002) 327
- [20]. Moy, D., Hoch, R. Hyperion Catalysts International Inc., US Patent 5569635 (1996)
- [21]. Gupta R.K., Dwivedy, I. Curr. Appl. Phys., 5 (2005) 163
- [22]. Journet, C., Bernier, P. Appl. Phys. A, 67 (1998) 1
- [23]. Teo, K.B.K., Singh, C., Chhowalla, M., Milne, W.I. in Encyclopedia of Nanoscience and Nanotechnology (ed H.S. Nalwa), American Scientific Publishers, 10 (2003) 1
- [24]. Jones, V. K., Neubauer, L. R., Bartholomew, C. H. J. Phys. Chem. 90 (1986) 4832
- [25]. Mehon, M., Andriotis, A.N., Froudakis, G.E. Chem. Phys. Lett. 320 (2000) 425
- [26]. Couteau, E., Hernadi, K., Seo, J. W., Thiên-Nga, L., Mikó, Cs., Gaál, R., Forró, L. Chem. Phys. Lett. 378 (2003) 9
- [27]. Mabudafhasi, M. L., Bodkin, R., Nicolaides, C. P., Liu X-Y., Witcomb, M. J., Coville, N. J. Carbon 40 (2002) 2737
- [28]. Prinsloo, F.F., Hauman, D., Slabbert, R. Proceedings of the 17th Biennial Conference on Carbon, (2001) 940
- [29]. De Jong, K., Van Dillen, A. J. 1999. Heterogeneous Catalysis: Preparation, Characterization and application Publicard: Utrecht. 274
- [30]. Duvenhage, D.J., Coville, N.J. Appl. Catal. 153 (1997) 43
- [31]. Huczko, A. Appl. Phys. A 74 (2002) 617
- [32]. Luo, M., Davis, B. H. Appl. Catal. A 246 (2003) 171

- [33]. Richardson, J.T. in "Fundamental and Applied Catalysis: Principle of Catalyst Development", eds Twigg, M.V. and Spencer, M.S. Plenum Press, New York, 1989
- [34]. O'Brien, R. J., Davis, B.H. *Cat. Lett.* 94 (2004) 1
- [35]. O'Brien, R. J., Xu, L., Spicer, R. L., Bao, S., Milburn, D. R., Davis. B. H. *Cat. Today* 36(1997) 325
- [36]. Wilfried, N.H., Zhang, Y., O'Brien, R.J., Luo, M., Davis, B.H. *Appl. Catal. A* 36 (2002) 77
- [37]. Dry, M. E., Shingles, T., Boshoff, L. J., Oosthuizen, G. J. *J. Catal.* 15 (1969) 190
- [38]. Luo, M., O'Brien, R. J., Bao, S., Davis, B.H. *Appl. Catal. A* 239 (2003) 111
- [39]. Anderson, R. B., Seligman, B., Schultz, J. F., Elliot, M. A. *Ind. Eng. Chem.* 44 (1952) 391
- [40]. Li, S., Krishnamoorthy, S., Li, A., Meitzner, G. D., Iglesia, E.J. *Catal.* 206 (2002) 202
- [41]. Rodriguez, N. M., Kim, M.-S., Baker, R. T. K. *J. Phys. Chem.* 98 (1994)13108
- [42]. Hoogenraad, M. S. Ph.D. thesis, Utrecht University (1995)

CHAPTER 4: Fe:Ru SMALL PARTICLE BIMETALLIC CATALYSTS SUPPORTED ON CARBON NANOTUBES FOR USE IN FISCHER-TROPSCH SYNTHESIS

4.1. Introduction

Bimetallic catalysts play an important role in many industrial catalytic processes and represent an area of intense research activity. The addition of a second metal component to a catalyst allows for the possibility of systematically altering the size and/or the electronic structure of a catalyst. The presence of a second metal component can also make its influence felt by modifying the adsorption characteristics of the catalyst surface, changing the reducibility of the catalyst or in certain cases altering the catalyst deactivation behavior. This has proven to be beneficial in bimetallic reforming catalysts [1].

Among the various bimetallic systems investigated, those of iron with noble metals such as Ru have drawn considerable attention over the decades because of their possible importance in the Fischer-Tropsch (FT) synthesis [2]. Alloying iron with

ruthenium results in a significant improvement in the stability of the catalytic system in FT synthesis compared with a one-component iron catalyst [3, 4]. Further, supported iron-ruthenium catalysts are assumed to combine the benefits of high metal dispersion and alloying [3]. Supported alloys of these two metals are also known to possess unique catalytic properties in hydrocarbon synthesis, particularly giving a high selectivity to propylene [4]. The hydrocarbon product distribution in CO hydrogenation reactions over Fe-Ru bimetallic catalysts has been found to vary dramatically with the relative proportions of the two component metals [5].

Numerous studies of different bimetallic Fe:Ru combinations have been reported in the literature, but a comparison of the reported results is difficult, since different authors have used different supports, methods of preparation, and metal loadings [6].

In many heterogeneous reactions, the active phase is spread on a support. A catalyst support is not merely a carrier but it may also contribute to the activity of the catalyst. Earlier studies have indicated that using carbon as a support to provide an inert, poorly interacting surface could moderate the catalytic behavior of metals such as iron and ruthenium [7-12]. In particular, it has been noted that CNTs provide a relatively inert support, suggesting that this is a unique system for the study of the catalytic behaviour of metals since it provides reduced support interactions. This also suggests the use of carbon nanotubes (CNTs) as an alternative to amorphous carbon.

Tubular carbon, as a support, exists in a number of forms including plates [13], fishbone structures (both filled and unfilled, usually referred to as carbon nanofibres (CNFs)) [13, 14] and classical nanotubes both as single-walled (SWCNTs) and multi-walled (MWCNTs) types [8, 15]. These materials have been used as supports in FT studies. Both Fe and Co have been supported on these materials [7, 8, 15-19]. The relationship between results obtained from these different forms of carbon has not been elucidated in this study and will be discussed elsewhere.

In a previous study, we have reported the use of carbon nanotubes as a support for iron catalysts in the Fischer-Tropsch synthesis [8]. The use of the tubular carbon as a support was found to stabilize highly dispersed iron particles formed from an aqueous impregnation technique using $\text{Fe}(\text{NO}_3)_3$ [7]. In addition, van Steen and Prinsloo [19] have studied Fe/CNF for FT synthesis and more recently Guzzi et al. [15] have compared the activity of Co and Fe/CNTs for FT synthesis.

While Ru has been supported on CNTs and the materials have been investigated in many catalytic reactions [20] (for example, NH_3 synthesis [21] and the hydrogenation of cinnamaldehyde [22]) the use of Ru on CNTs in the FT reaction has not previously been described. In this paper we report on the role of Ru as a co-catalyst for an Fe:Ru catalyst supported on MWCNTs for use in the FT reaction. The small particle Fe:Ru catalysts were also promoted with Cu and K, and the influence of these classical Fe FT promoters is described.

4.2. Experimental

4.2.1. Catalyst Preparation

CNTs were synthesized by the catalytic decomposition of C_2H_2 at $700^\circ C$ over iron supported on $CaCO_3$, as described elsewhere [7, 8, 23]. To avoid confusion with the catalyst used in the FT study, this catalyst will be referred to as the precursor catalyst. Approximately 2.5 g of the nanotubes and some amorphous material were formed for every 1 g of precursor catalyst used. A 30% HNO_3 solution was used to purify the CNT product [8, 24]. The recovered nanotube material was then washed with distilled water until neutral before being dried overnight at $120^\circ C$.

The carbon products of twelve CNT synthesis reactions were combined and thoroughly mixed to provide a homogeneous support material. Catalysts containing 10% iron supported on carbon nanotubes and promoted by 0.25% Ru were prepared by the incipient wetness (IW) impregnation process. In this method, $Fe(NO_3)_3 \cdot 9H_2O$ (7.21 g) and $C_8H_{12}O_8Ru_2$ (0.07 g), which was prepared in our laboratory according to the method described elsewhere [25], were dissolved in de-ionized water (18 ml) and added to 10 g of the carbon nanotube support. Three promoted catalysts (10FeRuCu, 10FeRuK and 10FeRuCuK) were similarly prepared by adding Cu, K or Cu and K to the 10% Fe catalyst. Thus KNO_3 (0.052 g; 0.2% K) and/or $Cu(NO_3)_2 \cdot 3H_2O$ (0.228 g ;

0.6% Cu) were added to an iron-ruthenium solution prepared as above and the mixture added drop-wise to 10 g of carbon nanotube support.

Keeping the Fe:Ru molar ratio the same, at 7.24, two other catalysts containing 5% and 2.5%Fe, i.e. 0.125%Ru and 0.0625%Ru (5Fe/0.125Ru and 2.5Fe/0.0625Ru) were also prepared by the incipient wetness (IW) impregnation method. For the preparation of these catalysts, $\text{Fe}(\text{NO}_3)_3 \cdot 9\text{H}_2\text{O}$ (3.605 g and 1.8035 g) and ruthenium acetate $\text{C}_8\text{H}_{12}\text{O}_8\text{Ru}_2$ (0.07 g, 0.35 g and 0.175g) were successively dissolved in de-ionized water (18 ml) and added to 10 g of the carbon nanotube support. Finally a 5% Fe catalyst loaded with 0.25% Ru (5Fe/0.25Ru) was also synthesised by the same procedures.

All the samples prepared were further dried in an oven (120°C, in static air overnight) and then heated in nitrogen at 220°C for 2.5 hours.

ICPOES (ICP Optical Emission Spectroscopy) analysis of the catalysts revealed that the metal ratios obtained on the CNT support are very close to those predicted from the catalyst preparation procedure (Table 4.1).

Table 4.1: Actual metal content of various catalysts as determined by ICPOES

Catalysts composition	Notation	%Fe	%Ru	%K	%Cu
5%Fe/0.25%Ru/CNT	5Fe/0.25Ru	5.6	0.3	0	0
10%Fe/0.25%Ru/CNT	10Fe/0.25Ru	11.8	0.4	0	0
10%Fe/0.25%Ru/0.2%K/CNT	10FeRuK	9.8	0.2	0.4	0
10%Fe/0.25%Ru/0.6%CuCNT	10FeRuCu	10.9	0.5	0	0.6
10%Fe/0.25%Ru/CNT/0.2%K/0.6%C	10FeRuCuK	10.7	0.3	0.6	0.7
5%Fe/0.125%Ru/CNT	5Fe/0.125Ru	4.9	0.13	0	0
2.5%Fe/0.0625%Ru/CNT	2.5Fe/0.0625Ru	2.8	0.06	0	0

4.2.2. Catalyst Characterization

A Du Pont 951 TGA (Thermo gravimetric analyzer), a JEOL JEM 100S (Transmission electron microscope) and a TPR (temperature programmed reduction) apparatus, constructed in our laboratory, were used to characterize the CNT and the FT catalysts supported on carbon nanotubes. All characterization analyses were performed according to standard procedures as described previously [8].

The surface areas of the carbon nanotubes and the prepared catalysts were determined using the BET method. Approximately 0.25 g of each sample was weighed, and then degassed at 120°C overnight. These samples were then analysed via N₂ physisorption

using a Micromeritics Tristar 3000 Surface Area and Porosity Analyser, and a comparison between the surface areas of the catalysts with high and low metal loadings was made.

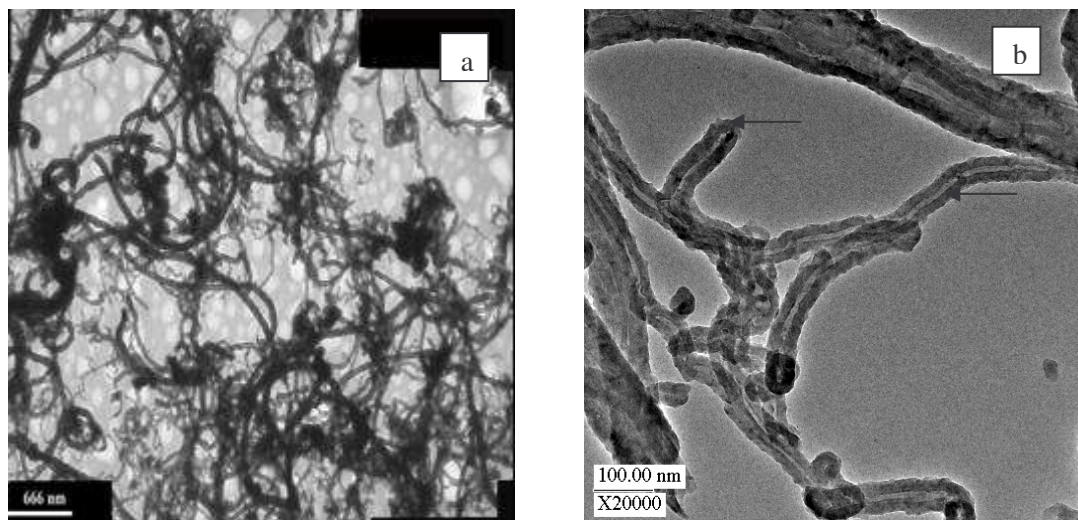
4.2.3. Catalytic measurements

The catalytic measurements were carried out in a fixed bed micro reactor as described previously [8, 26]. Fresh catalyst (0.3 g) was first reduced in a stream of pure hydrogen (350°C, 2 bar) for 24 hours and then cooled to the reaction temperature. The stream of pure hydrogen was then replaced by syngas (30% CO; 60% H₂; 10% Ar). Two sets of reaction data were collected: one set of reactions was carried out at the same flow rate, i.e. at a space velocity of 2142 h⁻¹, and a second set of reactions was carried out at similar conversions, at space velocities of approximately 4615 h⁻¹. Ar was used as an internal standard in order to ensure accurate mass balances. All the experiments were carried out at 275°C and 8 bar. The apparatus and all the experimental details have been described elsewhere [8]. Mass balance calculations similar to those used by Duvenhage and Coville [26] and described in a previous study [8] were used.

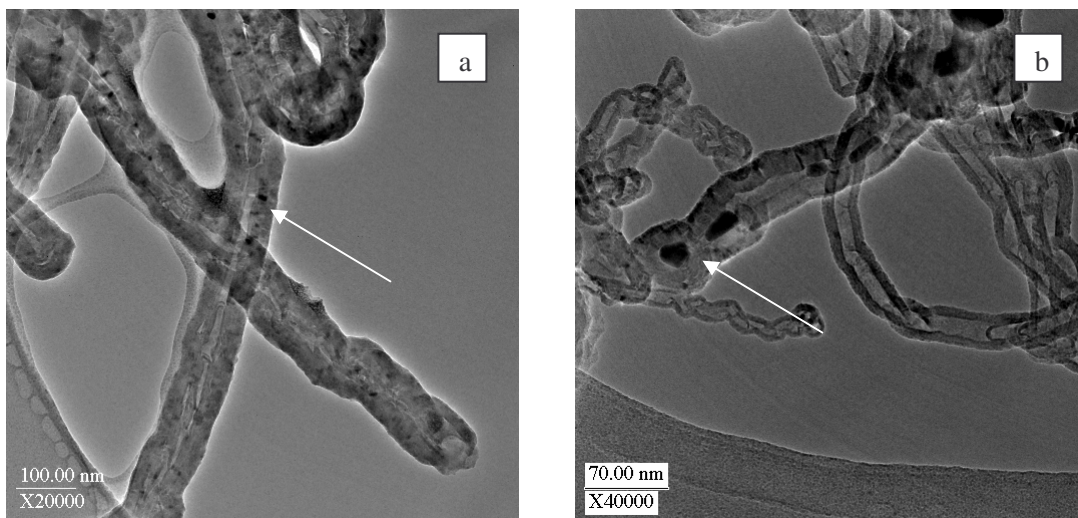
4.3. Results and Discussion

4.3.1. Catalyst characterization

Samples of the purified CNT material was analysed by TEM. The purified product is comprised of an interwoven matrix of tubes (Fig. 4.1a) that was shown to be comprised of multiwalled carbon nanotubes (MWCNTs) (Fig. 4.1b) with predominantly closed ends (Fig. 4.1b). The TEM images of the iron-ruthenium CNT catalysts revealed that the catalyst particles are well dispersed on the surface of the CNTs. The catalyst particles are very small (Fig. 4.2a; < 5 nm), and indeed smaller than those obtained when Fe alone was supported on the same CNTs [8]. The internal channel in the CNTs contains some residual material (Fe) not removed by the acid treatment (Fig. 4.2b).



Figures 4.1a and 4.1b: TEM images of the purified carbon nanotubes



Figures 4.2a and 4.2b: TEM images of iron-ruthenium based catalysts supported on carbon nanotubes

In general, the BET surface areas (Table 4.2) are very low for all the catalysts studied. Comparison of the 10Fe/0.25Ru sample with the 2.5Fe/0.0625Ru sample indicates that the range of surface areas determined for the different samples (40 versus 17 m²/g). These surface areas are much smaller than those reported by other workers (e.g. ref 15) and arise from the use of a weak acid washing to remove the support and Fe catalyst from the MWCNTs. This washing does not open the tubes (Fig. 4.2a).

Table 4.2: BET surface areas and pore volume of the different catalysts

Sample	BET Surface Areas ($\text{m}^2 \cdot \text{g}^{-1}$)	Pore Volume ($\text{cm}^3 \cdot \text{g}^{-1}$)
CNT	29	0.086
5Fe/0.25Ru	39	0.103
10Fe/0.25Ru	40	0.102
10FeRuCu	49	0.106
10FeRuK	38	0.090
10FeRuCuK	43	0.106
5Fe/0.125Ru	18	0.059
2.5Fe/0.0625Ru	17	0.059

TPR analyses were performed to evaluate the effect of Ru, Cu and K on the reducibility of the Fe/CNT material (Fig. 4.3). Two broad peaks are present in all the TPR-profiles. The first peak is assigned to the reduction of iron oxide. The second peak that is observed at temperatures above 550°C is assigned to both iron oxide particles interacting with carbon as well as the possible gasification of the carbon nanotubes since Fe can act as a catalyst for the formation of methane from CNTs and H₂. This latter phenomenon was described by van Steen and Prinsloo [19] and was observed in a previous study on iron supported on carbon nanotubes [8].

The TPR data reveal the classical effects expected on addition of traditional Fe promoters to the Fe:Ru catalyst. Thus, the addition of Cu lowers the reduction temperature while K has little effect relative to the unpromoted catalyst. It has been proposed that the reduction of iron catalysts, promoted by Cu, is the result of H₂ dissociation sites formed on Cu metal [27]. When copper is added to an iron catalyst, it is generally accepted that the reduction peaks associated with the transformation of CuO → Cu and Fe₂O₃ → Fe₃O₄ overlap [28].

A set of TPR experiments on different unpromoted catalysts (Fig. 4.4) in which either the same Fe:Ru ratio was used or the Fe content was kept constant and the Ru content was varied, was also carried out.

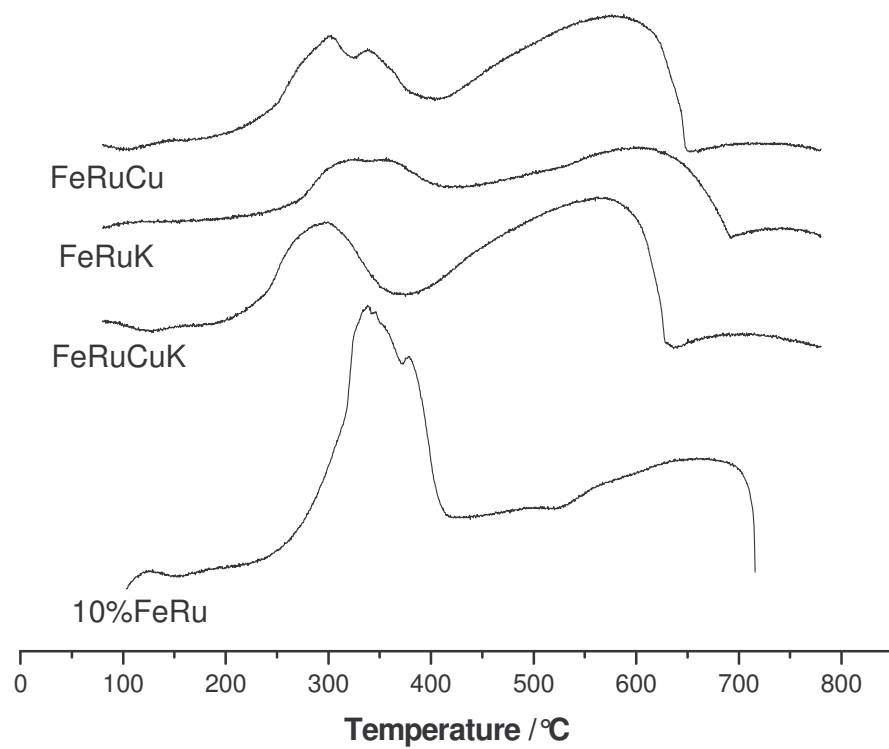


Figure 4.3: TPR profiles of various calcined catalysts.

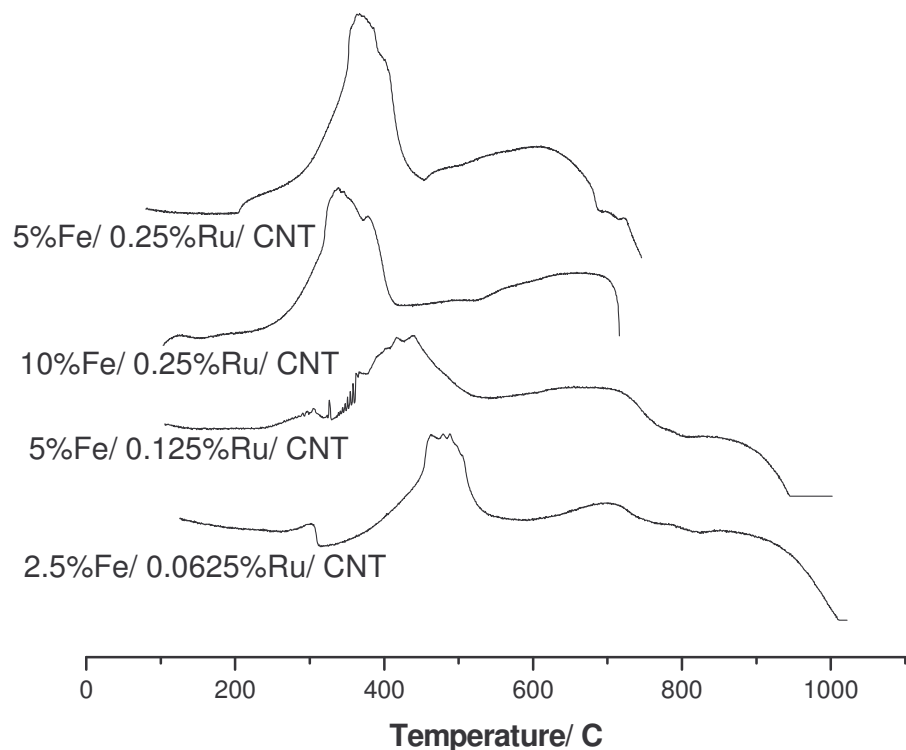


Figure 4.4: TPR profiles of various calcined catalysts with same Fe/Ru ratio

As the metal loading decreased for the complexes that had the same Fe:Ru ratio, the peaks in the TPR profiles were shifted to higher temperatures. For the 10Fe/0.25Ru catalyst the first peak is situated at ca. 340°C and the onset of the second peak occurs just above 600°C. For the 5Fe/0.125Ru and 2.5Fe/0.0625Ru catalysts the first peak shifts from 400°C to 450°C while the second peak occurs at about 700°C. The increase in reduction temperature (first peak shifted to the right) is associated with a dispersion effect which relates to increased Fe-carbon surface interactions.

In general, it is known that dispersion increases as the metal loading decreases [29]. Schay et al. [30] have shown that at low metal loading and high Fe:Ru ratios, ruthenium promotes the reduction of iron on samples prepared from co-impregnated Fe:Ru carbonyls on silica. Van der Kraan et al. [31] have shown that the presence of Ru lowers the reduction temperature for Fe supported on TiO₂. In a comparative study, Berry et al. [5] reported that as the ruthenium content in the iron-ruthenium catalysts is increased, the temperature corresponding to the reduction of iron on alumina or silica decreases.

A comparison between two catalysts (5Fe/0.125Ru and 5Fe/0.25Ru) in our study revealed the same trend; thus as the Ru content increased the reduction temperature corresponding to the reduction of Fe:Ru supported on carbon nanotubes decreased from about 440°C to below 400°C (Fig. 4.4).

The TPR profiles for the 5Fe/0.25Ru and 10Fe/0.25Ru catalysts reveal a shift of the TPR peaks to *higher temperature* as the Fe content decreases (Fig. 4.4, 370°C versus 340°C).. This suggests that in this instance the Fe-surface carbon interaction dominates (dispersion) over the ability of the Ru to reduce the Fe when the higher Fe:Ru ratio is used.

4.3.2. Catalytic activity

4.3.2.1. Effect of promoters

An attempt was made to determine the effect of promoters on both the activity (reactions carried out at constant flow rate) and selectivity (reactions at constant CO conversion). Fig. 4.5 shows the activity plots from the FT study in terms of the percentage conversion of CO, as a function of time on stream at constant flow rate. The data shown in Table 3 compares the CO conversion, rates of CO consumption, and the effect of additives on the activity of the different catalysts. All the reactions were performed under a set of standard conditions (275°C, 8 bar, H₂/CO = 2/1).

The initial CO conversion for all the catalysts studied increased and then stabilized within 15h to a value between 40 and 60%. The activity of 10Fe/0.25Ru was lowest (~ 40 %), and all of the promoted catalysts (10FeRuK, 10FeRuCu and 10FeRuCuK) exhibited higher conversions, namely between 50 and 60%. Of these three promoted catalysts, the 10FeRuCu catalyst had the highest conversion at about 60%. However, after a disturbance in the flow rate that occurred during this experiment the conversion dropped to about 54% but still remained steady at this value for the rest of the run.

After the initial increase, the conversion remained steady for the catalysts (104 h), except for 10FeRuK which declined very slightly from about 57% down to 53%.

The overall conclusion that can be drawn is that the catalysts are remarkably stable. This suggests that the metal particles are not sintering or being deactivated by carbon coverage with time.

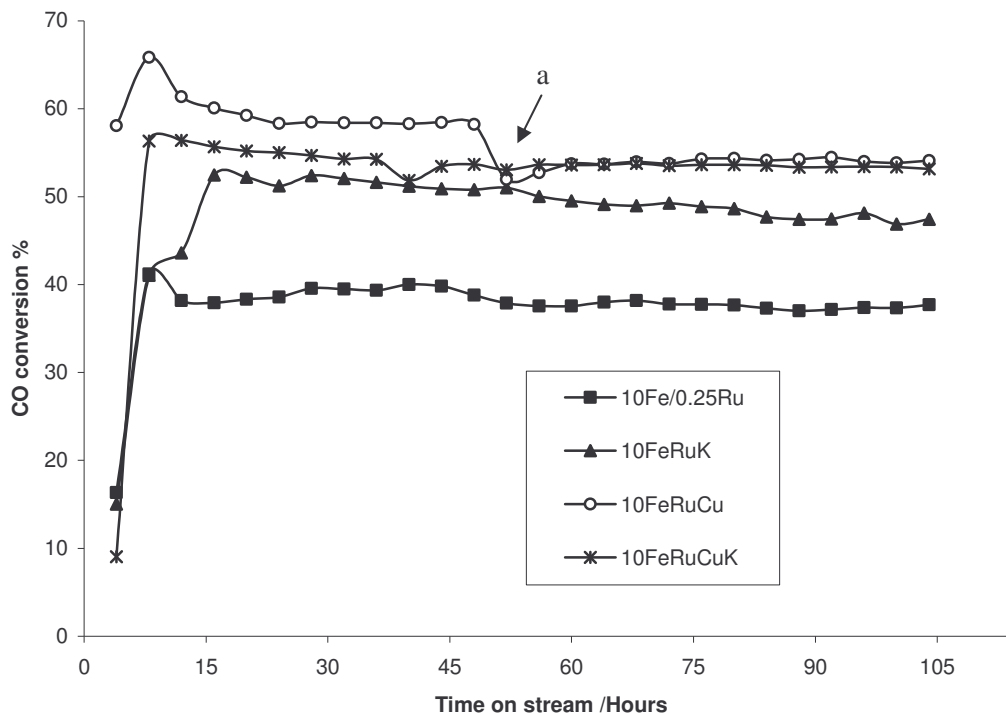


Figure 4.5: CO conversion with time on stream (same flow rate) for promoted Fe:Ru catalysts. The drop in conversion at (a) is attributed to a change in the flowrate.

Table 4.3: Activity and selectivity of Iron- Ruthenium catalysts

(Same flow rate, Large range of conversion: 60 – 36%)

Catalysts	10Fe/0.25Ru	10FeRuCu	10FeRuK	10FeRuCuK
CO conv.(%)	38	54	50	54
CO rate ^a	-1.36E-06	-1.80E-06	-1.74E-06	-1.80E-06
CO ₂ rate	6.28E-07	9.01E-07	8.48E-07	9.49E-07
FTS rate	7.33E-07	9.03E-07	8.94E-07	8.54E-07
Activity ($\mu\text{mol}/\text{sec}.\text{gFe}$)	45.39	60.13	58.05	60.11
Alpha (α)	0.61	0.54	0.72	0.68
Selectivity (%)				
C ₁	21.3	25.3	11.0	19.3
C ₂ -C ₄	41.4	44.3	23.3	41.6
C ₅ -C ₁₁	33.1	28.6	51.1	35.3
C ₁₂₊	3.9	1.7	5.6	3.0
C ₂ ⁼ / (C ₂ + C ₂ ⁼) ^b	13.0	4.7	46.9	25.4
CO ₂	10.2	14.6	13.8	15.4

^a Rate [mol/sec]

^b Olefin to total C₂ hydrocarbon weight ratio

Addition of Cu to the 10Fe/0.25Ru (10FeRuCu catalyst) resulted in a significant increase in CO reaction rate, CO₂ production rate and catalyst activity (Fig. 4.5 and Table 4.3). These trends are expected and are consistent with the TPR data i.e. with

the ability of Cu to lower the reduction temperature of Fe thus providing more active iron sites for catalysis [33, 34]. Product selectivities for the 10Fe/0.25Ru and 10FeRuCu catalysts are shown in Table 4.3. The low Cu loading did modify the catalyst selectivity, but not significantly. Methane and CO₂ selectivity have increased and the alpha value has decreased. For the 10FeRuK catalyst, an increase in olefinitivity and a decrease in CH₄ content relative to the Fe:Ru and 10FeRuCu catalysts are shown in Table 4.3. This is expected and is consistent with findings for Fe catalysts [35-38].

As shown in Fig. 4.5, the CO conversions are spread over a large range (36 – 60 %) and thus the observed differences in the catalyst behavior may simply be due to the different conversions. For a better understanding of the catalysts behavior, another set of FT reactions was then performed at a similar conversion by varying the flow rates. Data are shown graphically in Fig. 4.6. The CO conversion is spread between 20 and 28 %.

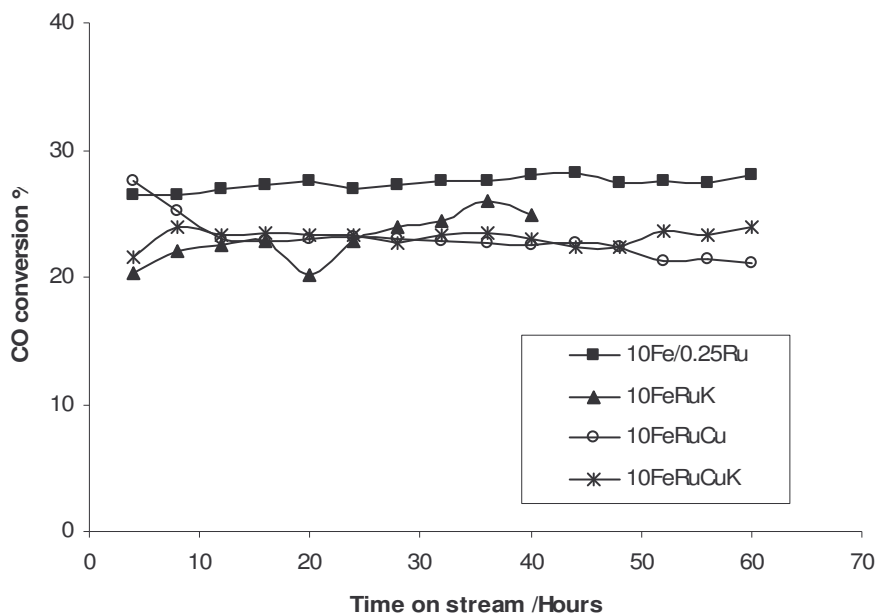


Figure 4.6: CO conversion with time on stream for promoted Fe:Ru catalysts

A comparison of the selectivities at similar conversion was made (Table 4.4). The predicted effect of K on olefin selectivity was observed. Little effect of K on the methane and hydrocarbon selectivity was observed, which was unexpected. The addition of Cu to the Fe:Ru catalyst generates a catalyst that produces a product that is more hydrogenated and again the result can be expected from the spillover effects associated with Cu. Thus, the overall effect of the promoters on the selectivity is similar to that expected for a typical Fe catalyst.

A comparison of the data in Tables 4.3 and 4.4 can also be made. In general, the selectivities to CO₂ and methane increase with increasing syngas conversion. At the

lower CO conversion, the olefin to paraffin ratio increased and the methane selectivity decreased for all the catalysts studied compared to the CO conversions at the higher conversion. This agrees with typical literature reports where increases in CO conversion have been shown in general to decrease the olefin to paraffin ratio [8, 39] and to increase the methane and the CO₂ selectivity [5].

Table 4.4: Activity and selectivity of Iron- Ruthenium catalysts

(Variable flow rates, conversions 20-30%)

Catalysts	10Fe/0.25Ru	10FeRuCu	10FeRuK	10FeRuCuK
CO conv. (%)	28	23	25	23
CO rate ^a	-1.97E-06	-1.72E-06	-3.32E-06	-7.47E-07
CO ₂ rate (WGS)	7.82E-07	8.14E-07	1.44E-06	2.82E-07
FTS rate	1.19E-06	9.04E-07	1.88E-06	4.66E-07
Activity				
($\mu\text{mol}/\text{sec} \cdot \text{gFe}$)	65.71	57.27	110.64	24.91
Alpha (α)	0.74	0.58	0.70	0.72
Selectivity (%)				
C ₁	14.7	16.8	14.5	11.4
C ₂ -C ₄	31.4	51.7	39.3	22.4
C ₅ -C ₁₁	48.9	30.5	46.0	62.1
C ₁₂₊	5.0	0.9	0.1	4.1
C ₂ ⁼ / (C ₂ + C ₂ ⁼) ^b	26.2	4.7	68.4	38.5
CO ₂	5.5	6.1	10.0	2.1

^a (mol/sec)

^b Olefin to total C₂ hydrocarbon weight ratio

4.3.2.2. Effect of Ruthenium

The effect of keeping the Fe:Ru ratio constant on the FT CO conversion is shown in Figure 4.7. As can be seen, the conversion increases with metal loading. However,

the decrease in the conversion is not linearly related to the metal loading, i.e. the CO conversion over the 10Fe/0.25Ru catalyst is not twice the conversion obtained over the 5Fe/0.125Ru catalyst and likewise for the 5Fe/0.125Ru and 2.5Fe/0.0625Ru.

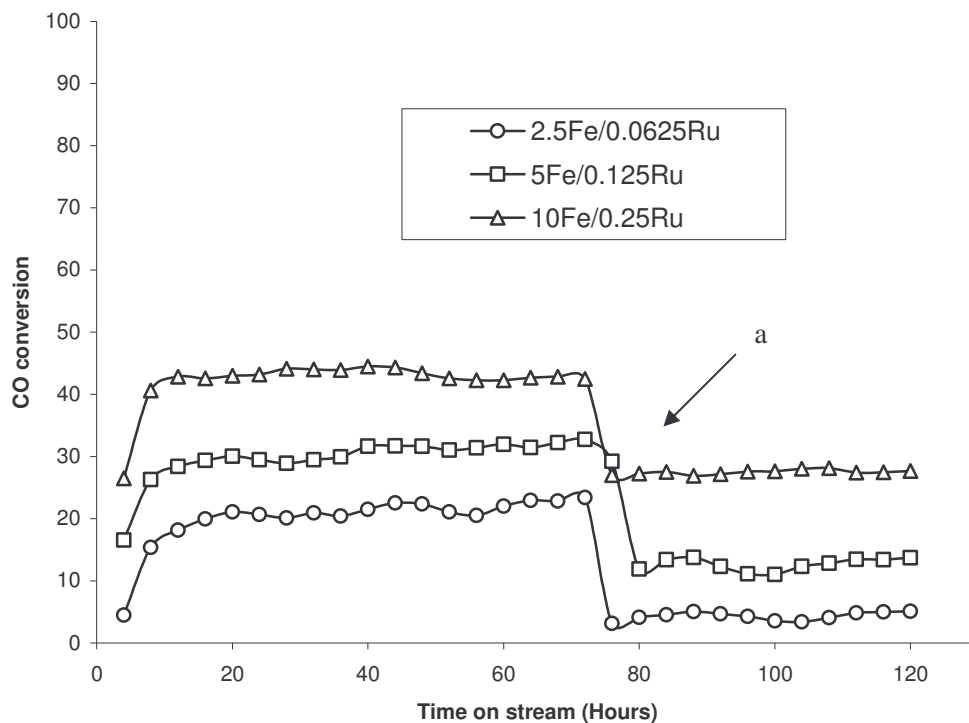


Figure 4.7: CO conversion with time on stream (same flow rate) for a series of Fe:Ru catalysts. The drop in conversion at (a) is due to a change in the flowrate.

In all three cases remarkable stability in the conversion data was noted. When the flow rates were changed after 70 h reaction, the reaction rapidly reached steady conversion level and again constant CO conversion was noted over the next 50 h.

Selectivity (and activity) data are also shown in Table 4.5. In general as the total metal loading increases the methane content and CO₂ content increase, while the product chain length increases slightly (the alpha values stay near constant). In these reactions the selectivity could be affected by conversion so no further analysis of the data will be given.

FT reactions involving the catalysts 10Fe/0.25 Ru and 5Fe/0.25Ru were also compared in terms of activity data (Fig 4.7; constant flowrate). The selectivity data are shown in Table 4.6. The methane selectivity increased while the C₅-C₁₁ fraction decreased with a decrease in the Fe loading, consistent with the lower Fe:Ru ratio of the latter catalyst.

Table 4.5: Activity and selectivity of catalysts with same Fe/Ru ratio

Catalysts	Same flow rates			Variable flow rates		
	10Fe/0.25Ru	5Fe/0.125Ru	2.5Fe/0.0625Ru	10Fe/0.25Ru	5Fe/0.125Ru	2.5Fe/0.0625Ru
CO conv. (%)	44	32	23	28	12	4
CO rate ^a						
CO ₂ rate	-1.36E-06	-7.65E-07	-5.52E-07	-1.97E-06	-9.30E-07	-6.56E-07
FTS rate ^b	6.28E-07	2.34E-07	9.30E-08	7.82E-07	2.56E-07	0.0
	7.33E-07	5.31E-07	4.59E-09	1.19E-06	6.64E-07	6.56E-07
Activity						
	45.39	25.51	18.40	65.71	30.99	21.86
Alpha(α)						
Selec (%)	0.61	0.58	0.61	0.74	0.60	0.61
C ₁						
C ₂ -C ₄						
C ₅ -C ₁₁	21.3	24.3	30.3	14.7	25.8	30.7
C ₁₂₊	41.4	45.9	44.2	31.4	41.8	44.9
C ₂ ⁼ /Total C ₂ ^c	33.1	28.7	21.1	48.9	29.5	24.4
CO ₂	3.9	0.8	0.3	5.0	2.5	0.0
	13.0	7.4	12.6	26.2	9.6	12.6
	10.2	3.8	1.5	5.5	1.5	0.0

^a Rate [mol/sec]

^b [μ mol/sec.gFe]

^c Olefin to total C₂ hydrocarbon weight ratio

Table 4.6: Activity and selectivity of 5%Fe/ 0.25%Ru catalyst at high and low conversion

Catalyst	High conversion: $\pm 55\%$	Low conversion: $\pm 20\%$
	5Fe/0.25Ru	5Fe/0.25Ru
CO rate	-1.81E-06	-1.94E-06
CO ₂ rate	8.91E-07	8.05E-07
FTS rate	9.18E-07	1.17E-06
Activity ($\mu\text{mol}/\text{sec}\cdot\text{gFe}$)	120.62	131.60
Alpha(α)	0.53	0.72
Selec (%)		
C ₁	29.4	21.1
C ₂ -C ₄	44.2	34.2
C ₅ -C ₁₁	26.5	40.6
C ₁₂₊	0.0	4.1
C ₂ ⁼ /Total C ₂	6.8	24.0
CO ₂	14.5	6.1

Table 4.7: Results of Fe-Ru catalysts supported on various materials

Catalyst	Temperature	H ₂ /CO	Activity	Conversion	Selectivity	
	(K)	Ratio	($\mu\text{mol.g}^{-1}.\text{s}^{-1}$)	(%)	C ₁ %	C ₂ ⁼ /C ₂
5Fe/0.25Ru	548	2:1	120.6	55.0	29.4	0.07
10Fe/0.25Ru	548	2:1	45.4	38.0	21.3	0.13
10FeRuCu	548	2:1	60.1	54.0	25.3	0.05
10FeRuK	548	2:1	58.1	50.0	11.0	0.47
10FeRuCuK	548	2:1	60.1	54.0	19.4	0.25
5% Fe /Carbolac ^a	503	3:1	-	3.0	23.0	0.35
0.97%Fe/ 0.77%Ru/C ^b	548	3:1	-	3.2	76.0	0.15
0.70%Fe/ 2.35%Ru/C ^b	548	3:1	-	4.4	88.0	0.11

^a Bartholomew et al. [28] comparable activity and C₂⁼ selectivity data not available.

^b Kaminsky et al. [29]

A comparison of the 5Fe/0.25Ru and 10Fe/0.25Ru catalysts at approximately the same flow rate (Fig. 4.7) reveals that the CO conversion and the methane selectivity of the latter are lower (Table 4.5 and 4.6). This indicates that although the higher relative Ru content should increase the reducibility of the 5Fe/0.25Ru catalyst compared to the 10Fe/0.25Ru catalyst, resulting in a higher CO conversion, this is not observed.

It is to be noted that Kaminsky et al. [10] also observed higher CO hydrogenation and methanation activities for catalysts with increasing Ru content. Contrary to the results of Kaminsky et al. [10], we found a lower CO₂ selectivity with the catalyst with the higher Fe content. It is to be noted however, that a slight increase in CO₂ selectivity has been observed as carbon builds up on the surface of Fe-Ru catalysts, and that this is accompanied by an increase in methane selectivity [32].

WGS and FTS rates for the 10Fe/0.25Ru and 5Fe/0.25Ru catalysts are also shown in Table 4.5. The WGS rate decreases with decreasing Fe content.

The effect of Ru content on the selectivity and activity of the catalysts was studied by keeping the Fe content constant and varying the Ru content i.e. by comparing the behaviour of the 5Fe/0.25Ru and 5Fe/0.125Ru catalysts. At a similar flow rate, the 5Fe/0.25Ru catalyst is far more active than the 5Fe/0.125Ru catalysts (Table 4.5 and 4.6); the increase of the Ru content increased the methane and the CO₂ selectivities. This increase in the CO₂ selectivity with the Ru content is unexpected [5, 10]. Furthermore, contrary to literature reports, the C₂ olefin selectivity did not increase with an increase in the Ru content.

Comparison of our data with similar iron, ruthenium and iron-ruthenium based carbon supported catalysts reported in the literature (Table 4.7) confirmed that when using ruthenium on carbon, the major product formed was methane. Ruthenium on carbon appears to be a methanation catalyst for FT synthesis. From Table 4.6, it can

be seen that the methane selectivity decreases with the decrease in ruthenium content. Although our experiments were carried out at high conversions, our methane selectivities are comparable with those obtained from the literature at low conversions. The low methane selectivity obtained by Bartholomew et al. [40] may be due to the low operating temperature used. It can be assumed that irrespective of the conversion, CNT supported Fe:Ru bimetallic catalysts yield lower methane selectivities compared to Fe:Ru bimetallic catalysts supported on other carbon materials. Using the same operating temperature as in our study and a H₂/CO ratio of 3, Kaminsky et al. [10] obtained a methane selectivity greater than 75% and low C₂ olefin fractions [10, 41]. To enhance the C₂ olefin yield and decrease the methane selectivity when using a Fe:Ru bimetallic catalyst in FT synthesis, the use of low H₂/CO feed ratio and promotion of the catalyst by K can be recommended.

4.4. Conclusion

In this study it has been shown that Fe:Ru bimetallic catalysts supported on carbon nanotubes are stable catalysts in FT synthesis. This implies that small particles (< 5 nm) are stabilised on the carbon and do not sinter significantly during the FT process. The catalysts reach steady state within 15 hours of reaction and remain stable for the rest of the reaction. The presence of ruthenium appears to facilitate the dispersion of the Fe particles on the surface of the CNTs, when compared to Fe/CNT catalysts [8].

In conclusion, the small particle Fe:Ru CNT supported catalysts show behaviour typical of Fe supported catalysts when (i) promoted with K and Cu and (ii) when Fe:Ru loadings and ratios are varied. The catalysts have the added advantage of a support interaction with the carbon that does not hinder reduction and yet produces a catalyst which does not sinter significantly in the FT reaction. It is thought that the moderate metal support interaction accounts for the catalyst stability.

References

- [1]. Guzzi, L. New trends in CO activation, ELSEVIER, vol. 64, 1991
- [2]. Kannan, K.R., Kulkarni, G.U., Rao, C.N.R. Catal. Lett. 14 (1992) 149
- [3]. Lázál, K., Reiff, W.M., Mörke, W., Guzzi, L. J. Catal. 100 (1986)118
- [4]. Ott, G.L., Fleisch, T., Delgass, W.N. J. Catal. 60 (1979) 394
- [5]. Berry, F.J., Liwu, L., Chengyu, W., Renyuan, T., Su, Z., Dongbai, L. J. Chem. Soc. Faraday Trans. I 81 (1985) 2293
- [6]. Niemantsverdriet, J.W., van Kaan, J.A.C., Flipse, J.F.C., van der Kraan, and A.M.J. Catal. Today 96 (1985) 58
- [7]. Jung, H. J., Walker Jr, P. L., Vannice, M. A. J. Catal. 75 (1982) 416
- [8]. Bahome, M.C., Jewell, L.L., Hildebrandt, D., Glasser, D., Coville, N.J. Appl. Catal. A: Genl 287 (2005) 60
- [9]. Vannice, M. A., Garten, R. L. J. Catal. 63 (1980) 255
- [10]. Kaminsky, M., Yoon, K. J., Geoffroy, G. L., Vannice, M. A. J. Catal. 91 (1985) 338
- [11]. Jones, V.K., Neubauer L.R., Bartholomew, C.H. J. Phys. Chem. 90 (1986) 4832
- [12]. Chen, A.A., Vannice, M.A., Phillips, J.J. Phys. Chem. 91 (1987) 6257
- [13]. Yu, Z., Borg, Ø, Chen, D., Enger, B.C., Frøseth, V., Rytter, E., Wigum, H. A. Holmen, Catal. Lett. 109 (2006) 43
- [14]. Winter, F., Bezemer, G.L., van der Spek, C., Meeldijk, J.D., van Dillen, A.J., Geus, J.W., de Jong, K.P. Carbon 43 (2005) 327
- [15]. Guzzi, L., Stefler, G., Geszti, O., Koppány, Zs, Kónya, Z., Molnár, É, Urbán, M., Kiricsi, I. J. Catal 244 (2006) 24

- [16]. Bezemer, G.L., Falke, U., van Dillen, A.J., de Jong, and K.P. Chem. Commun. (2005) 731
- [17]. Bezemer, G.L., Radstake, P.B., Koot, V., van Dillen A.J., Geus, J.W., de Jong, K.P. J Catal, 237 (2006) 291,
- [18]. Bezemer, G.L., Bitter, J.H., Kuipers, H.P.C.E., Oosterbeek, H., Holewijn, Xu, J. E X., Kapteijn, F., van Dillen A.J., de Jong, K.P. JACS, 128 (2006) 3956
- [19]. van Steen, E., Prinsloo, F. F. Catal. Today 71 (2002) 327
- [20]. Fu, X., Yu, H., Peng, F., Wang, H., Qian, Y. Appl. Catal. A: Genl (2007) doi:10.1016/j.apcata.2007.02.002
- [21]. Chen, H.-B., Lin, J.-D., Cai, Y., Wang, X.-Y., Yi, J., Wang, J., Wei, G., Lin, Y.-Z., Liao, D.-W. Appl. Surf. Sci. 180 (2001) 328
- [22]. Toebes, M. L., Prinsloo, F.F., Bitter, J.H., van Dillen A.J. de Jong, K. P., J Catal., 214 (2003) 78
- [23]. Mabudafhasi, M. L., Bodkin, R., Nicolaidis, C. P., Liu, X-Y., Witcomb, M. J., Coville, N. J. Carbon 40 (2002) 2737
- [24]. Couteau, E., Hernadi, K., Seo, J. W., Thiên-Nga, L., Mikó, Cs., Gaál, R., Forró., L. Chem. Phys. Lett. 378 (2003) 9
- [25]. Legzdins, P., Mitchell, R.W., Rempel, G.L., Ruddick, J.D., Wilson, G., J. Chem. Soc. A (1970) 3322
- [26]. Duvenhage, D.J., Coville, N.J. Appl. Catal. A: Genl 153 (1997) 43
- [27]. Li, S., Krishnamoorthy, S., Li, A., Meitzner, G. D., Iglesia, E. J. Catal. 206 (2002) 202

- [28]. Wu, B., Yian, L., Bai, L., Zhang, Z., Xiang, H., Li, Y. W. Catal. Communications 5 (2004) 253
- [29]. Guzzi, L., Schay, Z., Matusek, K., Bogyay, I. Appl. Catal. 22 (1986) 289
- [30]. Schay, Z., Lázál, K., Mink, J., Guzzi, L. J. Catal. 87 (1984) 179
- [31]. van der Kraan, A.M., Nonnekens, R.C.H., Stoop, F., Niemantsverdriet, J.W. Appl. Catal., 27 (1986) 285
- [32]. Ott, G. L., Fleisch, T., Delgass, W. N. J. Catal. 65 (1980) 253
- [33]. O'Brien, R. J., Davis, B.H. Cat. Lett. 94 (2004) 1
- [34]. O'Brien, R. J., Xu, L., Spicer, R. L., Bao, S., Milburn, D. R., Davis, B. H. Catal. Today 36 (1997) 325
- [35]. Anderson, R. B., Seligman, B., Schultz, J. F., Elliot, M. A. Ind. Eng. Chem. 44 (1952) 391
- [36]. Dry, M. E., Shingles, T., Boshoff, L. J., Oosthuizen, G. J. J. Catal. 15 (1969) 190
- [37]. Luo, M., O'Brien, R. J., Bao, S., Davis, B. H. Appl. Catal. A: Genl 239 (2003) 111
- [38]. Wilfried, H., Zhang, Y., O'Brien, R.J., Luo, M., Davis, B. H. Appl. Catal. A: Genl 36 (2002) 77
- [39]. Jung, H. J., Vannice, M. A., Mulay, L. N., Stanfield, R. M., Delgass, W. N. J. Catal. 76 (1982) 208
- [40]. Bartholomew, C.H., Jones, V.K., Neubauer, L.R. AIChE National Meeting, 1986
- [41]. Sommen, A. P. B., Stoop, F., Van der Wiele, K. Appl. Catal. A: Gen. 14 (1995) 277

CHAPTER 5: COBALT CATALYSTS SUPPORTED ON CARBON NANOTUBES FOR THE FISCHER-TROPSCH SYNTHESIS

5.1. Introduction

Fischer-Tropsch (FT) synthesis for converting syngas to hydrocarbons has been recognised as an important process in the production of transportation fuels and chemicals [1-3]. Due to the number of products that are formed in this reaction, the FT reaction system is possibly a complex reaction system and lack of control of the product selectivity has been considered as of the principal problems associated with this process.

Although several metals are active for the FT synthesis, only iron and cobalt catalysts appear economically feasible on an industrial scale [3]. The major difference between these two catalysts is the formation of the oxygen containing product, iron rejects a significant amount of the oxygen in the form of carbon dioxide rather than water while Co generates almost exclusively H₂O as the oxygen containing product. Since Fe generates CO₂, and since Fe can act as a catalyst in the water gas shift reaction, it

can be operated at significantly lower H_2/CO ratios (0.6-1.0) compared with cobalt [3, 4]. However, if syngas is available at a H_2/CO ratio of 2, there is an advantage to using Co based catalysts [4].

Cobalt based catalysts are typically more active for CO hydrogenation than iron catalysts, but they require lower reaction temperatures, since the selectivity to desired C_{5+} hydrocarbons and the quality of the diesel-range products formed over cobalt based catalysts become unacceptable at higher temperatures [4-6]. Iron based catalysts lead to more olefinic products, lower CH_4 selectivities without catalyst damage over a wider range of reaction conditions (temperature, H_2/CO ratio) than cobalt based catalysts [7].

The recent discovery of carbon nanotubes (CNT) has generated great interest in the scientific community [8-13]. Carbon nanotubes are attracting increasing attention as novel media for heterogeneous catalysis. The main advantage of using the CNTs as a support for catalysis reactions is that they possess both reasonable surface area and good conductivity compared with conventional carbon materials, such as graphite (low surface area) and activated carbon (poor electronic conductivity) [14].

Research on Fischer-Tropsch cobalt catalysts has been largely devoted to cobalt supported on oxidic supports such as alumina, silica and titania. A disadvantage of these support materials is their reactivity towards cobalt during either synthesis or catalysis that results in the formation of irreversible mixed compounds [15]. To

overcome these problems, the use of carbon nanotubes has been investigated and reported in the literature [15, 16]. Bezemer et al. [15] have demonstrated that carbon nanofibers (CNF) could be a promising support for the FTS with good activity and selectivity. A remarkable high C₅₊ selectivity of 86 wt% was also obtained for an unpromoted Co/CNF in the same study. And Yu et al. [16] have obtained a significant high C₅₊ selectivity by using platelet CNF supported cobalt catalysts. The activity obtained with these catalysts was comparable with that obtained with a Co/ γ -Al₂O₃ and their selectivity similar to the selectivity obtained with a Co/ α -Al₂O₃.

Recently we reported the use of the carbon nanotubes as a support for an iron based FT catalyst. In this paper, we report the catalytic performance of cobalt supported on carbon nanotubes in a FT fixed bed reactor. A series of cobalt catalysts was prepared by impregnation wetness method and calcined at different temperatures. The effects of the support, metal loading and calcination temperature on the physical properties of the catalysts were studied using different characterization techniques. The catalytic behavior of the new material we reported earlier.

5.2. Experimental

5.2.1. Catalyst preparation

The synthesis of the carbon nanotubes was performed in a quartz tubular reactor placed horizontally in a furnace [17, 18] at atmospheric pressure via the decomposition of acetylene over an iron catalyst supported on calcium carbonate. The supported iron catalyst (100 g) was heated from room temperature to 700°C in 2 hours and 20 minutes under a flow of hydrogen (100 ml min⁻¹). Maintaining the temperature at 700°C, the carbon nanotubes were allowed to grow over a period of 2 hours in pure acetylene (100 ml min⁻¹). After cooling in a flow of hydrogen (60 ml min⁻¹), the product thus produced was purified and washed in a 30% HNO₃ in a manner similar to that reported previously [17]. All the gases used were supplied by AFROX and were UHP.

Both iron and cobalt catalysts supported on carbon nanotubes were prepared by the incipient wetness (IW) impregnation process. In this method, Fe(NO₃)₃·9H₂O (7.21 g) and Co(NO₃)₂·6H₂O (0.07g) were dissolved in de-ionized water (18 ml) and added to 10 g of the carbon nanotube support. A series of bimetallic Fe/Co catalysts were also prepared by the co-impregnation procedure. During this preparation, 5%Fe and 5%Co were deposited by incipient wetness. All the catalysts prepared were further dried overnight in static air in an oven at 120°C. Thereafter the Co catalyst supported on

CNT was divided into four equal portions and each portion was calcined to a different temperature (220, 250, 300 and 350°C) in a flow of nitrogen for 2 hours and 30 minutes. These four different catalysts were referred as [Co(220), Co(250), Co(300) and Co(350)]. The Fe(220) and FeCo(220) catalysts were also calcined at 220°C in a flow of nitrogen for 2 hours and 20 minutes. After the calcinations, the catalysts were then allowed to cool to room temperature in flowing nitrogen and stored under air until they could be tested for catalytic activity.

5.2.2. Catalyst Characterization

The elemental composition of the catalysts was determined by using ICP optical emission spectroscopy. A Du Pont 951 TGA (Thermo Gravimetric Analyzer) was used to determine the decomposition temperature of the CNTs and catalysts. The sizes and morphology of the CNTs and the catalyst particles were determined using a JEOL JEM 100S Transmission electron microscope. A TPR (temperature programmed reduction) apparatus constructed in our laboratory was used for reduction studies. All characterization analyses were performed by classical procedures on apparatus described previously [17]. The determination of the surface areas and pore volumes of the carbon nanotubes and the prepared catalysts were achieved using the BET method. Approximately 0.25 g of each sample was weighed, and then degassed at 120°C overnight. The samples were thereafter analysed via N₂ chemisorption using a Micromeritics Tristar 3000 Surface Area and Porosity

Analyser, and a comparison between the surface areas and pore volume of catalysts was carried out.

5.2.3. Catalytic measurements

The catalytic measurements for FT activity were carried out in a fixed bed micro reactor as described previously [17, 19]. Two traps were placed below the reactor. The first, kept at 150°C, was used to collect the wax. The second, kept at ambient temperature, was used to collect a mixture of water and oil. The gas product from the reactor was directed to two on-line GC, a FID and a TCD, for analysis or vented to atmosphere. All the lines after the reactor were kept at 150°C to prevent the C₊₅ product from the reactor to condense [17]. The products were analysed using an on-line GC for the gaseous product and an off-line GC for the oil and wax as described previously [17, 19].

Fresh catalyst (0.3 g) was first reduced in flowing pure hydrogen at 350°C for 24 hours at a flow rate of 60ml min⁻¹ and a pressure of 2 bar. After reduction, the system was cooled to 275°C and the flow of hydrogen was then replaced by syngas (30% CO; 60% H₂; 10% Ar). For each experiment, three different reactant gas stream space velocities were used. A needle valve was used to control the volumetric flow through the reactor and also to maintain the pressure in the system at 8 bar throughout the reaction. The data was recorded and analysed as described elsewhere [17].

5.3. Results and discussion

5.3.1. Catalyst characterization

The CNT product of seven synthesis reactions were combined and carefully mixed to provide a homogeneous support material. The carbon nanotube yield was calculated as the mass of the product collected excluding the mass of the catalyst. Approximately 2.5 g of carbon nanotubes and some amorphous material was formed for every 1g of catalyst used. The CNTs were then purified with dilute HNO₃ [17] and the purified CNT material was characterized by TEM.

Metal salts (Fe, Co and Fe/Co) were then added to the CNTs as described and ICPOES (ICP Optical Emission Spectroscopy) analysis of the catalysts revealed that the metal weight percentages obtained on the CNT support were very close to those predicted from the catalyst preparation procedure (Table 5.1).

Table 5.1: Metal content of various catalysts

Catalysts	Notation	%Fe	%Co
10%Fe/ CNT	Fe(220)	10.6	0.0
5%Fe/ 5%Co/ CNT	FeCo(220)	5.3	5.1
10%Co/ CNT	Co(220)	0.0	10.2
10%Co/ CNT	Co(250)	0.0	10.4
10%Co/ CNT	Co(300)	0.0	10.3
10%Co/ CNT	Co(350)	0.0	10.0

The BET and pore sizes of the new materials were determined and data are given in Table 5.2. Given the results in Table 5.2, iron catalyst Fe(220) has the higher total surface area ($32.86 \text{ m}^2.\text{g}^{-1}$). It is possible that if the particles are small enough, the catalyst may become lodged in the pores of the catalyst support, thus reducing the overall surface area. In this present situation, it is assumed that the iron particles are bigger than the Co particles. It can also be noted from Table 5.2 that the surface area and the pore volume of the Co catalysts are increasing with the calcination temperature.

Table 5.2: Calcination temperature, BET surface area and pore volume of various catalysts

Catalysts	Calcination temperature	Notation	BET Surface area (m ² /g)	Pore volume (cm ³ /g)
10%Fe/ CNT	220°C	Fe(220)	32.9	0.071
5%Fe/ 5%Co/ CNT	220°C	FeCo(220)	19.3	0.062
10%Co/ CNT	220°C	Co(220)	21.7	0.065
10%Co/ CNT	250°C	Co(250)	22.7	0.073
10%Co/ CNT	300°C	Co(300)	25.8	0.086
10%Co/ CNT	350°C	Co(350)	26.6	0.101

Fig 5.1 shows TEM images of Fe particles supported on CNT. CNT are hollow with the graphite sheets parallel to the axis of the CNT. Catalyst particles trapped in the CNT can easily be seen. Fe particles can not be seen on the surface of the CNT support (Fig 5.1a). However, small Fe particles with sizes less than 1 nm can be seen on the same TEM image in dark field (Fig 5.1b).

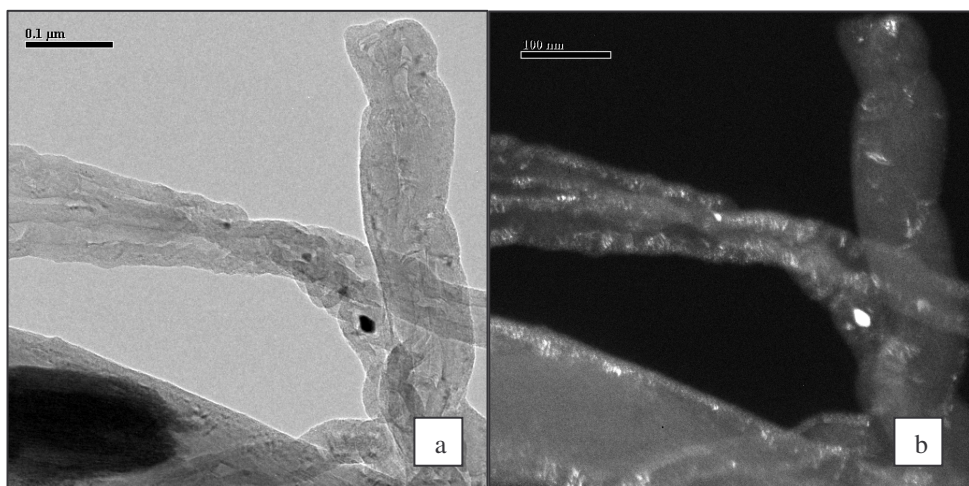


Figure 5.1: TEM images of Fe supported on CNT.

Fig. 5.2 shows the structure of the CNT and particle sizes of the Fe particles. CNT are really parallel type and hollow, very small Fe particles with not uniform diameter situated between the graphite sheets of the CNT are discernable on Fig. 5.2a and Fig. 5.2b. These Fe particles could not be seen in low resolution TEM image (Fig. 5.1a).

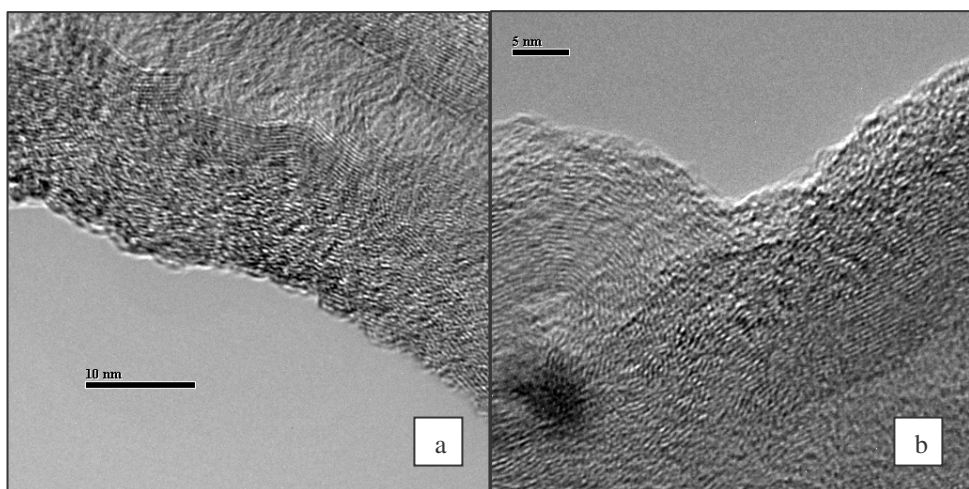


Figure 5.2: TEM images of the Fe supported on the CNT showing small Fe particles between the graphite of the CNT support.

TPR profiles of the Co based catalysts samples given in Fig. 5.3 show three reduction peaks for the Co catalysts calcined at temperatures of 250°C or higher. The three catalysts display the same TPR profile with the first peak increasing with decreasing the calcination temperature, the second peak increasing with the calcination temperature and the third peak overleaping with the second when increasing the calcination temperature. The first peak can be assimilated to the reduction of Co^{3+} to Co^{2+} . This indicates that Co_3O_4 is present in the calcined catalysts. The second peak, very weak for the Co(250) catalyst, is assimilated to the reduction of Co^{2+} to metallic cobalt. The third peak which is situated in the shoulder of the second for Co(300) and Co(350) catalysts, could be ascribed to the hydrogenation of the CNT to methane. The gasification of the CNT at low temperatures (350 - 400°C) in the presence of Co catalyst has also been observed by Bezemer et al [20]. The presence of three reduction peaks is not very distinct on the TPR profile of the catalyst calcined at a temperature of 220°C; this is an indication of an incomplete decomposition of the Co nitrate salt used in the impregnation step. The FeCo(220) catalyst presents three distinct peaks as the cobalt catalysts calcined at temperatures higher than 250°C but these peaks are smaller. This can probably due to the presence of smaller particles difficult to reduce on the surface of the catalyst. TPR studies reported for unsupported Fe:Co [21] and Fe:Co supported on alumina [22] and silica [23] have shown that effect of Fe on Co is to increase the Co temperature of reduction [20, 21].

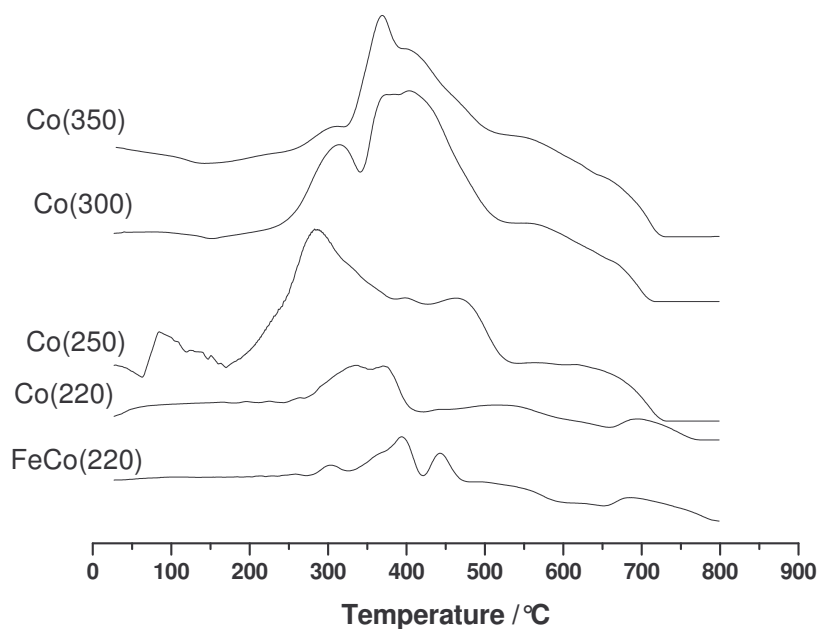


Figure 5.3: TPR profiles of different cobalt catalysts

5.3.2. Catalytic activity

FTS activity and selectivity of the catalysts were measured under a temperature of 275°C and a pressure of 8 bar. The FTS performance of the catalysts was studied at three different space velocities. FT reaction proceeds only on metallic cobalt, the differences on the performance of the catalysts was observed and could be attributed to the pretreatment conditions of the catalysts which resulted in different degree of reduction. This is often the case especially with small Co particles [24].

Fig. 5.4 shows the CO conversion with time and the stabilities of the catalysts for FTS during steady state conditions. For most of the catalysts studied, the steady state is reached after 24 hours. All the catalysts display a high CO conversion stability with time on stream and CO conversion is decreasing with increasing the flow rate.

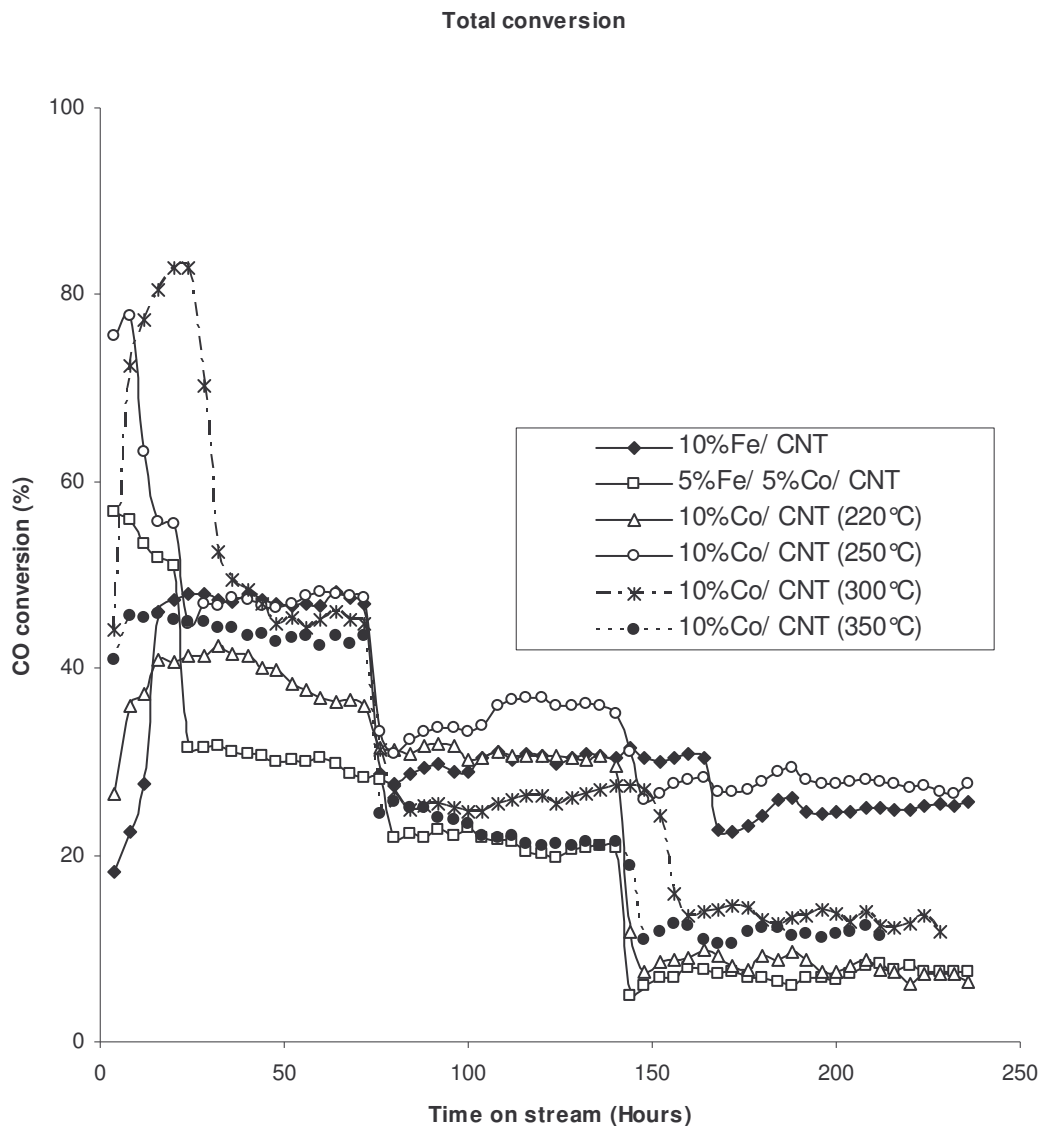


Figure 5.4: CO conversion with time on stream

Activities and selectivities of the catalysts at same GHSV are given in Table 5.3. For the catalysts calcined at 220°C, Fe catalyst display the highest CO conversion, activity and FT rate compared to FeC(220) and Co(220) catalysts. Co(220) and FeCo(220) catalysts have same CO conversion and almost the same activity. However, Fe catalyst gives product selectivities higher than the bimetallic catalyst. FTS rates for the two catalysts are different with the bimetallic catalyst having the lower the FTS rate. Fe catalyst yields the lowest methane selectivity and the highest C₂ olefin and CO₂ selectivity compared to the other catalysts calcined at the same temperature and all the Co catalysts used in this study. For the catalyst calcined at same temperature (220°C), the CO₂ selectivity decreases with the decrease in the Fe content. The decrease of the CO₂ selectivity with the Fe content was expected since Fe is a very active water gas shift catalyst.

Comparison between Co catalysts calcined at different calcination temperatures is also presented in Table 5.3. At same space velocity, the CO conversion increases with the calcination temperature, reaching a maximum with the Co(250) catalyst then decreases slightly and the same trend is observed with the FTS rate and the activity. At high calcination temperature 350°C, the Co catalyst is becomes simply a methanation catalyst with a methane selectivity of 91%. α value is decreasing with increasing the methane selectivity.

Table 5.3: Activity and selectivity of catalysts at same gas hourly space velocity

(GHSV = 2140 h⁻¹)

Catalysts	Fe(220)	FeCo(220)	Co(220)	Co(250)	Co(300)	Co(350)
Conv. (%)	46.8	30.6	30.7	46.6	45.3	43.6
CO rate	-1.38E-06	-9.58E-07	-8.87E-07	-1.56E-06	-1.34E-06	-1.24E-06
CO ₂ rate	4.19E-07	1.83E-07	5.97E-08	1.88E-07	1.65E-07	2.17E-07
FTS rate	9.61E-07	7.75E-07	8.28E-07	1.37E-06	1.18E-06	1.02E-06
Activity ($\mu\text{mol}/\text{sec.gCo, Fe}$) ¹	45.99	31.93	29.58	51.87	44.82	41.40
Alpha (α)	0.74	0.54	0.64	0.53	0.61	0.25
Selectivity (%)						
C ₁	18.71	43.28	29.36	46.26	35.32	91.79
C ₂ -C ₄	41.32	32.18	23.99	30.13	30.44	8.00
C ₅ -C ₁₁	36.67	22.46	36.13	23.60	28.81	0.21
C ₁₂₊	2.62	1.75	7.69	0.0	4.48	0.0
C ₂ ⁼ / (C ₂ + C ₂ ⁼)	11.51	5.02	4.73	4.96	5.45	0.0
CO ₂	6.81	2.97	0.97	3.05	2.68	3.56

¹ Activity was expressed per gram of Fe for Fe catalyst and per total mass of Fe and Co for the bimetallic catalyst

Comparison of activity and selectivity of different catalysts at different gas hourly space velocities is presented in Table 5.4, Table 5.5 and Table 5.6. CO conversion is decreasing with increasing the space velocity for all the catalysts. Iron catalyst produces the lower methane, highest CO₂ and C₂ olefin selectivity at all conversions compared to the bimetallic and Co catalysts.

For Fe(220) catalyst (Table 5.4), CO₂ selectivity decreases while C₂ olefin fraction, FTS synthesis rate and activity increase with increasing the space velocity. It was also noticed that for the FeCo(220) bimetallic catalyst, CO₂ selectivity decreases with the conversion but the methane selectivity increases to reach a maximum of 48.59% at a CO conversion of 21.2% then decreases. The FTS rate is increasing with the space velocity for the bimetallic catalyst.

Table 5.4: Activity and selectivity of catalysts at the different gas hourly space velocity

Catalysts	Fe(220)			FeCo(220)		
	2120	6000	10000	2140	3000	6000
GHSV (h^{-1})	2120	6000	10000	2140	3000	6000
Conv. (%)	46.8	30.6	24.5	30.6	21.2	6.4
CO rate	-1.38E-06	-2.29E-06	-3.11E-06	-9.58E-07	-1.25E-06	-1.80E-06
CO ₂ rate	4.19E-07	4.94E-07	6.85E-07	1.83E-07	2.35E-07	2.69E-07
FTS rate	9.61E-07	1.80E-06	2.42E-06	7.75E-07	1.02E-06	1.53E-06
Activity ($\mu\text{mol}/\text{sec}.\text{gCo, Fe}$) ¹	45.99	76.39	103.58	31.93	41.73	60.12
Alpha (α)	0.74	0.58	0.63	0.54	0.52	0.71
Selectivity (%)						
C ₁	18.71	21.27	20.78	43.28	48.59	39.12
C ₂ -C ₄	41.32	36.27	37.21	32.18	31.80	30.60
C ₅ -C ₁₁	36.67	33.95	36.81	22.46	18.93	30.27
C ₁₂₊	2.62	6.98	4.06	1.75	0.49	0.0
C ₂ ⁼ /(C ₂ + C ₂ ⁼)	11.51	15.42	16.77	5.02	3.54	5.89
CO ₂	6.81	2.87	2.39	2.97	2.72	1.56

¹ Activity was expressed per gram of Fe for Fe catalyst and per total mass of Fe and Co for the bimetallic catalyst

The data for Co(220) and Co(250) catalysts presented in Table 5.5 revealed that the FTS rate increases with increasing the space velocity. The activity increases with the space velocity. For the Co(250) catalyst the activity increases with the space velocity to a maximum of 63.75 $\mu\text{mol}/\text{sec}\cdot\text{gCo}$ and then decreases at high space velocity when using a calcination temperature higher than 250°C.

Results for cobalt catalysts calcined at temperatures equal or high than 300°C presented in Table 5.5 showed that the CO conversion also decreases with the space velocity but there is no trend for the FTS rate.

Catalysts activity was studied as function of the calcination temperature and it was noticed that below the calcination temperature of 250°C (Table 5.4 and Table 5.5), the activity increases with the space velocity. For the Co(250) catalyst the activity increases with the space velocity to reach a maximum of 63.75 $\mu\text{mol}/\text{sec}\cdot\text{gCo}$ and then decreases at high space velocity. Using a calcination temperature higher than 250°C, it is shown in Table 5.4 that the activity is decreasing with increasing the space velocity.

Table 5.5: Activity and selectivity of catalysts at different gas hourly space velocity

Catalysts	Co(220)			Co(250)		
	1620	2120	6670	2140	3330	4000
GHSV (h^{-1})	1620	2120	6670	2140	3330	4000
Conv. (%)	37.7	30.7	9.6	46.6	36.7	27.7
CO rate	-7.45E-07	-8.87E-07	-8.94E-07	-1.56E-06	-1.91E-06	-1.74E-06
CO ₂ rate	6.87E-08	5.97E-08	0.0	1.88E-07	2.23E-07	1.70E-07
FTS rate	6.76E-07	8.28E-07	8.94E-07	1.37E-06	1.68E-06	1.56E-06
Activity ($\mu\text{mol}/\text{sec.gCo}$)	24.84	29.58	32.16	51.87	63.75	57.88
Alpha (α)	0.58	0.64	0.62	0.53	0.65	0.61
Selectivity (%)						
C ₁	40.64	29.36	33.86	46.26	43.41	43.58
C ₂ -C ₄	25.64	23.99	24.69	30.13	25.30	25.03
C ₅ -C ₁₁	29.97	36.13	34.18	23.60	29.32	27.19
C ₁₂₊	2.98	7.69	5.97	0.0	1.62	3.64
C ₂ ⁼ /(C ₂ + C ₂ ⁼)	5.83	4.73	9.77	4.96	5.97	7.01
CO ₂	1.48	0.97	0.0	3.05	2.33	1.48

Fe catalyst gave the highest FT rate compare with Co and bimetallic catalysts. At same conversion, the highest FTS rate for Co catalysts 1.37E-06 $\mu\text{mol}/\text{sec.gCo}$ was achieved with the Co catalyst calcined at 250°C. In general, α value increased when

the methane selectivity decreased, this trend was observed for all the catalysts used in this study.

Table 5.6: Activity and selectivity of catalysts at the different gas hourly space velocity

Catalysts	Co(300)			Co(350)		
	2120	4000	6670	2140	4000	7500
GHSV (h^{-1})	2120	4000	6670	2140	4000	7500
Conv. (%)	45.3	30.7	9.6	43.6	36.7	27.7
CO rate	-1.34E-06	-9.31E-07	-8.40E-07	-1.24E-06	-8.13E-07	-9.40E-07
CO ₂ rate	1.65E-07	0.0	0.0	2.17E-07	0.0	0.0
FTS rate	1.18E-06	9.31E-07	8.40E-07	1.02E-06	8.13E-07	9.40E-07
Activity ($\mu\text{mol}/\text{sec.gFe}$)	44.82	31.04	27.99	41.40	27.11	31.33
Alpha (α)	0.61	0.67	0.71	0.25	0.61	0.63
Selectivity (%)						
C ₁	35.32	41.52	33.18	91.79	47.69	45.14
C ₂ -C ₄	30.44	30.87	26.03	8.00	30.52	27.86
C ₅ -C ₁₁	28.81	25.34	34.32	0.21	21.79	25.40
C ₁₂₊	4.48	1.81	5.65	0.0	0.0	1.31
C ₂ ⁼ /(C ₂ + C ₂ ⁼)	5.45	8.52	12.40	0.0	5.95	0.0
CO ₂	2.68	0.0	0.0	3.56	0.0	0.0

The Co catalysts displayed a relatively high activity varying from 29 to 51 $\mu\text{mol}/\text{sec.gCo}$. The activity of Fe catalyst and Fe-Co bimetallic catalyst used in this

study is also in the same range. The methane selectivity of the cobalt catalysts was higher and C₅₊ selectivity lower compared to those obtained by Yu et al [16] over cobalt catalysts supported on CNF. However, the methane selectivities obtained in this study are in agreement with the selectivities obtained by Bezemer et al [15] except that the catalyst calcined at 350°C has given a very high methane selectivity of 91%. High calcination temperature was indeed not beneficial for the cobalt catalyst supported on CNT. The highest C₅₊ selectivity obtained with the Co/CNT was 67% which is low compared to 81% reported in the literature and the α values obtained were also comparable to those reported [15].

5.4. Conclusion

Fe and Co catalysts supported on CNTs were synthesised. Very small catalyst particles well dispersed on the CNTs could be observed on HRTEM images. These particles were situated not on the surface of the CNTs but between the graphite sheets of the CNTs. The catalysts used in this study displayed high stability in FT synthesis at any GHSV.

Comparison between catalysts calcined at 220°C for their performance in FT synthesis using the same GHSV has revealed that Fe catalyst has the highest CO conversion, activity and FT rate. The Co(220) and FeCo(220) catalysts have same CO

conversion. The FTS rates for the two catalysts are different with the bimetallic catalyst having the lower the FTS rate.

In general, the chain growth probability increases with decreasing the methane selectivity, the CO₂ selectivity and C₂ olefin fraction decrease with decreasing the Fe content. High calcination temperature was indeed no beneficial for the cobalt catalyst supported on CNT. The highest C₅₊ selectivity obtained with the Co/CNT was relatively high. Fe supported on CNT gave lower methane selectivity compared to Co catalysts supported on CNT.

References

- [1]. Dry, M.E. Proc. of S. African Catal. Soc. Catalysis and Catalytic Processes, October 1993
- [2]. Mills, G.A. Catalysts for Fuels from Syngas, IEA Coal Research, London, 1988, pp. 34
- [3]. O'Brien, R.J., Xu, L., Spicer, R.L., Bao, S., Milburn, D. R., Davis. B.H. Cat. Today 36(1997) 325
- [4]. Guzzi, L. New trends in CO activation, Elsevier, vol. 64, (1991) 225
- [5]. Braly, R.C., Pettit, R.J. J. Am. Chem. Soc. 103 (1981) 1287
- [6]. Li, S., Krishnamoorthy, S., Li, A., Meitzner, G.D., Iglesia, E. J. Catal. 206 (2002) 202
- [7]. Krishnamoorthy, S., Li, A., Iglesia, E. Catal. Lett. 80 (2002) 77
- [8]. Rodriguez, N.M., Kim, M.-S., Baker, R.T.K. J. Phys. Chem. 98 (1994) 13108
- [9]. Iijima, S. Nature 354 (1991) 56
- [10]. Weaver, J.H. Science 265 (1994) 611
- [11]. Ebbesen, T.W., Ajayan, P.M. Nature 358 (1992) 220
- [12]. Nagy, J.B., Ivanov, V., Zhang, X.B. Science 265 (1994) 635
- [13]. Kiang, C.-H., Goddard III, W.A., Beyers, R. J. Phys. Chem. 98 (1994) 6612
- [14]. Liu, Z.-J., Yuan, Z.-Y., Zhou, W., Peng, L.-M., Xu., Z. Phys. Chem.Chem. Phys., 3 (2001) 2518
- [15]. Bezemer, G.L., van Laac, A., van Dillen, A.J., de Jong, K.P. Stud. Surf. Sci. Catal.147 (2004) 259

- [16]. Yu, Z., Borg, Ø, Chen, D., Enger, B. C., Frøseth, V., Rytter, E., Wigum, H., Holmen, A. *Catal. Let.* 109 (2006) 43
- [17]. Bahome, M.C., Jewell, L.L., Hildebrandt, D., Glasser, D., Coville, N.J. *Appl. Catal. A: General* 287, (2005) 60
- [18]. Lui, X-Y., Huang, B.-C., Coville, N.J. *Carbon* 40 (2002) 2791
- [19]. Duvenhage, D.J., Coville, N.J. *Appl. Catal.*, 153 (1997) 43
- [20]. Bezemer, G.L., Radstake, P.B., Koot, V., Dillen, A.J., Geus, J.W., de Jong, K.P. *J. Catal.* 237 (2006) 291
- [21]. Brown, R., Cooper, M.E., Whan, D.A. *Appl. Catal.* 3 (1982) 177
- [22]. Kalenczuk, R.J. *J. Chem. Tech. Biotechnol.* 59 (1994) 74
- [23]. Banerjee, D., Chakrabarty, D.K. *Ind. J. Tech.* 30 (1992) 81
- [24]. Sun, S., Fujimoto, K., Yoneyama, Y., Tsubaki, N. *Fuel* 81 (2002) 1583

CONCLUSIONS

Several methods are at present used to produce carbon nanotubes (CNTs), such as arc discharge, laser ablation, and chemical vapor deposition (CVD) procedures. The CVD method for the catalytic decomposition of hydrocarbons in the presence of a supported or unsupported metal catalyst at elevated temperatures is usually used to make CNTs. This method produces large amounts of CNT at low cost although purification of the products is needed after synthesis. The CVD method thus appears to be a very simple method for CNT synthesis but requires careful control of the operating conditions.

In this study the use of carbon (CNT) as a catalyst support for metal catalysts such as Fe, Co and Ru for use in the Fischer-Tropsch synthesis was investigated. Various characterization techniques were utilized to relate the performance of the catalysts to the physical and chemical properties of the catalyst and their performance in the FT synthesis. The results were compared with that of other carbon material supports as reported in the literature.

CNTs were synthesized by chemical vapor deposition method over iron supported on CaCO_3 using C_2H_2 as carbon source at atmospheric pressure and a temperature of

700°C. The characterization of CNTs was done by mean of SEM, TEM, HRTEM, chemisorption and TGA methods.

The TEM and SEM results showed that purified product is comprised of an interwoven matrix of tubes that were shown to be multiwalled (MWCNTs). The diameter of the CNTs was related to the particle size of the catalysts used. The crude product contained predominantly CNTs, with little amorphous carbon. The purification of the nanotubes and the oxidation of their surfaces was performed with dilute HNO₃ which resulted in removal of the Fe and CaCO₃ and enhancement of the CNT density.

CNT synthesis conditions were not optimized in this study. This was done by other workers in our group.

CNT supported FT metals catalysts were prepared, characterized and tested for Fischer-Tropsch activity.

TEM images of the catalysts supported on the CNTs revealed very small catalyst particles well dispersed on the surface of the CNT. In some cases, the internal channel of the CNT contained some residual material (Fe) not removed by the acid treatment. Most of tubes were noted to be closed.

The BET surface area of the purified CNT was found to be 113 m² g⁻¹. Loading of metal catalysts and promoters were shown to reduce the BET surface area of the CNT

supported catalysts. It was assumed that the catalyst particles were lodged in the pores of the catalyst support, thus reducing the overall surface area.

Comparison between the Fe/CNT and Co/CNT showed that the iron catalyst has a higher total BET surface area. The surface area and the pore volume of the Co/CNT catalysts were found to increase with increasing calcination temperature.

TGA analysis revealed that the ideal calcination temperature of the CNT supported catalysts should be around 220°C in nitrogen gas. Thus above 220°C, the CNT decomposes.

ICPOES (ICP Optical Emission Spectroscopy) analysis of the catalysts supported on CNTs revealed that the metal ratios obtained were very close to those predicted from the catalyst preparation.

The reduction behavior of the various catalyst precursors was studied by temperature-programmed reduction (TPR). The peak observed at temperature above 550°C in all the profiles was attributed to the gasification of the CNT support since transition metals can act as catalysts for the formation of methane through reaction of hydrogen with carbon nanotubes at temperatures above 500°C. The carbon gasification process was substantiated by passing the outlet gas from the TPR reactor through a GC. Methane was detected in this outlet gas at temperatures above 550°C. This shows that

gasification of the CNT occurs at high temperatures, apparently catalyzed by the FT metal catalysts, even in the absence of oxygen.

TPR profiles of the Co based catalysts samples showed three reduction peaks for the Co catalysts calcined at temperatures of 250°C or higher. The first peak could be assigned to the reduction of Co^{3+} to Co^{2+} . The gasification of the CNT occurred at even lower temperatures (350 - 400°C) in the presence of Co catalyst. The addition of ruthenium to the Fe catalysts supported on CNT was found to facilitate the dispersion of Fe particles on the surface of the CNT.

Part 1

The effect of catalyst preparation and catalyst promotion on the FTS activity, stability, and product selectivity of a series of Fe/CNT catalysts was investigated.

The CO conversion and product selectivity were not affected by the method of preparation namely of the catalysts. The main difference related to the CO_2 content, which was a little higher (9.81%) for the Fe/CNT prepared by the deposition precipitation method.

Iron supported on CNT gave catalysts with a remarkable high stability and activity. The activity for all the catalysts studied, was initially low but increased significantly within 15 hours and became stable for the entire experiment (20-120 h).

The effect of Cu and/or K addition on the FT activity and selectivity was also studied. The addition of potassium decreased the CO hydrogenation and increased the chain growth during FT synthesis reaction, producing higher molecular weight products (i.e., a higher α value). The C₂ olefin content also increased after the addition of potassium. It was found that potassium also decreased the methane selectivity and increased the WGS activity. Copper was introduced to facilitate reduction of the iron, but also increased the FTS reaction rate. It did not have a major effect on the product spectrum.

Part 2

The preparation of the catalysts described above was repeated but this time with Fe-Ru bimetallic catalysts supported on CNTs. The objective was to investigate the effect of Ru addition to the Fe catalyst. And the effect of Cu and K promotion on CO conversion, product selectivity and FT synthesis activity were also investigated. Comparison of catalyst selectivity and activity were determined at the same CO flow rate and also at similar CO conversions as selectivity depends on conversion.

The potassium promoted catalysts gave the highest yields of CO₂ and C₂ olefins and the lowest methane selectivity when compared to the unpromoted catalysts. The addition of Copper increased the catalyst activity but did not affect the Fischer-

Tropsch product selectivity. At low conversion the methane and CO₂ selectivity decreased and the C₂ olefin selectivity increased for all the catalysts studied.

It was shown that as the Fe content is increased, the methane and the C₂ olefin fraction selectivity decreased. Use of Fe supported on carbon nanotubes, without any promoter, revealed that the methane selectivity was lower and CO₂ selectivity was higher when compared with the ruthenium promoted iron catalyst supported on CNTs. In general, the selectivity to CO₂ and methane increased with increasing syngas conversion.

At low CO conversion (20% - 25%), the C₂ olefin to total C₂ hydrocarbon ratio increased and the methane selectivity decreased for all the catalysts studied. Higher FT synthesis rates and lower methane selectivities were achieved at similar CO conversion, by increasing the metal loading.

At the same conversion, promotion with K enhanced the activity of the catalyst and increased the C₂ olefin production, but the addition of Cu inhibited the performance of K.

TEM images of the iron-ruthenium catalysts supported on CNTs revealed that the catalyst particles were well dispersed on the surface of the CNTs. The catalyst

particles were very small (< 5 nm), and indeed smaller than those obtained when Fe alone was supported on the same CNTs.

Part 3

FT cobalt catalysts supported on CNTs were prepared as mentioned above and tested in FT synthesis. This time the catalysts were calcined at different temperatures. The objective was to investigate whether the calcination temperature could affect the distribution of the Co particles and hence the activity and selectivity of Co/CNT catalysts in Fischer-Tropsch synthesis (FTS). Various techniques (CO chemisorption, TPR, BET and Scanning Electron Microscopy) were utilized to relate the performance of the catalyst system to the physical and chemical properties of the catalysts.

All the catalysts displayed a high stability during the FTS. The CO conversion decreased with increasing space velocity. Fe supported on CNT gave the lowest methane selectivity.

Comparison of the catalysts calcined at 220°C for their performance in FT synthesis using the same GHSV, resulted in Fe catalyst having the highest CO conversion, activity and FT rate. The Co(220) and FeCo(220) catalysts had the same CO conversion. The FTS rates for the two catalysts are different, with the bimetallic catalyst having the lower FTS rate.

In general, the data revealed that the chain growth probability for the cobalt catalysts supported on CNTs increased with decreasing the methane selectivity, the CO₂ selectivity and C₂ olefin fraction decreased with decreasing the Fe content. High calcination temperature was indeed no beneficial for the cobalt catalysts supported on CNTs since methane selectivity was found to increase with cobalt catalysts calcination temperature. The highest C₅₊ selectivity obtained with the Co/CNT was relatively high. Co supported on CNT gave higher methane selectivity compared to Fe catalysts supported on the same CNT.

The preparation of the CNTs and different FT catalysts was successful, however, given the results obtained in this study, more catalysts characterization is needed since catalyst preparation and catalyst pre-treatment conditions would influence the performance of the catalyst in FT synthesis.

The interaction between the catalyst particles and CNT support need to be understood and the size of the catalysts particles should be controlled in the catalyst preparation stage. By controlling this interaction, it should be possible to improve the performance of the CNT supported catalysts in FT synthesis. This occurs since there is usually a relationship between dispersion and activity.